University of Bath

PHD

Novel optical fibres in mode-locked lasers and short pulse manipulation

Harvey, Clarissa

Award date:
2017

Awarding institution:
University of Bath

Link to publication

Alternative formats
If you require this document in an alternative format, please contact:
openaccess@bath.ac.uk

General rights
Copyright and moral rights for the publications made accessible in the public portal are retained by the authors and/or other copyright owners and it is a condition of accessing publications that users recognise and abide by the legal requirements associated with these rights.

- Users may download and print one copy of any publication from the public portal for the purpose of private study or research.
- You may not further distribute the material or use it for any profit-making activity or commercial gain
- You may freely distribute the URL identifying the publication in the public portal ?

Take down policy
If you believe that this document breaches copyright please contact us providing details, and we will remove access to the work immediately and investigate your claim.

Download date: 17. Aug. 2021

Novel optical fibres in mode-locked lasers and short pulse manipulation

submitted by

Clarissa May Harvey

for the degree of Doctor of Philosophy

of the

University of Bath

Department of Physics

August 2016

COPYRIGHT

Attention is drawn to the fact that copyright of this thesis rests with the author. A copy of this thesis has been supplied on condition that anyone who consults it is understood to recognise that its copyright rests with the author and that they must not copy it or use material from it except as permitted by law or with the consent of the author.

This thesis may be made available for consultation within the University Library and may be photocopied or lent to other libraries for the purposes of consultation.

Signature of Author .....

Clarissa May Harvey

To my family and loved ones.

Abstract

This thesis covers work developing novel optical fibres for use as a delay fibre to decrease the pulse repetition rate of a short pulse mode-locked fibre laser operating at 1064 nm . The limits on the length of these laser cavities, and in turn the pulse repetition rate, was found to be the nonlinear phase shift accumulated by a pulse in one round trip of the laser cavity. The addition of extra fibre increases the cumulative nonlinear phase shift to the detriment of fundamental mode-locked pulses. Here, different optical fibres were developed with negligible nonlinear response to minimise additional nonlinearity when extending the laser cavity length. The fibres included large mode area (LMA) solid core fibres, hollow core photonic crystal fibres (PCF) and the more recently developed negative curvature anti-resonant hollow core fibre (NCF).

The LMA fibres had an increased modal area which decreases the intensity of the guided light and thus decreases the nonlinear response. These fibres were used to reduce the repetition rate of a 20 MHz mode-locked fibre laser to 7.6 MHz operating at 1064 nm with a pulse duration of approximately 4 ps .

The use of a hollow core fibre reduces the nonlinearity experienced by a pulse by changing the medium the light is propagating through. The low nonlinear response of air allowed for the reduction of a 4 ps pulse operating at 1064 nm and 37 MHz to be reduced to 27 MHz in PCF hollow core fibre and to a record 5.4 MHz in NCF. The PCF was found to be limited by polarisation effects and high fibre attenuation. However, the results using NCF showed no detriment to the near transform limited pulse. The use of hollow core fibre as a method of reducing the pulse repetition rate of mode-locked fibre lasers was demonstrated.

The NCF developed for this work was also used as a means to induce spectral broadening of a high power, amplified pulse pulse by the means of self phase modulation in a single pass through the fibre. A pulse was broadened by self phase modulation alone producing a symmetrical and broad spectrum that was controlled by the pressurisation of argon within the hollow NCF core. Using a grating pair on the fibre output a pulse of 10 ps at 1064 nm was compressed to 420 fs with an output pulse energy of 8 µJ .

Acknowledgements

Thank you to Jonathan Knight, William Wadsworth and Paulo Almeida for your supervision and guidance throughout.

Fei Yu, Thank you for sharing your knowledge of negative curvature fibre and the guidance in drawing them.

Jim for all the guidance when I first started.

Stephanos thanks for always reminding me to eat lunch and take coffee breaks.

Jon and Adrian for the informative and mentally stimulating diversions.

To all the members of CPPM that have made working here a pleasure and helped in proof reading.

Thank you to Ruth for your friendship and being a sounding board throughout.

Also thanks to Anatoli, John, Mike and all those in Fianium who have been welcoming to my many visits and provided continual assistance.

To my parents for the support and proof reading.

Special thank you to Simon for all the support over the years.

Funding acknowledgements go to the EPSRC and TSB for project funding and to Fianium ltd. for providing funding, supplying fibre laser components and expertise.

Abbreviations

SESAM	Semiconductor saturable absorber mirror
MLFL	Mode-locked fibre laser
EDFL	Erbium doped fibre laser
YbDFL	Ytterbium doped fibre laser
SPM	Self phase modulation
XPM	Cross phase modulation
MI	Modulation instability
SRS	Stimulates Raman scattering
GVD	Group velocity dispersion
FWHM	Full width half maximum
CFBG	Chirped fibre Bragg Grating
WDM	Wavelength division multiplexer
CW	Continuous Wave
NLSE	Nonlinear Schrödinger equation
LP	Linearly polarised
NCF	Negative curvature fibre
HWP	Half wave plate
PBS	Polarising beam splitter
OSA	Optical spectrum analyser
ASE	Amplified spontaneous emission
LMA	Large mode area
HCF	Hollow core fibre
PCF	Photonic crystal fibre
NCF	Negative curvature anti-resonant fibre

Common variables

Pulse propagation

ν & ω	[s^{-1}] Frequency and angular frequency of light respectively
λ	[m] Wavelength of light
$E(z,t)$	Electric field profile as a function of distance along fibre and time
$U(z,t)$	Electric field profile normalised to unity
$A(z,t)$	Pulse envelope as a function of distance along fibre and time
$P(z,t)$	[W] Pulse power as function of position and time, equivalent to $P_0\|U(z,t)\|^2$
P_0	[W] Peak input pulse power
ϕ	Phase
$\chi^{(n)}$	Material susceptibility
α	[$\mathrm{dB\,m^{-1}}$] Fibre attenuation
v_p	[$\mathrm{m\,s^{-1}}$] Phase velocity
v_g	[$\mathrm{m\,s^{-1}}$] Group velocity
$\beta(\omega)$	[m^{-1}] Propagation constant
$\beta_n(\omega)$	[ps^n /m] Coefficients of the Taylor expanded propagation constant
D	[$\mathrm{ps\,nm^{-1}\,km^{-1}}$] Fibre dispersion
γ	[$\mathrm{W^{-1}\,m^{-1}}$] Nonlinear coefficient
n_0	Linear refractive index
n_2	[m^2/W] Nonlinear refractive index
g	[m^{-1}] Fibre gain
E_{sat}	[J] Gain saturation

SESAM parameters

ΔR	Modulation depth
$q(t)$	Absorption as a function of time
A_{ns}	Non-saturable loss
q_0	Unsaturated absorption, saturable absorption, absorbance, Small signal absorption
τ_A	Recovery time
$P_{sat}, E_{sat}, F_{sat}$	Saturation power, energy and fluence.

Contents

Chapter 1

Introduction

Optical fibres are an increasingly useful tool in many areas of both physics research and in industry. New fibres are continuously being developed for a multitude of purposes. The areas of interest here are in generating short optical pulses in mode-locked fibre lasers and in manipulation of short pulses.

A mode-locked laser is known for producing short pulses of picosecond or femtosecond duration at a high repetition rate of megahertz to gigahertz. Many industrial applications require energetic short pulses for applications such as micromachining and research interests can lie in the study of optical nonlinear effects arising from high intensity light in pulses propagating through optical fibre.[1] Extending the performance of mode-locked lasers can give access to further extremes of intensity, pulse repetition rates, pulse durations or pulse energies. The main focus of this thesis is to push the boundaries of low pulse repetition rates in mode-locked fibre lasers whilst maintaining the characteristic short pulse produced by such lasers. A low pulse repetition rate is of interest as it can provide pulses that have high energy or peak power while maintaining a low average power. This makes a useful tool for studying nonlinear effects that depend on only peak power. Low pulse repetition rates are accomplished by extending the length of the laser cavity thereby increasing the round trip time of the pulse within the laser cavity. However, the increased path length also increases the effects of dispersion, nonlinearity and fibre loss on the pulse

which can result in distortion or even the break up of the optical pulse. This work developed optical fibres that could be introduced into a laser cavity to increase the length while minimising additional nonlinear and dispersive effects. This included the study of large area, all solid silica optical fibres as well as the development of silica fibres designed to guide light within a hollow core.

The hollow core fibres developed were also tested for other purposes, namely in using them to spectrally broaden an optical pulse to allow for further compression to a shorter pulse. This spectral broadening can be fine controlled within hollow core fibre by filling the fibre with a suitable gas and pressure.

The synopsis of this thesis is as follows:

Chapter 2 introduces optical fibres in their different forms and covers necessary theory of fibre propagation.

Chapter 3 discusses the methods used to fabricate the optical fibres used in this thesis and goes into further detail on the negative curvature hollow core fibre used in this work.

Chapter 4 covers the background and theory of lasers and introduces the methods of producing pulses of light from mode-locking a laser cavity.

Chapter 5 briefly covers the numerical models developed in this work that were used to investigate the properties of the mode-locked fibre lasers studied in this work and aid in their design. The models also covered pulse propagation in gas filled hollow core fibre which was studied in the chapter 8.

Chapter 6 presents the experimental results of low repetition mode-locked laser cavities constructed with a large mode area fibre as a delay fibre to extend the cavity length while minimising additional nonlinear phase shift of the pulse within the fibre.

Chapter 7 also presents results from low repetition mode-locked lasers but instead exploits the low nonlinearity of hollow core fibres to extend the cavity length with

negligible additional nonlinear phase shift.

Chapter 8 moves away from the construction of mode-locked fibre lasers and investigates the use of the hollow core fibres developed as a means to spectrally broaden an optical pulse through a single pass with the goal of pulse compression. The spectral broadening was a nonlinear effect, which was controlled by filling the hollow core fibre with varying pressures of gas.

Chapter 9 gives the final summary of the work as well as prospects for future work in this area.

Chapter 2

Optical Fibres

2.1 Introduction

This chapter will cover the necessary background of optical fibre theory for this thesis. The theory is introduced in the context of step index fibres for simplicity but is applicable to fibres of other guiding mechanisms discussed toward the end of the chapter. Maxwell's equations can be solved with the boundary conditions imposed by an optical fibre, resulting in multiple transverse modes of light where the light propagates in the same pattern with no change except for phase,[2] these are discussed in section 2.3.1. When considering how light propagates through a fibre it is useful to examine the propagation constant, which is introduced in section 2.3. This describes the phase velocity of a mode through a fibre and how that can vary with frequency giving rise to dispersive effects talked about in section 2.4. Section 2.5 introduces some of the key points of light polarisation that are relevant to this work. A key phenomena in this thesis is nonlinear optics. The velocity of light within a medium is defined by the refractive index $n = c/v$ with c being the speed of light in a vacuum and v is the speed of light in the medium. Nonlinearity arises from the refractive index of the guiding material changing with the intensity of the guided light. The change in refractive index gives rise to many different nonlinear effects such as self-phase modulation from the interaction of light with the electrons in the

material, or Raman which arises from light exciting vibrational modes of molecules. The relevant nonlinear effects are reviewed in section 2.6.

The mathematical description of how dispersion and nonlinearity interact and effect a propagating pulse is given by the nonlinear Shrödinger equation (NLSE) introduced in section 2.7. This is a partial differential equation that describes how the light propagates in both distance and time. The NLSE has non trivial, stationary solutions referred to as solitons. These only occur in specific dispersion regimes and are discussed in section 2.7.

Fibre loss and its relevance are discussed in section 2.8. This chapter concludes with an introduction to different kinds of structured fibre and other guiding mechanisms. Many different types of fibre exist, constructed from different glasses, doped glasses and micro-structures, to achieve specific goals such as controlled nonlinearity, dispersion or transmission windows. This thesis focuses on hollow core fibres which are introduced in section 2.9 and the design and fabrication are elaborated on in chapter 3.

2.2 Step index fibre

Step index fibres are typically considered to be the standard type of optical fibre. These fibres are all solid and consist of a core material surrounded by a cladding material. The cladding material is designed to have a lower refractive index which reflects the light back into the high index core fulfilling the conditions or total internal reflection.[2] The light is only reflected if it is below the critical angle, θ_c, which leads to a maximum angle of acceptance of input light, θ_{NA}, which is related to the numerical aperture of the fibre as $NA = n \sin \theta_{NA}$. These fibres are usually made from silica which has been doped with ions, for example germanium or fluorine, to achieve a different refractive index in the core and cladding. This is shown diagrammatically in figure 2.2.1. The core of an optical fibre is of the order of a few microns radius. At this size the wave properties of light are apparent and the confinement of the light can be thought of more as a balance between the diffraction

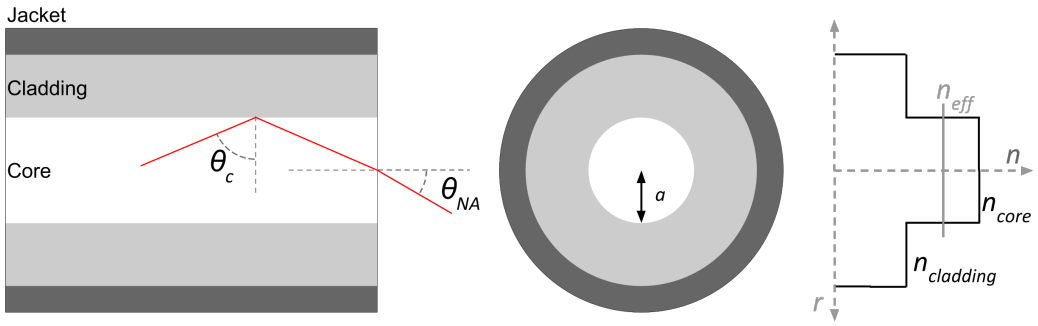

Figure 2.2.1 Step index fibre showing fibre cross section along the optical axis (left), the cross section perpendicular to the optical axis (middle) and the refractive index profile (right). The light is confined to the core of radius a.

of the light in the core and reflection at core-cladding interface. The cladding provides a boundary condition to which Maxwell's equations can be solved. The stable solutions are known as the transverse modes of the fibre where the light propagates without change except for phase.[2] Each mode of a fibre will propagate with its own effective refractive index n_{eff} with $n_{\text{cladding}} < n_{\text{eff}} < n_{\text{core}}$. If a fibre only supports one mode it is a single mode fibre else it is a multi-mode fibre. The mode in a single mode fibre or the mode with the highest n_{eff} in a multi-mode fibre is known as the fundamental mode and the rest are referred to as higher order modes. The fundamental mode will have a Bessel profile with the highest intensity propagating through the centre of the core.

A type of fibre that is similar to the step index fibre which is also used in this work is graded index fibre. Graded index fibre is all solid but has a gradual variation in refractive index between the high index of the core and the lower index of the cladding. These have an advantage of preserving mode size under bending.[3]

2.3 Wave equation and propagation constant

To effectively describe how light propagates through a fibre the wave equation is often used which arises from solving Maxwell's equations:

$$\nabla \times \mathbf{E} = -\frac{\partial \mathbf{B}}{\partial t}, \tag{2.3.1}$$

$$\nabla \times \mathbf{H} = \mathbf{J} + \frac{\partial \mathbf{D}}{\partial t}, \tag{2.3.2}$$

$$\nabla \cdot \mathbf{D} = \rho_{\mathrm{f}}, \tag{2.3.3}$$

$$\nabla \cdot \mathbf{B} = 0, \tag{2.3.4}$$

where $\mathbf{E}$ is the electric field vector; $\mathbf{H}$ is the magnetic field vector; $\mathbf{D}$ is the electric flux density; $\mathbf{B}$ is the magnetic flux density; $\mathbf{J}$ is the current density vector; ρ_f is the charge density.

Within a medium the permittivity, ε_r, and permeability, μ_r, are taken into account along with the electric polarisation, $\mathbf{P}$ and magnetic polarisation, $\mathbf{M}$, the electric and magnetic flux density can be expressed as

$$\mathbf{D} = \varepsilon_0 \mathbf{E} + \mathbf{P} = \varepsilon_0 \varepsilon_{\mathrm{r}} \mathbf{E} \tag{2.3.5}$$

$$\text{and } \mathbf{B} = \mu_0 \mathbf{H} + \mathbf{M} = \mu_0 \mu_{\mathrm{r}} \mathbf{H}. \tag{2.3.6}$$

In optical fibres there are no free electrical charges and it is a non-magnetic medium. Thus the terms, $\mathbf{J}$, ρ_f and $\mathbf{M}$ are zero.

By taking the curl of equation 2.3.1, substituting in equations 2.3.5, 2.3.2, 2.3.6, using identity $\nabla \times \nabla \times \mathbf{E} \equiv -\nabla^2 \mathbf{E}$ one can arrive at the wave equation:

$$\nabla^2 \mathbf{E} - \frac{1}{v^2} \frac{\partial^2 \mathbf{E}}{\partial t^2} = \mu_0 \frac{\partial^2 \mathbf{P}}{\partial t^2}, \tag{2.3.7}$$

where v is the velocity of light in a medium and is related to the speed of light, c, and the refractive index, n, by $v = c/n = 1/(\sqrt{\varepsilon_0 \varepsilon_r \mu_0 \mu_r})$.

A solution to the wave equation including fibre loss and assuming a plane wave

approximation of the light within a fibre, the electric wave can be expressed as a distance, z, and time, t, dependent amplitude $E(z,t)$:

$$\mathbf{E}(\mathbf{x},\mathbf{y},\mathbf{z},t) = \mathbf{E}_0(\mathbf{x},\mathbf{y})e^{i(\beta z - \omega t + \phi - i\alpha z)}, \tag{2.3.8}$$

where E_0 is the spatial amplitude of the wave, ω is the frequency of the wave, ϕ is the phase offset, α is the fibre attenuation coefficient and β is the propagation constant defined by:

$$\beta = n_{\text{eff}}k = n_{\text{eff}}\frac{2\pi}{\lambda},$$

where k is the wave vector which is dependent on the wavelength λ. The propagation constant β is the component of the wave vector in the direction of propagation in a fibre. In free space $\beta = k$. The propagation constant β can be used to describe the phase velocity of the light but also its frequency dependence describes the dispersive properties of the fibre.

2.3.1 Multi-mode fibre

A multi-mode fibre is a fibre that supports more than one transverse fibre mode. Each of these modes are defined by the fibre geometry and are spatially invariant along the length of the fibre. The modes only experience a phase change during propagation. In a fibre core, the core-cladding interface can be considered as a boundary condition to the wave equation which can then be solved to produce the mode field patterns. The modes for a circular core are well known and are solved as Bessel functions shown in figure 2.3.1 The existence of a given mode can be determined using the normalised frequency, V,[2] defined as:

$$V = 2\pi\frac{a}{\lambda}\sqrt{n_{\text{core}}^2 - n_{\text{clad}}^2},$$

where a is the core radius and n_{core} and n_{clad} are the effective refractive indices of the core and cladding respectively. For a given V, a fibre guides a number of modes.

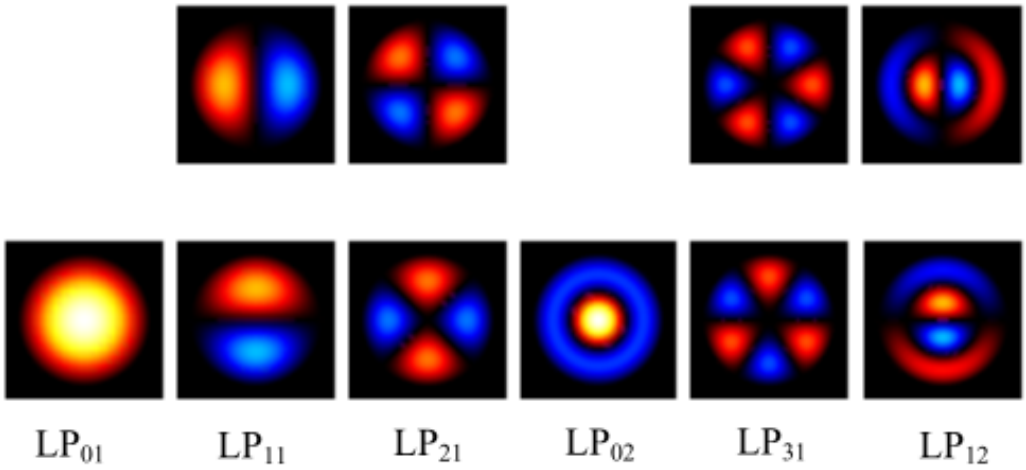

Figure 2.3.1 Fibre modes of a circular core referred to as the the linearly polarised (LP) modes where the polarisation is in an identical state at any point in the spatial field pattern and LP_{01} is the fundamental mode. The red and blue show different phases within the mode pattern. Image courtesy of Tim Birks.

Therefore each mode will have a corresponding cut-off V value. A single mode fibre will have a V less than 2.405.[2]

More complicated fibre geometries require numerical analysis to determine the mode shape. This is applicable to asymmetric fibre cores and to modes that can exist in the cladding of a fibre. Coupling between modes is a concern in mode-locked fibre lasers as it can disrupt mode-locking.[4] Coupling between core and cladding modes is also a mechanism for loss as cladding modes experience high attenuation. Controlling coupling to the cladding modes can improve fibre transmission.[5]

2.4 Dispersion

The refractive index and thus the propagation constant are dependent on frequency. Light travelling through a fibre will have a finite spectral bandwidth so this means different components of the light will travel at different speed through the fibre. For pulses this can lead to a spread or compression of the pulse depending on the initial

conditions and dispersion parameters. The dispersion can arise from the material properties of the medium (material dispersion) and the geometric properties of the waveguide (waveguide dispersion).

The main forms of dispersion that are generally important in fibres are chromatic and modal dispersion. Chromatic dispersion describes both material and waveguide dispersion and will affect any light travelling through the fibre. Second is modal dispersion which is applicable to multi-mode fibres and describes the propagation differences of each mode. Modal dispersion can be in the form of spatial mode dispersion or polarisation mode dispersion which describes the propagation differences between different spatial modes and polarisation states within a fibre respectively.

2.4.1 Material dispersion

The material dispersion can be calculated from the wavelength dependent refractive index given by the Sellmeier equation:[2]

$$n^2(\lambda) - 1 = \sum_{\mathrm{j}=1}^{m} \frac{A_\mathrm{j}\lambda^2}{\lambda^2 - B_\mathrm{j}^2}, \tag{2.4.1}$$

where A_j and B_j are measured Sellmeier coefficients of the material. The above equation is the standard for optical fibres and is applicable to solid materials with the Sellmeier coefficients of silica given by Malitson.[6]

However, for a gas the refractive index is dependent on the temperature and pressure of the fluid. The Sellmeier equation for a gas at a given temperature, T, and pressure, p, at wavelength, λ, is given by:[7]

$$n^2(\lambda, p, T) - 1 = \frac{p}{2p_0}\frac{T_0}{T}\left[\sum_{j=1}^{m} \frac{A_\mathrm{j}\lambda^2}{\lambda^2 - B_\mathrm{j}^2}\right]_{p_0,T_0} \tag{2.4.2}$$

where p_0 and T_0 are 1 bar and 0°C respectively.

The chromatic dispersion arises directly from the frequency dependence of the propagation constant. To classify the different dispersive effects it is useful to expand

the propagation constant as a Taylor series.

$$\beta(\omega) = n(\omega)\frac{\omega}{c} = \beta_0 + \beta_1(\omega - \omega_0) + \frac{1}{2}\beta_2(\omega - \omega_0)^2 + \frac{1}{6}\beta_3(\omega - \omega_0)^3 + ... \quad (2.4.3)$$

where

$$\beta_{\mathrm{m}} = \left(\frac{\mathrm{d}^m\beta}{\mathrm{d}\omega^m}\right)_{\omega=\omega_0} (m = 0, 1, 2, ...). \quad (2.4.4)$$

Each subscript of β corresponds to a different dispersive order. β_0 is the initial phase and is often omitted from descriptions of fibre. β_1 is the group delay and describes the group velocity, v_{g}, of a pulse envelope that has a group refractive index, n_{g}; $\beta_1 = \frac{1}{v_{\mathrm{g}}} = \frac{n_{\mathrm{g}}}{c}$. β_2 is the group velocity dispersion (GVD) and is the most relevant to this work. This determines the spread of a pulse as it propagates and can have a large impact on the structure of a pulse and the optical phenomena it is subject to. It is also useful to introduce the dispersion parameter D which is related to β_2 as $D = \frac{\mathrm{d}\beta_1}{\mathrm{d}\lambda} = -\frac{2\pi c}{\lambda^2}\beta_2$. β_3 is known as the third order dispersion which can distort a pule but is usually only relevant in the case of ultra-short pulses or when β_2 is small. Higher orders do exist but the effect is increasingly small and not covered in this thesis.[2]

The group velocity dispersion is wavelength dependent and has an important property of switching signs at a particular wavelength known as the zero-dispersion wavelength. A positive group velocity dispersion β_2 is known as normal dispersion and negative β_2 is known as anomalous dispersion. Physically this means that in normal group velocity dispersion longer wavelengths of light travel faster than shorter wavelengths; this is known as normal dispersion as this is the regime of visible wavelengths of light in many glasses. In the anomalous dispersion regime the opposite is true with longer wavelengths travelling slower then shorter wavelengths. A fibre that exhibits negligible waveguide dispersion can be modelled using the Sellmeier equation 2.4.1. The GVD can then be plotted as a function of wavelength, figure 2.4.1. The zero dispersion wavelength is located at approximately 1300 nm . Wavelengths shorter than this are in the normal dispersion regime and longer wavelengths are in

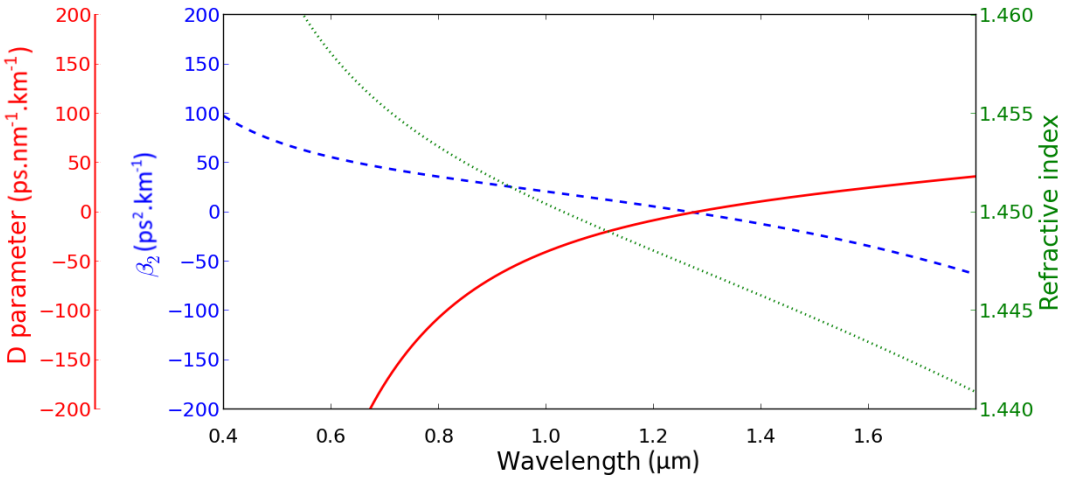

Figure 2.4.1 The refractive index (green dotted) calculated from the Sellmeier equation 2.4.1 using the coefficients of fused silica. The corresponding β_2 and dispersion parameter D are shown in blue dashed and red solid lines respectively.

the anomalous dispersion regime.

Figure 2.4.1 also shows the D parameter mentioned previously and shows its sign change at the zero dispersion wavelength. The GVD experienced by a pulse induces a frequency variation across a pulse known as a chirp. GVD is also relevant in the interplay between certain nonlinear effects, which only manifest in certain GVD regimes. These nonlinear effects will be discussed later in section 2.6.

2.4.2 Waveguide dispersion

Waveguide dispersion arises from the geometry of the waveguide. The inhomogeneity introduced by boundary conditions at a core-cladding interface create a different propagation constant for the wave vectors that compose the guided light. In a free space plane wave the wave vector is in the propagation direction and has no waveguide dispersion. When confined to a waveguide, the propagation constant is a distribution of wave vectors confined in the core. The different wave vectors are wavelength dependent and so give rise to dispersive effects. The waveguide disper-

sion is typically small compared to the material dispersion at 1 µm, but becomes important in the cases of small core fibres and of low material dispersion fibres such as hollow core fibres.[2]

In the case of hollow core fibres the waveguide dispersion can be estimated using the capillary modal. This is where the core is approximated by a cylindrical tube and the waveguide dispersion can be given by:[8]

$$n_{01}(\lambda) = 1 - \frac{\lambda^2 j_{01}^2}{8\pi^2 a^2}, \tag{2.4.5}$$

where $n_{01}(\lambda)$ is the wavelength dependent refractive index of the fundamental mode of the fibre, j_{01} is the first zero of the J_0 Bessel function used to describe the fundamental mode, and a is the core radius. Using this equation the waveguide dispersion can be estimated, though it is not applicable to complicated waveguide shapes it is sufficient to estimate the waveguide contribution to the overall dispersion of the fibres used in this thesis.

2.4.3 Modal dispersion

As discussed previously the chromatic dispersion is composed of contributions from the material dispersion and the waveguide dispersion. The total chromatic dispersion is applicable to one given mode and each mode will have a slightly different propagation constant. This means that as light travels in a multimode fibre the modes will eventually spread apart reaching the fibre end at different times. This is known as modal dispersion. Modal dispersion occurs between the transverse spatial modes of a fibre and can also occur between two polarisation modes of a fibre. The polarisation modes of a fibre tend to have a close propagation constant and thus small modal dispersion compared to spatial mode dispersion.

2.5 Polarisation

An electromagnetic wave is composed of electric and magnetic waves propagating in the same direction. The amplitudes of the electric and magnetic fields oscillate in orthogonal directions. Polarisation in optics refers to the orientation of the amplitude oscillation of the electric wave. If all the waves within a beam of light are in the same orientation then it is linearly polarised. If the oscillation orientation rotates it is circularly or elliptically polarised. If the orientation is randomly distributed in space or time then the light is said to be depolarised. It is possible to have different proportions of the light in the same orientation and can be partially polarised which can be described as the degree of polarisation.

Polarisation of the light can have an impact for different applications and is of importance to the stability of a fibre laser. In an isotropic material such as bulk silica the polarisation of the light will remain unchanged when propagating through. However, some materials and fibre geometries exhibit birefringence where different polarisation states experience a different refractive index. This can change the polarisation state by either rotating it, converting between elliptical and linear or depolarising light. Birefringence can occur in naturally non-isotropic materials but can also appear in silica fibres when the structure is under stress; breaking the symmetry of the molecular structure. In fibres this can occur through tight bending, compression or having an asymmetric core shape. Some fibres have birefringence deliberately engineered into them through the addition of stress rods either side of the core. This has the effect of creating two axis of the fibre to guide different polarisation states without distortion from bending or other effects. These are polarisation maintaining (PM) fibres. Both PM and non-PM fibres were used in this thesis and the differences between the two were found to have an impact of the performance of mode-locked lasers as discussed later in chapters 6 and 7. Comparative micro-graphs of PM and non-PM fibre is shown in figure 2.5.1.

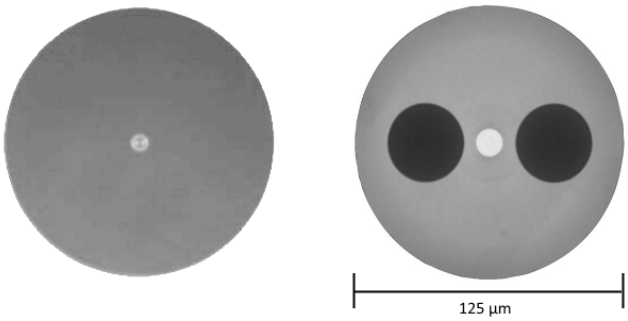

Figure 2.5.1 Micrographs from Thorlabs dataheets of non-PM step index fibre and PM panda fibre (YB1200-6/125DC-PM fibre).

2.6 Nonlinearity

The field of nonlinear fibre optics is extensive and covers many optical phenomena. This section will describe the phenomena relevant to this thesis as well as a brief introduction to the origins of them.

2.6.1 Dielectric material polarisation

Silica is a dielectric material meaning that when light passes through it the dipole moments within the material are displaced. This dipole displacement also has a polarisation associated with it and is a mechanism through which light interacts with the material. The constitutive relation for light travelling through a medium is given by equation 2.3.5. In an optical fibre the permeability is approximately one[2] meaning the refractive index is given by

$$n^2 = \epsilon_r. \tag{2.6.1}$$

It is useful to introduce the electronic susceptibility tensor, $\chi_\mathrm{e} = \epsilon_\mathrm{r} - 1$ where ϵ_r is the relative permittivity of a material. The electronic susceptibility relates the electric field, $\mathbf{E}$, to the polarisation density of the dipoles in a material $\mathbf{P}$ as $\mathbf{P} = \epsilon_0 \chi_\mathrm{e} \mathbf{E}$ where ϵ_0 is the electric permittivity of free space.

To classify the optical phenomena in this thesis it is useful to expand the polarisation density with a Taylor expansion:

$$\mathbf{P_x} = \mathbf{P}_0 + \epsilon_0\chi^{(1)}\mathbf{E} + \epsilon_0\chi^{(2)}\mathbf{EE} + \epsilon_0\chi^{(3)}\mathbf{EEE} + ... \tag{2.6.2}$$

where $\chi^{(1)}$ is the linear susceptibility which relates to the linear refractive index and the fibre attenuation discussed later. $\chi^{(2)}$ and higher are the nonlinear susceptibilities that govern different nonlinear effects.

Combining equations 2.6.2, 2.3.5 and 2.6.1 the refractive index n can be given as:

$$n = \sqrt{1 + \chi^{(1)} + \chi^{(2)}\mathbf{E} + \chi^{(3)}\mathbf{EE}...} \approx n_0 + n_2\mathbf{EE}, \tag{2.6.3}$$

this can then be split into linear and nonlinear parts in terms of electric field or intensity I,

$$n = \sqrt{1 + \chi^{(1)}} + \chi^{(3)}/2n_0\mathbf{EE} = n_0 + \frac{2\chi^{(3)}}{2n_0c\epsilon_0 n}I = n_0 + n_2 I \tag{2.6.4}$$

where the linear refractive index $n_0 = \sqrt{1 + \chi^{(1)}}$ and the nonlinear refractive index is $n_2 = \frac{2\chi^{(3)}}{2n_0c\epsilon_0 n}$. The refractive index is dependent on the light intensity, which gives rise to the nonlinear effects observable at sufficient intensities of light.

2.6.2 Self-phase modulation

The Kerr effect arises from $\chi^{(3)}$ nonlinearities with the basis being that the refractive index is dependent on the intensity of the incident light. This can manifest in two ways. Spatially a beam with a higher intensity of light in the centre will create a higher refractive index at that point and will focus light to the centre of the beam, this effect is known as Kerr lensing. Secondly, in the time domain for a pulse of light it means the refractive index seen by the pulse is larger at the peak amplitudes of the pulse. This causes a nonlinear phase shift of the components of the pulse. This

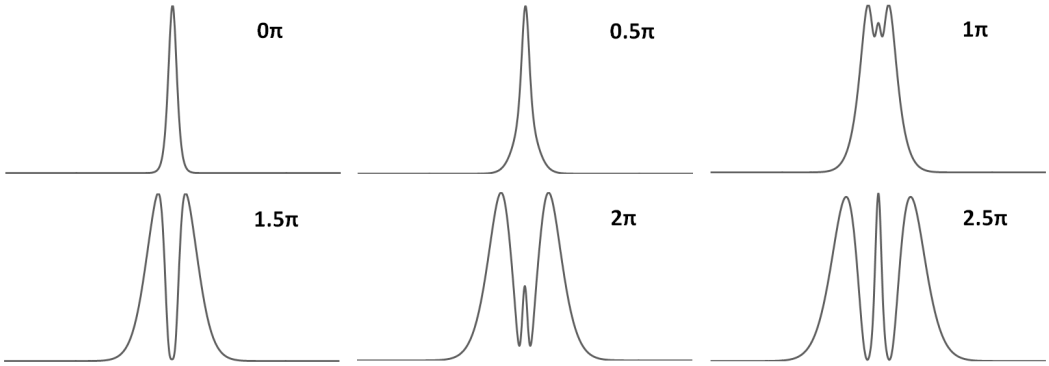

Figure 2.6.1 Example normalised spectra of an initially transform limited pulse after undergoing a phase shift (labelled) induced by SPM.

nonlinear phase shift (ϕ_{NL}) is given by:

$$\phi_{NL} = \gamma P_0 L_{\text{eff}} = \frac{2\pi n_2}{\lambda A_{\text{eff}}} P_0 L_{\text{eff}}, \tag{2.6.5}$$

where P_0 is the peak power, L_{eff} is the effective fibre length taking into account fibre losses (which is discussed further in section 2.8), $\gamma = \frac{2\pi n_2}{\lambda A_{\text{eff}}}$ is the nonlinear coefficient, n_2 in the nonlinear refractive index, λ is the light wavelength and A_{eff} is the effective mode area within the fibre. As a pulse propagates down a fibre it accumulates nonlinear phase shift. This does not directly affect the pulse duration but will broaden the bandwidth of the pulse resulting in a chirp. This process is called self-phase modulation (SPM). The spectral broadening from SPM is characterised by the introduction of a series of peaks in the pulse spectrum which is proportional to the accumulated phase shift as shown in figure 2.6.1. The number of peaks is defined as M and is related to the phase shift ϕ as:[9]

$$\phi = (M + 0.5)\pi. \tag{2.6.6}$$

2.6.3 Modulation instability

Scalar modulation instability (MI) arises from fluctuations in the amplitude of a continuous wave (CW) or pulsed laser. The effects of self-phase modulation and anomalous dispersion compress these fluctuations and can turn a CW laser into a pulse train, or modulate a pulse to have periodic amplitude fluctuations across its duration. In the spectral domain this manifests in the generation of new frequencies either side of the main pulse spectrum. The new frequencies will be generated according to the modulation instability gain curve determined by:[9]

$$g(\Omega) = |\beta_2 \Omega|(\Omega_c^2 - \Omega^2)^{\frac{1}{2}}, \tag{2.6.7}$$

where β_2 is the group velocity dispersion, Ω is the angular frequency shift from the central pulse frequency, Ω_c is the cut off frequency shift after which no new frequencies are generated from the main pulse (though this effect can cascade and 2nd order MI frequency peaks can be generated at sufficient powers). Ω_c is defined by the nonlinear coefficient (γ), peak power (P_0) and the group velocity dispersion (β_2) by:

$$\Omega_c = \frac{4\gamma P_0}{|\beta_2|}. \tag{2.6.8}$$

The MI generated frequencies with the highest gain are found at $\Omega_{\max} = \pm\frac{\Omega_c}{\sqrt{2}}$, shown in figure 2.6.2.

2.6.4 Raman effect

The Raman effect is the production of new frequencies of light based on the interaction between light and molecular vibrations. This interaction occurs in two forms where energy is either transferred to the material from the photon or from the material to the photon. The photon can lose energy (lower frequency) exciting the vibrational or rotational energy of the molecule in question as an optical phonon, where the new photon frequency is called a Stokes wave. Conversely, the material can impart some energy to a photon increasing the photon energy producing higher

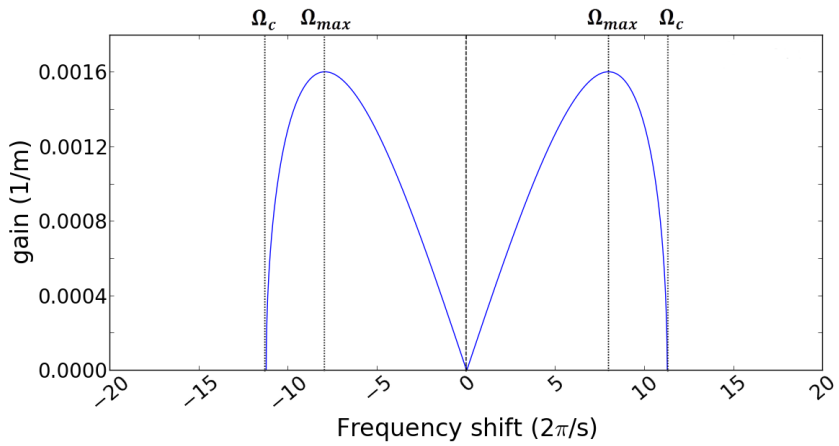

Figure 2.6.2 Example MI gain as function of angular frequency shift. Gain curve was generated for a pulse of 500 kW peak power, $\gamma = 2.6 \times 10^{-6}\,\mathrm{W}^{-1}\,\mathrm{m}^{-1}$ and a central wavelength of 1064 nm.

frequency light as the anti-Stokes wave. The Raman effect can be a useful tool in areas such as spectroscopy[10] or as a laser gain mechanism.[11] However, it is not always a desired effect as it can add an extra level of complexity to optical systems and compete with other nonlinear effects, creating highly structured pulse spectra.[12] The Raman effect can be minimised by propagating at low power or in a vacuum. However, some applications still require high nonlinearity, such as spectral broadening for pulse compression. In these cases a monatomic gas, i.e. a noble gas, can be used that does not have vibrational or rotational modes to excite and so does not have a Raman response.[12]

2.7 Nonlinear Schrödinger equation and solitons

As a pulse propagates through a medium it is subject to both dispersion and nonlinear effects, specially self-phase modulation. These two effects can strongly shape a pulse. The amount of dispersion experienced by a pulse is dependent on the pulse spectral bandwidth and affects the pulse duration. The nonlinearity is dependent on the pulse peak power, and in turn the pulse duration as a shorter pulse will have

a higher peak power, and affects the pulse spectrum. The interdependency of the dispersion and nonlinearity mean both need to be considered simultaneously when describing pulse propagation.To describe the overall effect of these the nonlinear Schrödinger equation is used. This partial differential equation is show is given as:

$$i\frac{\partial A}{\partial z} + \frac{i\alpha}{2}A - \frac{\beta_2}{2}\frac{\partial^2 A}{\partial t^2}\gamma|A|^2 A = 0, \tag{2.7.1}$$

where $A = A(z,t)$ is the time and distance dependent pulse envelope , z is the propagation distance along the fibre, α is the loss coefficient, β_2 is the group velocity dispersion, t is time in the reference frame of the pulse, and γ is the nonlinear coefficient. This equation is heavily used to describe pulse propagation within a fibre and many numerical methods have been developed to solve it, such as the split step Fourier method[13] which will be reviewed in chapter 5.

A special case solution of the equation is in the anomalous dispersion regime where $\beta_2 < 0$. In this regime the effects of nonlinearity and dispersion oppose one another and can cancel out resulting in a stable propagation with no change in pulse parameters apart from attenuation. This solution is known as a soliton. The analytical solution is:

$$A(t) = N\,\mathrm{sech}^2(t/\tau), \tag{2.7.2}$$

where N is the soliton order shown in equation 2.7.3 and τ is the pulse duration in $1/e^2$ width[9]

$$N = \gamma P_0 \frac{\tau^2}{|\beta_2|}. \tag{2.7.3}$$

For the case of $N = 1$, the soliton is known as a fundamental soliton and was first reported in surface waves on water in 1834[14] and later in fibres in 1980.[15] There are solutions to the NLSE that exhibit similar behaviour but have a periodic amplitude fluctuation in distance or time. These are known as higher order solitons[9] where $N > 1$. This periodicity gives rise to the descriptive parameter of a soliton period, z_s:

$$z_\mathrm{s} = \frac{\pi\tau^2}{2|\beta_2|}. \tag{2.7.4}$$

If a pulse is propagating in the anomalous dispersion regime and has sufficient intensity to induce SPM then it will tend to a soliton shape even if it is initially the wrong duration or shape.[9] A pulse will transition into a soliton usually by shedding some energy until it reaches the steady state parameters. This energy is shed a dispersive wave that propagates in the same direction. This makes soliton propagation quite stable and relatively easy to excite.

In a system constructed of many components, such as a laser, the pulse is not always subject to constant GVD or nonlinearity and can undergo discrete changes in parameters. Solitons in such lasers will then experience a certain periodicity in the laser cavity round trip. A soliton in such a system will be identical at a given point in the laser cavity, e.g. at the output coupler, even though it may change duration, energy or bandwidth as it travels through a cavity. These can be referred to as self-similar or breathing solitons as each pulse exiting the cavity is identical to the previous pulse. These still have soliton like properties but can be made in different regimes. For example, at 1064 nm the light is in the normal group velocity dispersion regime of silica, but a self-similar soliton can be generated in a 1064 nm laser cavity provided there is a component that applies enough anomalous dispersion to the pulse, such as a chirped fibre Bragg grating.

2.8 Fibre loss

As light propagates through a fibre, some of it is lost due to absorption or scattering by the material or from imperfect confinement. For a given fibre, the loss is typically quoted in dB/km. For many practical purposes it is possible to simplify the mathematics by introducing an effective fibre length $L_{\text{eff}} = \frac{1-exp(-\alpha L)}{\alpha}$ for a fibre of length L with and absorption coefficient α, such that a lossy fibre can be equated to a shorter, loss-less fibre when dealing with nonlinear effects. This is used through the experimental sections when calculating fibre properties from measured results of self-phase modulation or modulation instability. The effective length is also used in the numerical modelling in chapter 5 to optimise the calculations.

The absorption coefficient α discussed previously is related to the imaginary part of the linear susceptibility while the linear refractive index is related to the real part:[16]

$$\alpha(\omega) = \frac{\omega}{nc}\Im[\chi^{(1)}(\omega)] \tag{2.8.1}$$

$$n(\omega) = 1 + \frac{1}{2}\Re[\chi^{(1)}(\omega)]. \tag{2.8.2}$$

These equations mean that the frequency dependent linear refractive index can be determined from the fibre loss using Kramers-Kronig relations:[16]

$$n(\omega) = 1 + \frac{c}{\pi}\int_0^\infty \frac{\alpha(\Omega)}{\Omega^2 - \omega^2} d\Omega. \tag{2.8.3}$$

This is a useful tool as it means the refractive index, and in turn the dispersion, can be estimated from the measured transmission of a fibre. This gives an indication of the shape of the group velocity dispersion curve across the transmission band of the fibre and what the zero-dispersion wavelength is.

2.9 Other guiding mechanisms and hollow core fibre

The physics presented in this chapter so far has been explained in the context of solid core, step index fibres. These are the standard type of fibre and useful for introducing the main concepts of light in an optical fibre. However, different guiding mechanisms do exist that do not depend on a high refractive index in the core to refract light. The two other guiding mechanisms in use are photonic band-gap guidance and anti-resonant guidance. Fibres of these different types are shown in figure 2.9.1. A photonic band-gap fibre has a periodic structure surrounding the core of either holes in the glass or rods of a different glass or dopant. Individually, these act as partial mirrors but are placed in a larger structure designed to manipulate the wave-vectors of the light in the cladding to suppress cladding modes and keep the light in the core, and can be considered a kin to a 2D Bragg mirror.[17] Anti-resonant fibres use a

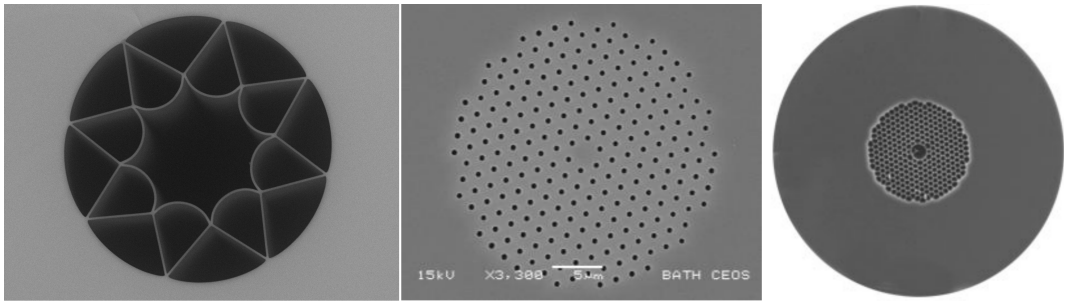

Figure 2.9.1 Right to left: NCF antiresonant fibre drawn in house with a core of 34 µm , photonic band-gap fibre with air holes drawn in house, Hollow-core photonic crystal fibre (Thorlabs HC-1060 with 10 µm core).

thin wall around a core. The thin wall and core mode can be thought of as coupled resonators and are designed to be in antiresonance and minimise the amplitude in the thin wall and the rest of the support structure.[18] Further engineering of the geometry of these fibres can then minimise coupling into leaky cladding modes and improve fibre transmission. The concepts described so far in this chapter are applicable to both photonic band-gap fibres, anti-resonant fibres as well as step index fibres. The key differences between the photonic band-gap and anti-resonant guidance with simple step index fibres is that these fibres allow further engineering of the waveguide dispersion and the core does not require a higher refractive index than the cladding. A low refractive index core is of particular interest in this thesis. The main consequence of this is that a fibre can be constructed that has a hollow core. The majority of hollow core fibres used in this thesis are of anti-resonant design. The theory, design and fabrication of such fibres will be discussed later in chapter 3.

Chapter 3

Fibre Design and Fabrication

3.1 Introduction

For this work many different types of optical fibres have been used and fabricated. Chapters 6 and 7 cover work in mode-locked fibre lasers. These fibre lasers contain many different types of fibre in one cavity and will be discussed further in the relevant chapters. The main component pigtails and gain fibre used in the laser cavities in chapters 6 and 7 are commercially bought fibres. The delay fibres used to lengthen the laser cavities were custom made for the purpose and drawn in house. Chapter 6 covers the work done with large mode area fibres. The large mode area fibres consisted of either step index fibre or graded index fibre. The fabrication of these will be discussed in section 3.2. Chapter 7 covers the laser cavities constructed using hollow core fibre as the delay fibre. The same fibres are then used in chapter 8 to create self-phase modulation on an existing pulse by filling the fibre with gas. Section 3.3 covers the design and fabrication of the negative curvature hollow core fibre used in both chapters 7 and 8.

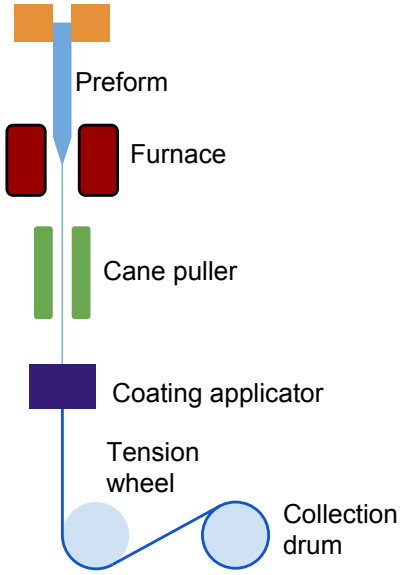

Figure 3.2.1 Diagram of a fibre tower. Cane puller is for drawing canes only. Coating applicator, tension wheel and collection drum are for drawing to fibre.

3.2 All solid fibres and tapered fibre

Solid optical fibres fabricated for this project were done using a fibre tower. A large scale version of the fibre structure known as a preform is constructed or bought and is then drawn down into fibre through a furnace. A diagram of a fibre drawing tower is shown in figure 3.2.1. The glass preform is held in a chuck and lowered into the furnace at controlled rate. The furnace heats the glass and the softened glass is then pulled into a thinner form with the same structure. The preform can be pulled into an intermediary stage called a cane which is thinner than the preform but still much larger than the final fibre. Canes are normally rigid and are drawn using the cane puller shown in figure 3.2.1. Everything below the cane puller shown in figure 3.2.1 is used when drawing to fibre only. The fibre is pulled through the furnace by the force of the turning collection drum through a coating applicator. The fibre is then wound onto a collection drum.

The outer diameter (OD) of the fibre is monitored as it comes out of the furnace. The OD of the fibre or cane is controlled by the preform feed and draw speed. Adjusting the applied tension by changing the draw speed allows for the thickness to be controlled and tapers can be made directly on the tower.

The large mode area fibres (LMA) used in chapter 6 were initially drawn by Jim Stone. Further step and graded index fibres, both tapered and non-tapered, were drawn by myself and Ben Cemlyn.

3.3 Negative Curvature Fibre

Negative curvature, hollow-core anti-resonant fibre (referred to as NCF) is a type of leaky mode fibre that guides light using an anti-resonant method, as total internal reflection is not applicable to hollow fibres. The leaky mode definition means the modes are not traditional bound modes but instead have decaying light in the transverse direction that is blocked by the cladding structure. These modes experience waveguide loss but not in sufficient amounts to distort the mode shape.[19] Negative curvature fibre was first trialled in a "Kagome" fibre[20,21] and found to significantly improve the fibre guidance of the core mode. Further study then revealed that the negative curvature wall was an excellent guiding mechanism and could be used without the Kagome structure simplifying the fibre design.[22]

3.3.1 Fibre design

The majority of fibre fabricated for the low repetition mode-locked laser cavity project was of the negative curvature, hollow-core anti-resonant design. This is based on the design by Fei Yu et al.[23] but designed to have a central wavelength of 1064 nm . The design of this fibre requires several factors to be taken into account. The notable ones that will be discussed here are: the wall thickness, curvature, core size, cladding capillary size and the draw down ratio. These factors are shown illustratively in figure 3.3.1.

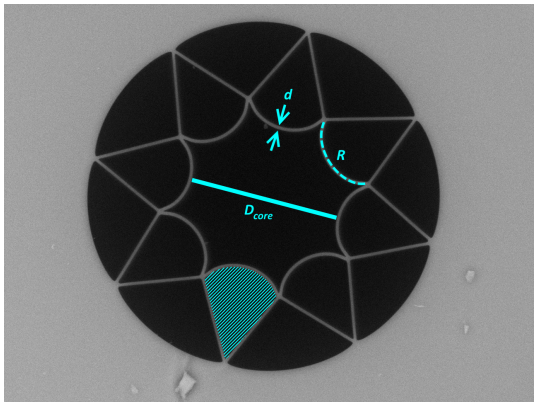

Figure 3.3.1 Visualisation of key parameters of NCF. d is the wall thickness, D_{core} is the core diameter, R is the radius of curvature of the core walls and the hashed area is the area of the cladding capillaries. Background image is an SEM image of an existing fibre.

Wall thickness

The wall thickness is an important parameter as it is related to both the wavelengths included in the transmission bands and the attenuation of the fibre.

The position of the transmission bands can be approximated by the anti-resonant reflecting optical waveguide (ARROW) model.[24] This model is based on viewing the main core mode and the cladding modes as two coupled resonators. As such they will have a resonance wavelength where light will be transmitted through the core wall. Away from these wavelengths the light can be guided provided it is prevented from coupling with other cladding modes. Under the ARROW model the resonant wavelength, λ_{m}, is given by:

$$\lambda_{\text{m}} = \frac{2n_1 d}{m}\sqrt{\frac{{n_2}^2}{n_1} - 1}, \tag{3.3.1}$$

where n_1 and n_2 are the low (air) and high (glass) refractive indices, d is the wall thickness and m is an integer denoting the order of the resonance. λ_{m} corresponds to the points of high attenuation between the transmission bands. For a given cladding material the position of the transmission bands are determined by the wall thickness

d. The main transmission band located between λ_1 and λ_2 is the band normally used for operation. The main dependences that can be determined by examining equation 3.3.1 is that λ_m is proportional to n_2 and d, so if these are increased then the transmission band widens and shifts to longer wavelengths. However, increasing n_1 will shift the transmission band to longer wavelengths but narrow the transmission band.

The transmission band can be shifted by altering the core medium. This can be done by filling the fibre with a gas or liquid. As the gases used in this thesis have a refractive index close to one[25] the affect on the fibre transmission from gas filling is assumed to be negligible. For the case of filling with a liquid with a high refractive index then changes to the transmission window would need to be taken into account.

The wall thickness has also been shown to impact the fibre attenuation both from simulations and experimentally by Yu et al.[24] Ideally, the wall thickness should be as thin as possible to prevent coupling between core and cladding modes.

Wall curvature

In addition to the parameters set by the ARROW model for guidance, the fibre geometry also plays a key role in core-cladding mode coupling and thus transmission properties. The wall curvature is set by inflating the cladding capillaries during fabrication to expand the wall into the core. To achieve low loss a thin wall is desirable.[26] However this has to be done such that the design wavelength is still in the transmission window. The other geometric properties that need to be considered are the curvature of the walls and the size of the connecting nodes in this fibre. Decreased radius of curvature generally increases the confinement although this is not a simple correlation as shown by in figure 3.3.2. However, practically when fabricating this, the nodes connecting the NCF walls will also increase in size and start to guide light. This means light from the core will couple to the lossy node wave-guides and increase the fibre loss.

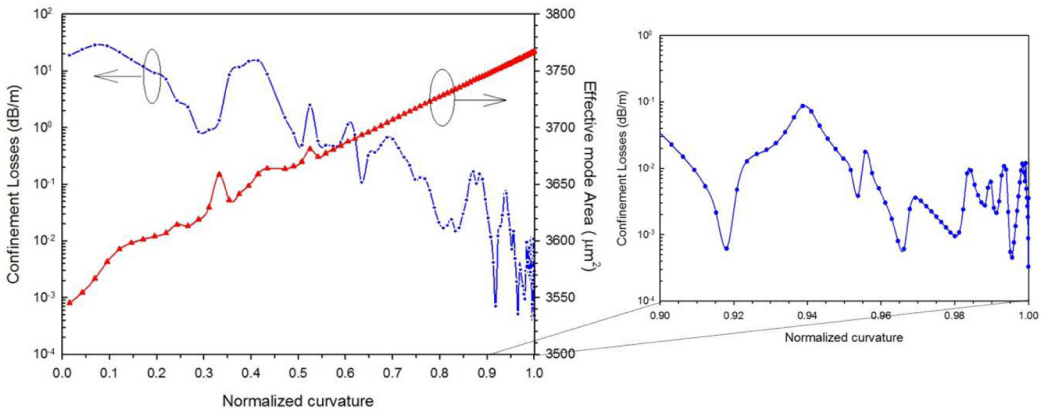

Figure 3.3.2 Confinement of core mode for varying curvatures simulated by Belardi et. al.[5]

Core and cladding capillary size

The diameters of the cladding capillaries and the core also play a role in the performance of the fibre. The cladding capillaries can guide their own"air modes" which act as a loss mechanism to the core if core light can couple to them from the core.[5] The phase matching conditions between the core and the air modes of the cladding also determine the single mode and multi mode guiding properties of the fibre. The fibres fabricated and used in this thesis all have 8 cladding capillaries as that was a proven design.[23] The core size of the fibres drawn has resulted in the fibres supporting the LP_{11} mode in addition to the fundamental mode.

Draw down ratio

There are also fabrication constrictions that need to be taken into account in the design stage. Namely the limit on draw down ratio from preform to fibre. This arises from the effect of surface tension opposing the inflation of the capillaries to form the curved wall while the preform is in the furnace. This becomes more prevalent for smaller fibres, i.e. fibres designed for short wavelengths ($\lesssim 2\,\mu m$). Previous fabrication has found the ideal ratio is approximately 10 to 1 cane to fibre diameter

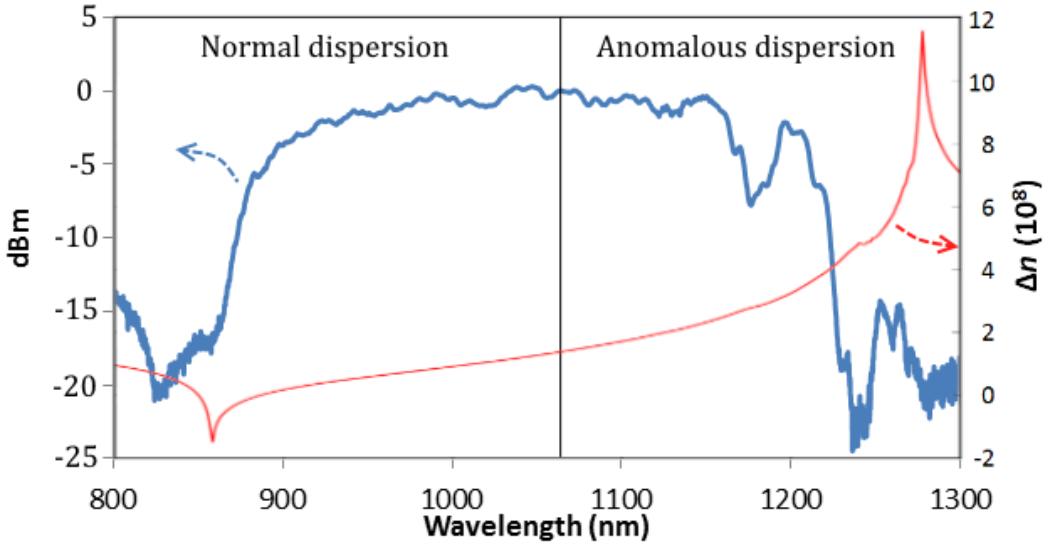

Figure 3.3.3 Example transmission spectra (blue line) measured with a design wavelength of 1064 nm (black line). The red line is the calculated variation in refractive index using the Kramers-Kronig relation discussed in section 2.8.

for fibres designed for 1064 nm. Slightly larger draw down ratios are possible but require higher pressures during the draw and proved to be more sensitive to draw parameters and thus more difficult to produce a consistent quality of fibre. This was the main limitation on drawing long lengths of fibre as the fibre length is dictated by the draw down ratio and the length of the preform.

To further improve the quality of the fibre at short wavelengths an outer jacket of fluorine doped silica is used. This directly has no impact on the optical properties of the fibre as it is far from the core and cladding light. The benefits arise from fluorine doped silica having a lower melting point than pure silica. This allows for a more uniform heating of the fibre as it is drawn through the furnace thus reducing distortions and asymmetry in the final fibre.

Fibre dispersion

For a fibre with an air or gas filled core, the material dispersion is low, meaning that the waveguide dispersion needs to be considered. The variation in refractive index (and thus the chromatic dispersion) can be approximated from the transmission window shape from the Kramers-Kronig relations.[16] The zero-dispersion wavelength of the fibre lies near the centre of the transmission window with longer wavelengths being in the anomalous dispersion regime and shorter wavelengths in the normal dispersion regime as shown in figure 3.3.3. The desired dispersion regime at the operation wavelength needs to be taken into account when engineering the position of the transmission band. Though the zero dispersion wavelength can be fine tuned by pressurising with different gases.[27]

3.3.2 Negative curvature fibre fabrication

NCF fabrication is divided into two main sections: fabricating canes and jacketing the canes and drawing to fibre. The canes are the intermediary stage where the fibre structure has been constructed in a large rigid cane that is then ready to be drawn to fibre. The jacket refers to a glass tube to which the cane is inserted.

The canes were designed using a MATLAB script, originally constructed by Fei Yu, taking the factors discussed in the previous section into account to produce a stacking guide. Inputs include target core size, fibre diameter and dimensions of the two jacket tubes. An example of the output design is given in figure 3.3.4. Appropriate silica tubes were selected or drawn to match the design with some adjustments made to the design based on what tubes are available. The stack used to make this fibre is shown in figure 3.3.5. The canes are made by inserting eight smaller, thin capillaries into a larger silica tube. At this stage the main silica tube has an outer diameter of 25 mm and has an inner diameter approximately 10 mm . Two supporting tubes are placed in the core at each end of the stack to separate the cladding capillaries. The stack is then drawn down to cane of approximatively 2 mm . At this stage the capillaries are fused to each other and the outer jacket as shown in figure 3.3.6a.

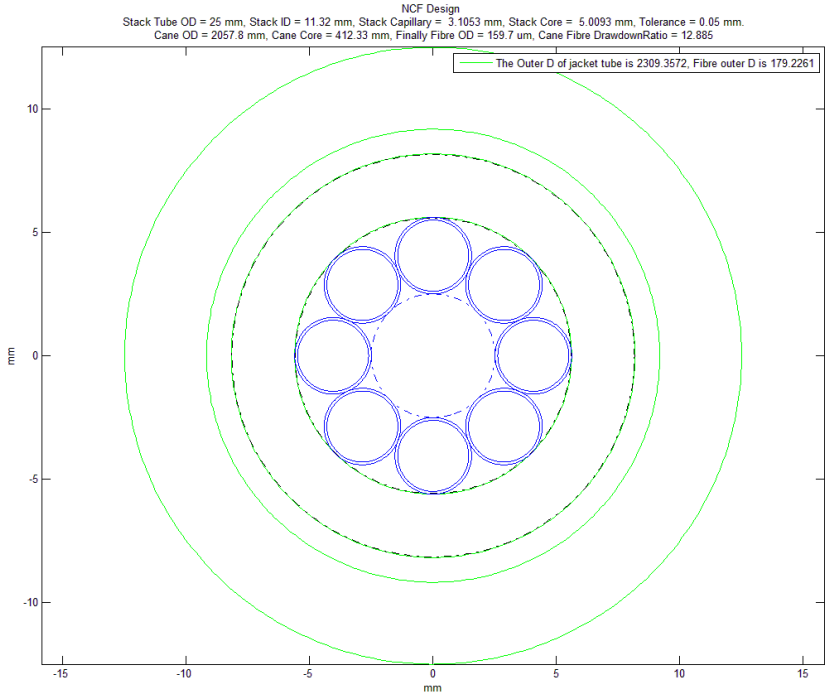

Figure 3.3.4 Example NCF design produced for an operation wavelength of 1064 nm showing the size of glass tubes needed for the two out jackets, the cladding structure and the central supporting tube. Design was created as part of this work using an existing MATLAB script.

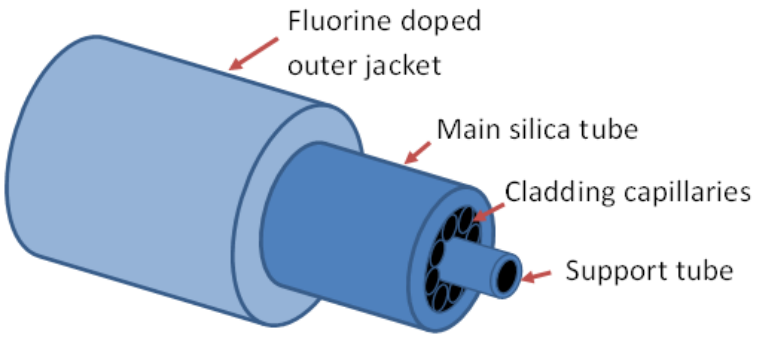

Figure 3.3.5 Diagram of NCF preform.

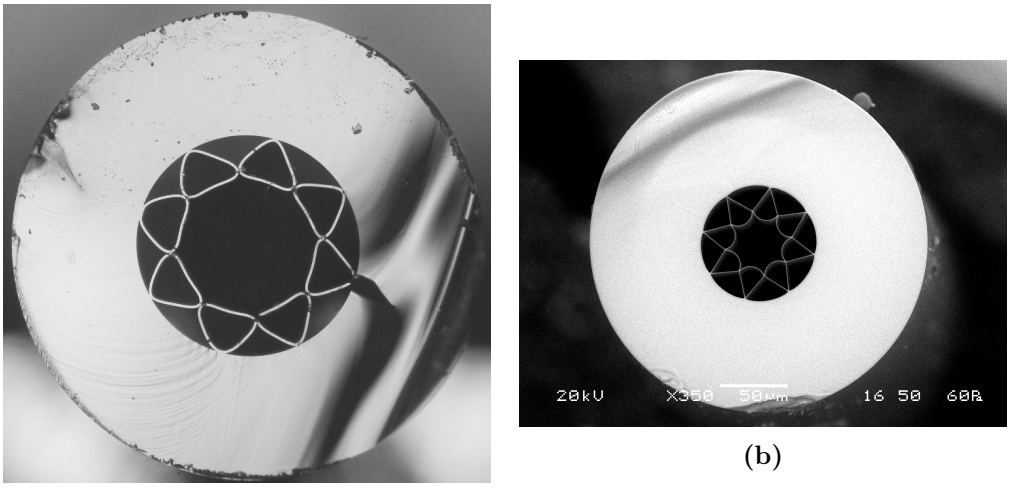

(a) (b)

Figure 3.3.6 Left: NCF cane with a 2 mm outer diameter diameter. Right: Completed fibre with a fluorine doped silica outer jacket Fibre outer diameter is 244 µm, inner cladding structure is ≈ 60 µm and a core diameter of ≈ 34 µm.

The second stage consisted of threading the cane into a fluorine doped silica outer jacket. A small capillary is inserted into the core to allow for a different pressure to be applied to the cladding structure and the core as shown in figure 3.3.7.

The cane was drawn to a fibre in the fibre tower with a coating being applied to the outside. The fibres had a final outer diameter of approximately 240 µm for fibres drawn with a fluorine doped silica outer jacket. Some fibres drawn for this work did not have a fluorine outer silica jacket and thus have a smaller outer diameter of approximately 160 µm. The final fibres had a core diameter of approximately 35 µm.

The final fibre drawing stage required precise parameters to maintain the cladding structure and provide the correct curvature to guide light adequately. Although the drawing parameters can be roughly calculated, the precise values were found by trial and error. Figure 3.3.8 shows three examples of unsuccessful fibre draws before the correct parameters were found. The typical parameters used to draw low loss NCF are given in table 3.1.

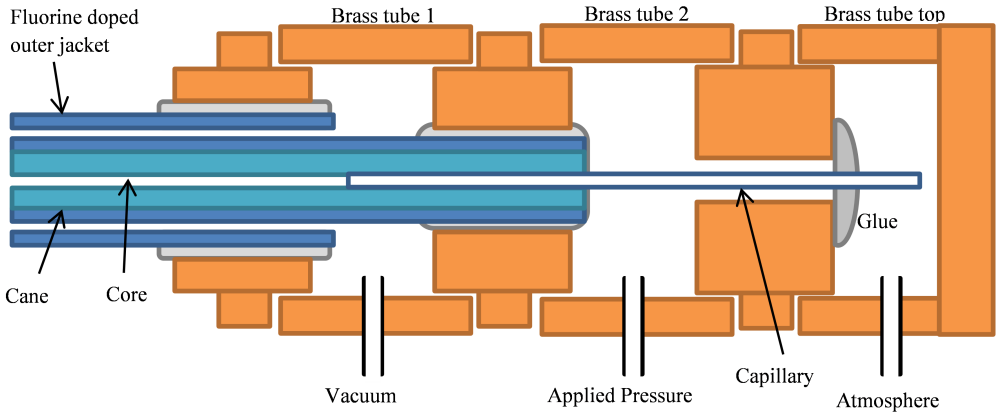

Figure 3.3.7 Pressurisation schematic of the NCF cane. The core is pressurised at atmospheric pressure and monitored. The cladding is then pressurised to inflate the cladding walls in toward the core. The vacuum collapses the fluorine doped outer jacket when one was used.

Draw Speed	6.7	m/s
Feed Speed	75	mm/min
Temperature	1955	°C
Pressure in cladding	19	Pa above room
Tension	220	g
Outer Diameter	245	µm

Table 3.1 Typical fibre draw parameters of the hollow-core negative curvature fibre designed to guide 1064 nm .

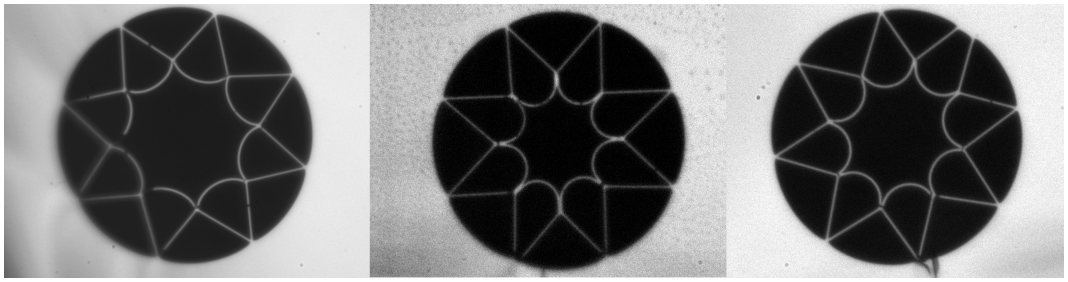

Figure 3.3.8 Examples of three different fibre draws resulting in inadequate fibre. Left: the furnace temperature was too high resulting in under inflation, middle: the pressure in the cladding was too high resulting in over inflation and right: capillary over attached resulting in strong asymmetry.

3.3.3 Fibre characterisation

The initial characterisation of the fibre gives a good idea of how it will perform in a laser cavity. The first characterisation performed was to photograph the cladding structure through a microscope. This was normally done during the draw to monitor the curvature. The core diameter is measured at this point using a calibrated scale in the microscope image. The wavelength transmission was also measured for each fibre. This was done by sending a white light from a Xenon-bulb or a supercontinuum into a standard SMF-28, step index fibre that was then butt-coupled or focused onto the end of the NCF. The output was then measured with an optical spectrum analyser. It is customary to perform a cut back measurement where the fibre is cut shorter by a known amount and the relative change in output spectrum power can then be used to calculate the fibre attenuation. As the fibres drawn for this work were required to be as long as possible this was not done to most of the fibres. Instead the attenuation was estimated for the design wavelength through measuring the fibre throughput. The ratio of light of a given wavelength measured coming out of the fibre relative to the light incident gives an upper value of the fibre attenuation.

The mode pattern was also analysed by focusing a CCD camera on the fibre end using lenses and a ytterbium ASE source centred at 1030 nm . As the core diameter

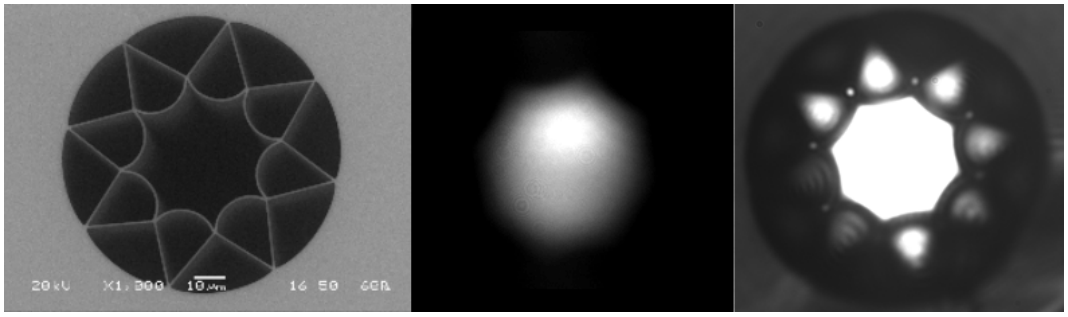

Figure 3.3.9 Micrographs imaging the fibre end of a low loss 48 m NCF. Left: SEM image of fibre end structure. Middle: Optical micrograph showing the core mode profile. The asymmetry in the intensity pattern indicates higher order modes present in addition to the fundamental mode as discussed in section 2.3.1. Right, overexposed optical micrograph showing the illuminated fibre structure, air guided cladding modes and the modes guided in the nodes between the negative curvature walls taken by illuminating the entire fibre input.

is known at this point, micrographs were taken with the structure illuminated and again with only the core mode excited to scale the image and measure the mode field diameter. The mode purity is also qualitatively assessed at this point by the symmetry of the mode pattern and its resilience to physical fibre perturbation. The air guided cladding modes and node modes can also been seen at this stage. These modes are shown in figure 3.3.9. It is worth noting the difference in intensity between the air guided cladding modes. These show the differences in guiding capabilities in the cladding structure as these relative intensities did not change with offsetting the incident spot on the fibre or by bending the fibre. This shows there is some asymmetry in the fibre structure. As seen in the SEM image in figure 3.3.9 the core has some ellipticity. These asymmetries can create a birefringence in the core that needs to be take into account when managing polarisation within a laser cavity.

Chapter 4

Mode-locked Fibre Lasers

4.1 Introduction

This chapter covers the necessary theory of mode-locked fibre lasers (MLFL) that are relevant to the experimental chapters 6 and 7. A brief introduction is given with a historical context. Section 4.2 gives the overview theory of a laser cavity followed by the information on the laser gain used in this thesis. Section 4.4 covers the methods used to create a mode-locked laser and the different operating regimes of such a laser are described in section 4.5 and characterising laser pulses in section 4.6.

The main focus of the MLFL work in this thesis is in reducing the repetition rate. The challenges and existing work in this area is summarised in section 4.7. The chapter concludes by covering some of the more specialist laser components used in this thesis in section 4.8.

MLFLs are a type of pulsed laser that are known for producing ultra-short pulses ($<$10 ps) at high repetition rates (50 MHz to GHz). They are an industry standard in many applications[28,29,30] but also are of interest in scientific research both as a tool and as the subject of research. The short, high intensity pulses allow for study of nonlinear optics and they are the work horse in the study of ultra-fast optics.[28]

Two main types of mode-locked laser that exist are solid state (bulk) mode-locked lasers and optical fibre mode-locked lasers (MLFL). Both have advantages

and disadvantages that make them suitable for different applications. Solid state lasers are constructed out of free space components and the light is directed with mirrors and lenses. These lasers can handle high power as the beam can be spatially broadened to lower intensity where needed. Maintenance is a factor in the continual operation of these lasers, as they periodically require precise re-alignment to operate efficiently. Conversely fibre lasers are not known for producing high power as they are subject to the damage thresholds and nonlinear limitations in optical fibres. Fibre mode-locked lasers do have the advantage of being robust and produce an output beam with good spatial beam quality. Fibre lasers do not require continual alignment to function and long lengths can be wound into a compact appliance. A more thorough discussions of the differences can be found in Paschotta.[31] This thesis is based on fibre lasers and the rest of this chapter introduces the theory specific to those lasers using the optical fibre theory from chapter 2.

4.1.1 Historical background

The mode-locked laser was first demonstrated in 1963.[32] The term arose a year later[33] along with the first experimental example of an active mode-locked laser.[34] The first passive mode-locked laser came in 1965.[35] It wasn't until 1972 that the first stable pulse train was seen.[36]

From 1961, fibre lasers were being developed in conjunction with mode-locked lasers.[37] After 22 years of development the first MLFL was shown in 1983.[38] During the 1980s there were many developments in different types of MLFL, examples being frequency modulated MLFL[39] and amplitude MLFL.[40]

More recently, mode-locked lasers have been produced with interests in extending specific performance limits. For example; a shortest pulse of 28 fs ,[41] highest repetition rate of 160 GHz,[42] and low repetition rates. It is the low repetition rate that is of interest in this thesis and the existing work will be discussed in section 4.7.

4.2 Laser cavities

A laser in its most basic form consists of a repeating path of light that has output components to use the light and a gain component to compensate for losses within the cavity. A cavity will support a number of standing waves around a central frequency ν_0 with a frequency separation of:

$$\Delta\nu = \frac{c}{\int_0^L n(z)\mathrm{d}z}, \tag{4.2.1}$$

where c is speed of light, n is the refractive index at point z in the laser cavity and L is the cavity round trip length.

4.3 Laser gain

The key component of a laser is the gain which arises from stimulated emission. Stimulated emission is one of three main kinds of interaction of a photon with a gain medium which occur from the excitation and de-excitation of electrons in the gain medium; the other two are absorption and spontaneous emission. The wavelengths that can experience gain is finite due to the allowed electron transitions. A laser will have a finite set of longitudinal modes that are both supported by the cavity from equation 4.2.1 and are in the gain spectrum. A representation of this is shown in figure 4.3.1. In this work the gain medium used was an Ytterbium doped silica fibre pumped by a laser diode. The electron transitions used are between the $^2\mathrm{F}_{5/2}$ and $^2\mathrm{F}_{7/2}$ manifolds of the Yb^{3+} ion.[43] The pump and signal wavelengths of the relevant transitions are shown in figure 4.3.2. The gain spectrum also determines the minimum pulse duration achieved by a laser. As a pulse shortens in time it broadens in wavelength. Any pulse components outside the gain spectrum do not get amplified so the pulse duration cannot be reduced beyond that point.

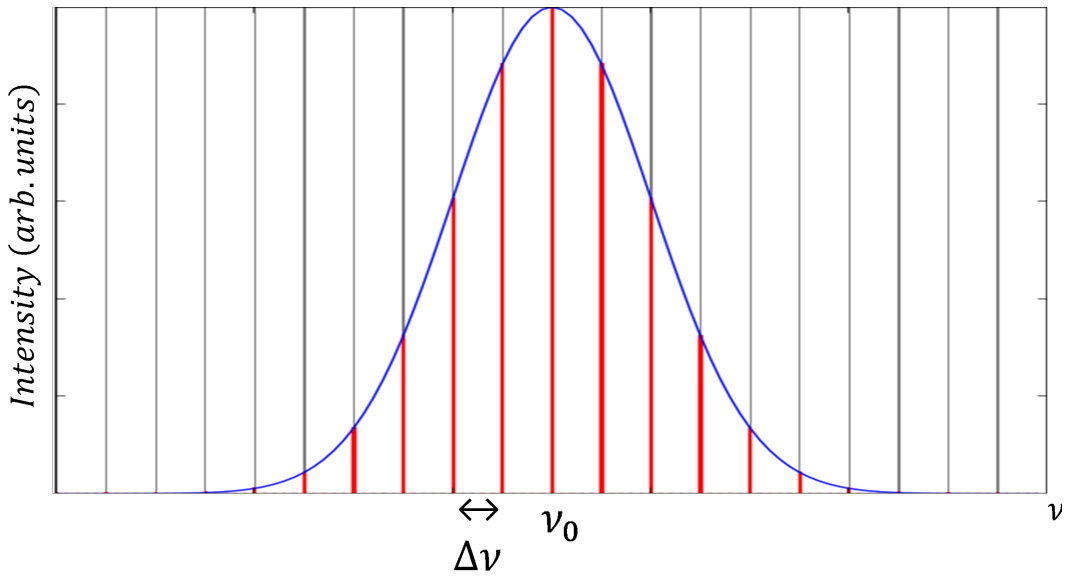

Figure 4.3.1 Illustration of the gain spectrum (blue), the supported cavity modes (grey) and the supported laser modes that can be amplified (red).

4.3.1 Absorption

Absorption is when a photon passes its energy to an electron putting the electron into an excited state. This can act as a loss mechanism to the light as the energy becomes stored by excited electrons in the gain medium. A material can have multiple allowed electron transitions and these transitions are further blurred by local electric or magnetic fields or by interactions with phonons. These give rise to a range of wavelengths that comprise the absorption spectrum.[44] The optical absorption cross-section of the ytterbium doped fibre is shown in figure 4.3.3. The optical cross-section defines the strength of an interaction between light and an ion for a transition corresponding to the wavelength of light. The pump wavelength used in this work is 980 nm which corresponds to the peak absorption of the Ytterbium doped gain fibre.

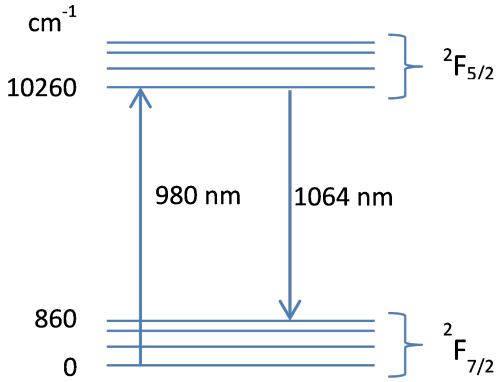

Figure 4.3.2 Energy level diagram showing the $^2F_{5/2}$ and $^2F_{7/2}$ manifolds of Yb^{3+}.

4.3.2 Spontaneous emission

Excited electrons will eventually decay back to a lower energy state and emit a photon of equivalent energy after a period of time known as the upper state lifetime. This process is spontaneous emission. Light emitted from spontaneous emission can be emitted in any direction and be of any wavelength from allowed electron transitions. As with absorption, there is a range of possible emitted wavelengths that comprise the emission cross-section, show in figure 4.3.3. This light is generally incoherent.

4.3.3 Stimulated emission

An optical pump energy can be applied to a gain medium to excite the ions into a higher state. In the presence of gain, amplified spontaneous emission (ASE) is obtained when electrons de-excite and emit a photon at any frequency in the emission spectrum. ASE is produced if a gain medium is pumped without a laser cavity or in cavities at powers below the laser pump threshold. ASE can be useful as an incoherent light source. In this work it was used for alignment of cavity components at low power.

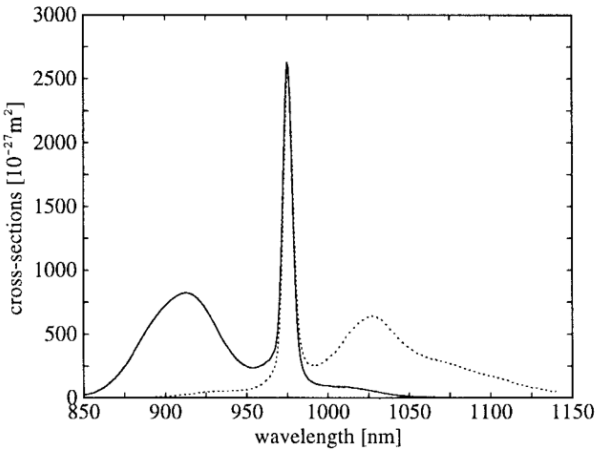

Figure 4.3.3 The absorption (solid) and emission (dotted) spectra of ytterbium doped fibre from Paschotta et. al.[45] The laser transition cross-section quantifies the probability of a photon-electron interaction occurring at that wavelength.

Stimulated emission is the mechanism for laser gain. As a photon passes an excited electron, the electron transitions to a lower energy state emitting a photon of the same frequency, phase and direction as the incident photon. Population inversion is achieved when there are more excited ions than non-excited ions in the gain material. When a cavity has sufficient external pump power to supply gain, the stimulated emission is self sustaining. This is the laser pump threshold. Applying further pump power increases the gain of the laser light and will increase the laser output power proportionally.

4.3.4 Gain saturation

The number of excitable ions in a given volume of gain media is finite. Thus at high enough pump powers, the amount of gain saturates. The saturable gain, g, for a pulsed laser is determined by:

$$g = \frac{g_0}{1 + \frac{E_\mathrm{p}}{E_\mathrm{sat}}} \tag{4.3.1}$$

where g_0 is the small signal gain coefficient, E_{sat} is the saturation energy and E_{p} is the pulse energy. The gain saturation is an important consideration for both numerical modelling and in designing the laser cavities.

Another saturation effect to consider is the pump saturation with length of the gain fibre. As the pump light is absorbed it is attenuated and the level of population inversion decreases with fibre length. At longer lengths of gain fibre the gain will become less efficient. In the absence of any pump light, the gain fibre absorbs the signal wavelength causing additional loss within the laser. Thus, for a given pump power there is an optimum length of gain fibre. The pump power in this work is limited by the maximum output power of the pump diode. The optimum gain fibre length was determined experimentally and is given in the relevant designs in chapters 6 and 7.

4.4 Mode-locking methods

A laser cavity does not have a single operation frequency but rather has many longitudinal modes that fit as standing waves within the cavity as shown in figure 4.3.1. The output of the laser can then be assumed to be the sum of the time, t, dependent electric fields, $E(t)$, of each of the supported modes.

$$E(t) = \sum_{n=-N}^{N} E_{\mathrm{n}} e^{i\phi_{\mathrm{n}} - i\omega_{\mathrm{n}} t}, \tag{4.4.1}$$

where E_{n}, ϕ_{n}, ω_{n} are the amplitude, phase and frequency of the nth mode and N is the total number of supported modes. If the phases of the longitudinal modes can be aligned at a given point then they will constructively interfere to produce a spike in amplitude at that point. This is shown diagrammatically in figure 4.4.1 for four longitudinal modes of a laser. In practice there would be many more longitudinal modes in a laser cavity combining to make a pulse significantly more intense than the equivalent CW operation.

The methods of mode-locking a laser cavity to produce a pulsed output can be

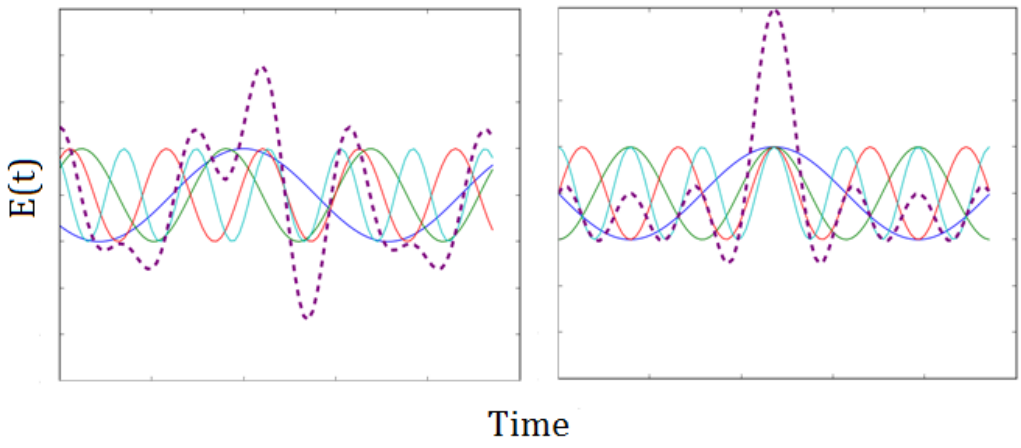

Figure 4.4.1 Diagram of the electric wave of four longitudinal modes of a laser in random phase (left) and when mode-locked (right). The purple dashed line shows the cumulative electric field in each case.

categorised as either active mode-locking or passive mode-locking. Both methods operate by applying a modulation to the amplitude or phase of the light within the laser cavity. This modulation induces a phase relationship between the longitudinal cavity modes and suppress (amplitude modulation) or phase shift (frequency modulation) the modes that are out of phase. Active mode-locking is achieved by direct modulation of the cavity using an electro-optic, acousto-optic or other kind of actively controlled component within the cavity. Passive mode-locking uses a non-linear component that applies modulation in response to the pulse itself without external control, such as a saturable absorber mirror (discussed later in section 4.4.1), Graphene,[46] carbon nanotubes,[47] Kerr lensing[48] or polarisation rotation.[49] The mode-locking method used in this thesis is semiconductor saturable absorber mirrors (SESAMs). These are an industry standard for mode-locking and the behaviour of such devices is reasonably well known.[50]

4.4.1 Saturable absorbers

SESAMs are passive components requiring little alignment and can achieve short pulse durations. The SESAM works on a principle of photon absorption in a semiconductor to provide intensity discrimination. Incident photons are absorbed by electrons and excited from the valence to the conduction band within the material. When the valance band is depleted the SESAM is saturated and incident photons are then reflected. The relaxation of electrons from the conduction band gives the SESAM a temporal response known as the recovery time. The SESAM acts as either a fast or slow saturable absorber depending on whether the recovery time is shorter or longer than the incident pulse duration.

SESAM not only provides mode-locking, parameters of SESAM can define mode-locking threshold, self starting behaviour, power limitations, define minimum pulse duration, pulse break up energy, pulse stability, tolerance of scattering effects, reflections, and noise. They also have an intrinsic loss known as the non-saturable loss that attenuates some of the incident light regardless of the level of saturation.

A saturable absorber can then be described by the change in absorbance, q, with time, t :

$$\frac{dq}{dt} = -\frac{q(t) - \Delta R}{\tau_{\mathrm{A}}} - \frac{P(t)}{E_{\mathrm{sat}}} q, \tag{4.4.2}$$

where ΔR is the modulation depth; τ_{A} is the recovery time; E_{sat} is the saturation energy and P is the incident pulse power.[51,52] To model the SESAM pulse interaction equation 4.4.2 must be solved with the correct conditions.

For fast saturable absorption where τ_{A} is much less than pulse length the absorbance can be modelled as:

$$q(t) = \frac{q_0}{1 + \frac{P}{P_{\mathrm{sat}}}} \tag{4.4.3}$$

where q_0 is the small signal absorbance and $P_{\mathrm{sat}} = E_{\mathrm{sat}}/\tau_{\mathrm{A}}$ is the saturation power.

For slow saturable absorption where τ_A is greater than the pulse length the absorbance becomes dependent on how much of the pulse power is still stored in the

upper states of the SESAM and becomes:

$$q(t) = q_0 \exp -\frac{1}{E_{\text{sat}}} \int_{-\infty}^{\tau} P(t)dt \tag{4.4.4}$$

SESAMs were modelled in this project as part of numerical simulations of the modelocked cavities, typical τ_{A} values for SESAMs used in this project are ≈30 ps. Further discussion of the theory involved and how that translates to the model is discussed in chapter 5.

4.5 Mode-locked laser operating regimes

The behaviour of a mode-locked laser cavity is dependent on the pump energy being supplied to the cavity. Going through from low to high pump power the laser will go through; ASE operation, CW operation, Q-switched mode-locking, fundamental mode-locking and finally multi-pulsed at high pump powers. The fundamental mode-locking regime is the region of interest in this work as this is the case when a single pulse is existent in the laser cavity. The range of cavity powers where fundamental mode-locking exists is defined by the mode-locking threshold and the multi-pulse threshold so these will be discussed further.

4.5.1 Q-Switched mode-locking

Q-switched lasers are a type of pulsed laser which is independent of mode-locked lasers. Q-switched lasers work on the principle of controlling the cavity net loss (or Q factor). The cavity loss is increased via a shutter or optical switch to prevent lasing in the cavity while continually pumping the gain medium. Reducing the cavity loss, i.e. opening the shutter, releases the energy stored in the gain medium as a single energetic optical pulse. Pulses from a Q-switch laser are typically nanoseconds in pulse duration and low pulse repetition rates defined by the speed of the shutter within the cavity.

In mode-locked lasers the net cavity loss is dependent on the intensity of the

pulses within the cavity due to the imposed saturable absorption as described previously. This variation in net cavity loss can result in Q-switched mode-locking. This typically manifests as a modulation on the pulse peak power. This can be either unstable, with the pulse peak power changing seemingly randomly from pulse to pulse, or it can form a stable modulation with the peak power varying in a roughly sinusoidal pattern repeating every few nanoseconds.

Q-switched mode-locking is normally unwanted behaviour and careful cavity design can minimise it. It tends to happen at lower cavity powers close to the mode-locking threshold which effectively increases the minimum cavity power where the mode-locked laser is practically useful. Q-switched free mode-locking can be achieved when the pulse energy E_p satisfies:[53]

$$E_p^2 > E_{gain,sat} E_{abs,sat} \Delta R, \tag{4.5.1}$$

where $E_{\mathrm{gain,sat}}$ is the saturation energy of the gain medium, $E_{\mathrm{abs,sat}}$ is the saturation energy of the saturable absorber and ΔR is the modulation depth of the saturable absorber. The pulse energy can be defined in terms of the average cavity power, P_{av}, and the pulse repetition rate, ν_{rep}, or the effective cavity round trip length, L with the refractive index at distance z through the cavity, $n(z)$:

$$E_{\mathrm{p}} = \frac{P_{\mathrm{av}}}{\nu_{\mathrm{rep}}} = \frac{P_{\mathrm{av}} \int_0^L n(z)\mathrm{d}z}{c}. \tag{4.5.2}$$

From this the minimum average cavity power that produces Q-switch free mode-locking can be determined. It also scales with cavity length, such that in longer cavities a lower average power is needed to produce Q-switch mode-locking. This is advantageous for designing a long cavity with fundamental mode-locked pulses.

4.5.2 Multi-pulsed mode-locking

At high pump or cavity powers, each pulse can break up into multiple pulses co-propagating through the laser cavity. This break up occurs when a pulse accumulates

a large nonlinear phase shift as it propagates through the cavity. This is the nonlinear phase shift induced by self-phase modulation as discussed in section 2.6. The affect of this phase shift depends on the dispersion regime the pulse is propagating through. In the anomalous dispersion regime the dispersion can compensate for the phase shift and soliton propagation is possible allowing cavities of long lengths to be made. However, in the normal dispersion regime the dispersion does not compensate for the phase shift and the pulse will break up when the accumulated phase shift in one round trip reaches π.[54] The nonlinear phase shift, ϕ_{NL} per round trip in the fundamental mode-locking region of operation is:

$$\phi_{\mathrm{NL}} = \gamma P_0 L_{\mathrm{eff}} < \pi. \tag{4.5.3}$$

This is also length dependent so this multi-pulsing threshold will decrease with increased cavity length. This limits the performance of the laser at long cavity lengths. Increasing the multi-pulsing threshold was the main focus of the work in chapters 6 and 7 allowing longer cavities to be constructed without the pulse accumulating excessive nonlinear phase shift. A means to do this is to decrease the nonlinear coefficient γ. Methods for this include increasing the mode area in the fibre and reducing the nonlinear refractive index n_2, which are discussed in chapters 6 and 7 respectively.

A mode-locked laser operating in the multi-pulse regime usually operates either in bunched pulse mode-locking or harmonic mode-locking. Bunched pulse mode-locking (sometimes referred to as burst pulse mode-locking) where many pulses propagate through the cavity in a cluster and stay very close in time. The pulse separation in bunched pulse mode-locking can be unstable and drift with time. The pulses in this regime can also be temporally close and appear as a single broader pulse. This is usually identifiable by an interference pattern being produced in the pulse spectra. Such patterns are shown in chapter 6 and 7. Harmonic mode-locking is where each pulse is equally separated in time, this is the regime used for work in increasing the repetition rate of mode-locked lasers. Increasing cavities power

significantly higher than the multi-pulse threshold can cause further pulse break up leading to a higher harmonic with many pulses equally spaced in time propagating around the laser cavity.

4.6 Mode-locked laser pulse characteristics

A soliton or a self-similar soliton will have a sech^2 pulse shape as a solution to the nonlinear Schödinger equation discussed in section 2.7. A soliton can be identified from the measured shape of the temporal envelope and the pulse spectrum. In fibre lasers, solitons also exhibit characteristic Kelly side bands.[55] As a pulse interacts with the discrete components of a laser cavity it experiences discrete changes in dispersion, loss or gain. At these points the pulse sheds energy in the form of a dispersive wave to reach stable soliton parameters again. The phase matching of the co-propagating dispersive wave with parts of the main pulse result in sharp spikes in the pulse spectrum appearing symmetrically either side of the main peak as shown in figure 4.6.1. Kelly side bands are an indication of soliton like behaviour.

Another factor to consider when characterising a pulse is the time-bandwidth product. This indicates if a pulse has any chirp. An ideal output pulse for this work is chirp-free, also known as transform limited. This means that the time-bandwidth product will be at a minimum for the pulse shape. A sech^2 soliton will have a time-bandwidth product of 0.315 for a transform limited pulse measured at the FWHM.

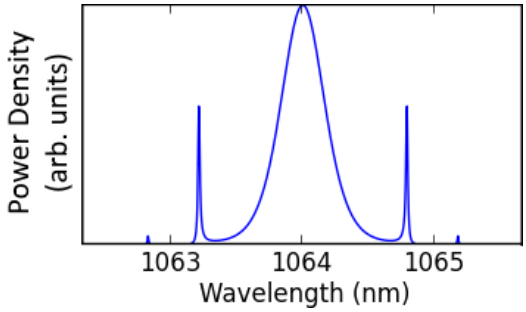

Figure 4.6.1 Example spectrum of a numerically simulated mode-locked laser cavity showing first and second order Kelly side bands.

4.7 Low repetition mode-locked lasers

The main focus of the mode-locked laser work in this thesis is in pushing the limits of low pulse repetition rates. This is accomplished by increasing the laser cavity length and thus increasing the round trip time of the pulse within a cavity. This means each pulse has a higher pulse energy for the same average pump power. This is useful for applications that want high peak power or pulse energy but low average power such as micro-machining or supercontinuum generation.[28] A low repetition rate pulse can also result in high pulse energy for a given amplification energy as the applied energy will be split between fewer pulses.

Current methods of achieving low repetition rate typically involve using a pulse-picker which uses precisely controlled opto-electronics to select specific pulses and filter out unwanted pulses. Pulse pickers are generally expensive and also require more amplification stages to reach the same output power as energy is being thrown away in the pulses that are filtered out.

The challenge of creating a low repetition rate mode-locked laser is to ensure the fundamental mode-locking regime is possible for a given cavity length. The cavity average power range that corresponds to the fundamental mode-locking regime is defined by a range of average cavity powers between the mode-locking threshold, P_{min}, and the multi-pulsing threshold, P_{max} as discussed in the previous section.

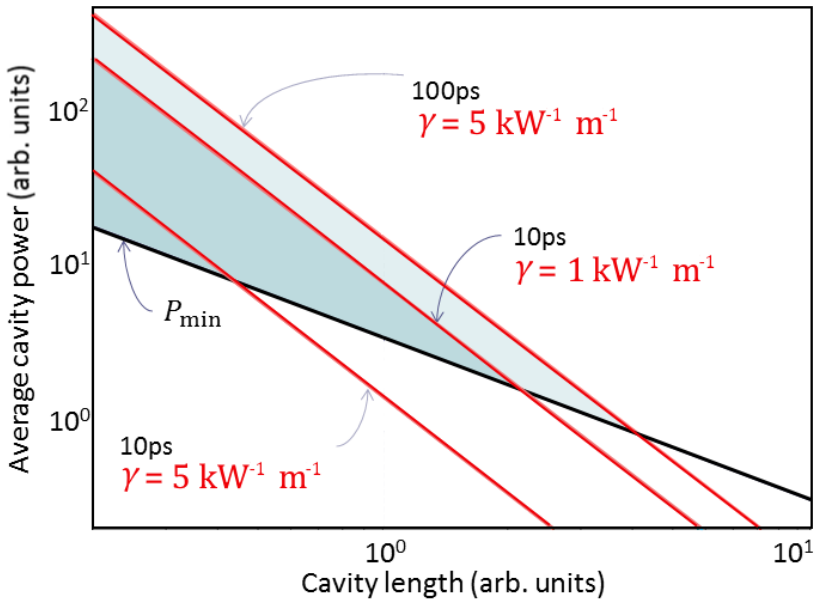

Figure 4.7.1 An illustration of the fundamental mode-locking range (blue area) enclosed between the black and red lines. The black P_{min} line is the minimum average power needed for mode-locking as a function of laser cavity length, above this line the cavity will produce mode-locked pulses. The red lines are upper average power limit, P_{max}, given for three different combinations of pulse duration and γ, above these lines a cavity will operate in a multi-pulsed regime.

Both of these thresholds decrease with increasing cavity length and converge at long cavity lengths. At cavity lengths longer than the thresholds convergence, the laser will operate in a multi-pulsed regime at all powers above the mode-locking threshold and no fundamental mode-locking can be achieved. In figure 4.7.1, P_{max} converges with the lower limit P_{min} showing the limitation of cavity length on the fundamental mode-locking regime. The cavity length where the lower and upper limits converge can be controlled to a certain extend by using different pulse durations or values of γ. A laser with a long cavity length and fundamental mode-locking operation requires a longer pulse duration or a smaller nonlinear coefficient γ.

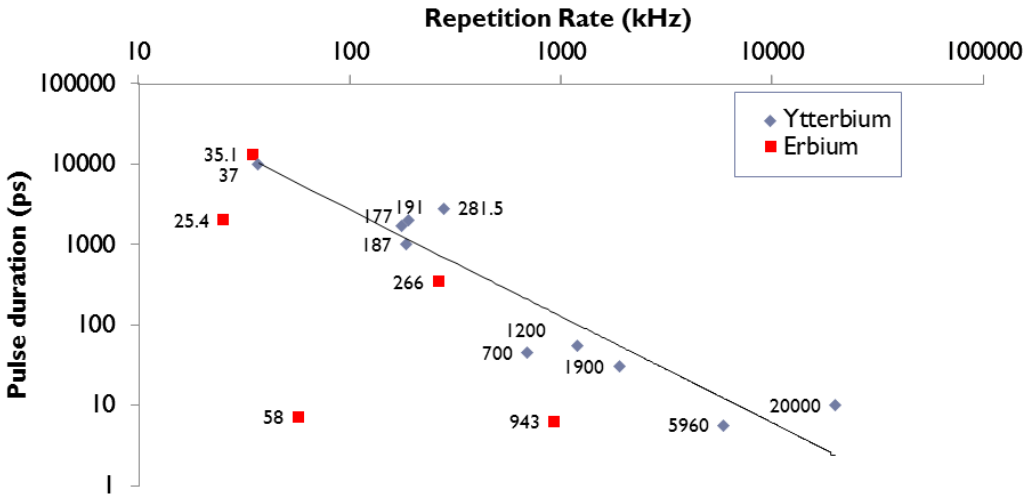

Figure 4.7.2 Review of reported low repetition mode-locked lasers for ytterbium based lasers operating at ≈1 µm and erbium based lasers operating at ≈1.5 µm. The numbers are the quoted repetition rate in kHz. The references for each repetition rate are: Yb: [37][56] ; [177][57] ; [187][58] ; [191][59] ; [217.4][60] ; [281.5][61] ; [700/1900][62] ; [1200][63] ; [948][64] ; [5960][65] ; [2000] Commercial Laser (Fianium) Er: - [25.4][66] ; [35.1][67] ; [58][68] ; [266][69] ; [943][70]

4.7.1 Existing mode-locked lasers

A summary of achieved low repetition rates is shown in figure 4.7.2. Two types of mode-locked lasers are shown in figure 4.7.2; erbium and ytterbium based lasers. Erbium based lasers characteristically work at 1.5 µm which is in the anomalous dispersion regime of silica and ytterbium based lasers which operate at 1 µm and is in the normal dispersion regime of silica. Erbium based lasers can use the anomalous dispersion to propagate over long lengths as shown by the lack of correlation between the repetition rates achieved and the pulse duration. However, for ytterbium based lasers they are constricted by the π limit on the nonlinear phase shift. As this is a nonlinear effect dependent on peak power, P_0 in equation 4.5.3, this limits the repetition rate achieved for a given pulse width. A longer pulse has a lower peak power and can reach a longer cavity length before breaking up. This explains the

correlation seen in the ytterbium based laser points in figure 4.7.2. The work in chapters 6 and 7 in this thesis tries to break away from this correlation by control of the cavity nonlinearity. The area of interest is using a pulse that is less than 10 ps and moving to 5 MHz or below.

4.7.2 Self starting

The creation of an initial mode-locked pulse in a laser cavity is a probabilistic occurrence reliant on background noise. Once a random spike in background noise occurs, this is then amplified and reinforced by the saturable absorber and becomes the main pulse propagating through the cavity. The parameters of the laser govern how likely a sufficiently random spike will occur and lead to a property known as self starting. If a mode-locked laser always produces a pulse when is it switched on it is referred to as self starting. Not all have this property and sometimes external intervention is required to induce the initial spike in background CW light. This can happen by physically perturbing the fibre to modulate the attenuation in it, by starting the laser at a higher pump power and reducing it to the desired level or by inducing a Q-switch pulse by either blocking and unblocking the laser cavity or switching it off and on again.

4.8 Relevant cavity components

A mode-locked fibre laser consists of a gain medium, output coupler and mode-locking element connected by optical fibres in its most basic form. However, other components can be used to achieve different laser parameters and designs. This section discusses the components used in the lasers built for this thesis.

Laser diodes - the gain fibre in this work is pumped optically using a CW laser diode at 980 nm . These are electronically powered and controlled. Laser diodes consist of a small laser cavity that use semi-conductor materials that can be electronically pumped to create population inversion. Laser diode power can be fine controlled by controlling the applied current. The laser diodes used in this work

operated at few hundred milliwatts to provide the pump power to the gain fibre.

Wavelength Division Multiplexers (WDMs) - The pump light is coupled into the laser cavity fibre by means of a wavelength division multiplexer (WDM). These components direct different wavelengths of light through different optical fibre pigtails. This allows for 980 nm to be directed into the cavity without 1064 nm light being directed back toward the pump laser diode.

Isolators - A useful component is a fibre coupled optical isolator which allows light to travel in one direction through it but not in the reverse direction. This is useful to protect sensitive components from damage and to minimise reflections back into the cavity. Individual isolators operate for a finite bandwidth so different isolators may be required in different parts of the cavity to block specific wavelengths where needed.

Circulators - Circulators direct light between specific fibre optical pigtails. Unlike WDMs which operate on different wavelengths, circulators typically work for a narrow bandwidth. The circulator will typically have many ports and are designed to take input light from one port and transmit it to the next port in the series while preventing light from travelling back to the previous port in the series. These devices were used to incorporate reflective components into a ring cavity as shown in the laser cavity designs in chapters 6 and 7.

Chirped fibre Bragg grating (CFBG) - A CFBG is used as an output coupler in this work. The design of the CFBG can control how much light is coupled out of the cavity and how much is reflected back in. These operate on the principle of a Bragg grating which uses a periodic fluctuation in refractive index designed to reflect a desired amount of light a particular wavelength. The bandwidth of fibre Bragg gratings is usually small with the ones used in this work having a bandwidth of a few nanometers. The properties of a Bragg grating can reflect light but the grating can also be designed to apply a chirp. The chirp in this case is a gradual variation in the spacing between the periodic fluctuations of the refractive index in the fibre. This means different wavelengths will be reflected at different points within the grating.

This has the effect of applying a chirp to the reflected pulse of light. This design allows for more control over the dispersion applied to a pulse within a laser cavity. In this case it applies a large amount of anomalous dispersion to the pulse (of the order of tens of $\mathrm{ps}\,/\,\mathrm{nm}$). This will give the cavity a net anomalous dispersion and create a self-similar soliton in the laser cavity. The anomalous dispersion applied by the CFBG is much larger than the total dispersion in the rest of the cavity so the CFBG defines the pulse duration within the cavity.

Chapter 5

Numerical Modelling

5.1 Introduction

Numerical simulations have been a useful tool in the majority of experiments conducted in this thesis. The designs of mode-locked fibre lasers used in chapters 6 and 7 were tested and optimised with numerical simulations before construction. The nonlinear effects studied in chapter 8 were also tested and compared to numerical simulations.

Although commercial packages, such as Fiberdesk, exist for modelling pulse propagation it was useful to develop code in house to have greater flexibility with the simulation parameters and develop an understanding of the underlining physics.

The numerical simulations constructed are based on the split-step Fourier method (SSFM) to model a pulse propagating through an optical fibre. This is covered in section 5.2. The pulse interaction with discrete cavity components, such as a SESAM, is modelled with the relevant transformations and these are covered in section 5.3. The complete numerical model simulates a pulse propagating through a virtual laser cavity composed of lengths of sequential fibre and cavity components. The pulse was repeatedly propagated through the virtual cavity as necessary.

The simulation results were compared to measurements of known mode-locked lasers to test the validity of the code. This is covered in section 5.4. The pulse

output from a mode-locked laser may be identical from pulse to pulse but that does not give information of how much the pulse changes as it propagates through a round trip of the cavity. Having large amount of loss or dispersion in discrete components can distort a pulse heavily and can impact the over all stability of the laser. This variation is difficult to measure experimentally in a laser but analysis through numerical modelling can give information on this. This is covered in section 5.5.

5.2 Split-step Fourier Method

A pulse propagating through a fibre is governed by the non-linear Schrödinger equation (NLSE) discussed in chapter 2. Analytical solutions to the NLSE are rare and numerical solutions are used for situations where the analytical solution is not applicable. The pulse is subject to dispersion and nonlinear effects, which are both counter dependent. The dispersion effects the pulse duration and is based on the spectral width while the nonlinearity effects the spectral width and is based on the pulse duration via peak power. To simulate this, it is not accurate to apply them separately for the whole fibre length. The SSFM works by separating the nonlinearity and dispersion and alternately applying them to small segments of fibre. With a small enough step size the SSFM can then be approximated to a continuous application of nonlinearity and dispersion.

This method is derived from expressing the NLSE in the form normalised to the pulse duration T_0, fibre dispersion length, $L_D = T_0/|\beta_2|$, and peak power, P_0 :[9]

$$i\frac{\partial U}{\partial \xi} = sign(\beta_2)\frac{1}{2}\frac{\partial^2 U}{\partial \tau^2} - N^2|U|^2U, \tag{5.2.1}$$

where $U = A\sqrt{P_0}$ is the electric field normalised to the peak power, $\xi = z/L_D$ is the propagation distance normalised to the second order dispersion length of the fibre, β_2 and β_3 are the group velocity dispersion and third order dispersion respectively, N is the soliton order that was given in equation 2.7.3, $\tau = T/T_0$ and $\text{sign}(\beta_2) = \beta_2/|\beta_2|$. The dispersive and nonlinear parts of the equation can then be

separated out into operators on the normalised electric field U:

$$\frac{\partial U}{\partial \xi} = \left(\hat{D} + \hat{N}\right) U, \tag{5.2.2}$$

where the operators $\hat{D}$ and $\hat{N}$ are the dispersion and nonlinear operators respectively given by:

$$\hat{D} = \frac{i}{2}\left(\text{sign}(\beta_2)\omega^2 + \frac{1}{3}\beta_3\omega^3\right)$$
$$\hat{N} = iN^2$$

where ω is the frequency in the Fourier domain. These operators are then applied to the field profile alternately as:

$$U\left(L,T\right) \approx e^{-\frac{1}{2}h\hat{N}}\left(\prod_{m=1}^{M} e^{h\hat{N}}e^{h\hat{D}}\right)e^{\frac{1}{2}h\hat{N}}U\left(0,T\right), \tag{5.2.3}$$

where L is the length of fibre and h is the step size being evaluated. The nonlinearity and dispersion are applied in the temporal and spectral domains respectively. To take this into account, the pulse profile undergoes a Fourier transform between applying nonlinearity and dispersion, thus earning the name split-step Fourier method.

The SSFM has a trade off where a small step size increases the accuracy of the simulation but at the cost of simulation time. There is some trial and error in finding a sufficiently small step size which is done by running identical simulations with an increasingly smaller step size until a negligible difference is found.

5.3 Code overview

The numerical simulation was based on creating a normalised electric field, $U(z,t)$, with a sufficiently large but finite temporal window and array resolution. This field was then manipulated as needed by the SSFM in the optical fibres or by the corresponding laser cavity component model. The main laser cavity components

used in the simulations are SESAMs, chirped fibre Bragg gratings, passive optical fibre, and optical gain. These components were introduced in chapter 4 and the simulation of these is discussed here.

5.3.1 SESAM

There are multiple ways to model the effect of a SESAM on an electric field. These are known as fast or slow saturable absorption which depend on whether the pulse duration is longer or shorter than the SESAM recovery time respectively as discussed in section 4.4.1. The pulse durations considered in this work were between 4 ps and 50 ps . The SESAMs used had a specified recovery time of 30 ps so both regimes of saturable absorption were developed in the code. The differences between these regimes was tested for all the applicable pulse durations and found that the fast saturable absorption model provided adequate results compared to the slow saturable absorption model even for the short 4 ps pulses simulated. The fast saturable absorption has the advantage of being computationally faster so became the default simulation method.

5.3.2 Chirped fibre Bragg grating

The chirped fibre Bragg grating transmits a proportion of the light out of the cavity in addition to applying a dispersion to the pulse. The loss is modelled as an output coupler and reduced the electric field amplitude by the relevant amount. The dispersion is modelled in the spectral domain as an instantaneous dispersion:

$$U = \mathcal{F}(\mathcal{F}^{-1}(U).e^{\frac{i}{2}\beta_2\omega^2}), \tag{5.3.1}$$

where β_2 is the group velocity dispersion applied by the CFBG and ω is angular frequency. This is applied in the same manner as dispersion in the SSFM but can be considered to be instantaneous and applied in a single calculation. As the application of the CFBG dispersion is separate to the SSFM and applied in a single step it is

not necessary to normalise with respect to dispersion length for this component.

5.3.3 Fibre gain

The gain calculations are incorporated into the split-step Fourier method by adding a proportion of the gain in each unit step, δz:

$$U(z+\delta z,t) = U(z,t)\sqrt{e^{g.\delta z}}, \tag{5.3.2}$$

where g is the gain coefficient. This coefficient is subject to saturation effects as described in section 4.2. The saturated gain is calculated from the small signal gain coefficient, g_0, the saturation energy of the gain fibre, E_{sat}, and pulse energy, E_{p}:

$$g = \frac{g_0}{1+\frac{E_{\text{p}}}{E_{\text{sat}}}}. \tag{5.3.3}$$

The gain is calculated by entering a value for g_0 in the code along with the saturation energy E_{sat}. The variable g_0 is the variable used to control the cavity power and is adjusted to simulate the cavity at different pump power and to produce pulse energies equivalent to physical cavities as needed.

Typical parameters used for the respective cavity components in the simulations are shown in table 5.1. A passive extension fibre is the fibre under test in each experiment. The simulation starts with an input electric field, U, of either noise or a predefined pulse. The electric field is then transformed by the function for a component in the laser cavity and passed to the next cavity component. This simulates the pulse propagating through a laser cavity. The entire cavity loop is repeated until a steady state solution is found when the pulse has negligible change at each encounter with the output coupler over many loops through the cavity.

The simulations can be started from noise or from a specified pulse and successive loops will eventually converge on the stable solution. The convergence time is quicker for an input pulse that is similar to the steady state solution though starting from noise can give a rough indication of how easily a set up will self start.

Simulation Parameters	Temporal array size	1024-4096
	Half-pulse interval	100-1000 ps
Output Coupler	Loss	60%
CFBG	Dispersion	10 or 40 $\mathrm{ps\,nm^{-1}\,km^{-1}}$
SESAM	Saturation Fluence	$90\,\mu\mathrm{J/cm^2}$
	Saturable absorption	0.3
	Non-saturable absorption	0.1
	Spot diameter	10 - 20 µm
	Temporal response	30 ps
	Modulation depth	0.2
Gain fibre	Length	0.3 - 0.7 cm
	Dispersion	17 $\mathrm{ps\,nm^{-1}\,km^{-1}}$
	MFD	6 µm
	n_2	$3.2e-20\mathrm{m^2/W}$
	Gain	140 ± 25 $\mathrm{dB\,m^{-1}}$
	Gain saturation	5 - 10 pJ

Table 5.1 Typical component parameters used in simulations. The parameters of the extension fibres are given in the relevant sections.

The numerical model covers the nonlinear and dispersive effects covered in the NLSE shown in section 2.7.1 to third order dispersion and can incorporate the relevant cavity components. However, this numerical model does not cover the spatial intricacies of modes or polarisation dependent effects such as polarisation dependent loss through polarisers. It is also an idealised version of a laser and was not subject to environmental conditions like temperature fluctuations. Overall, the simulations are designed to give an idea of whether a cavity would produce stable pulses and the range of cavity powers where fundamental mode-locking occurs but it does not predict how stable a cavity will be or how well it will self start.

5.4 Testing simulations

The code for each component of the laser cavity simulations was tested in comparison to existing pulse propagation software Fiberdesk. The entire simulation code was tested by comparing the stable solutions produced to measurements of existing

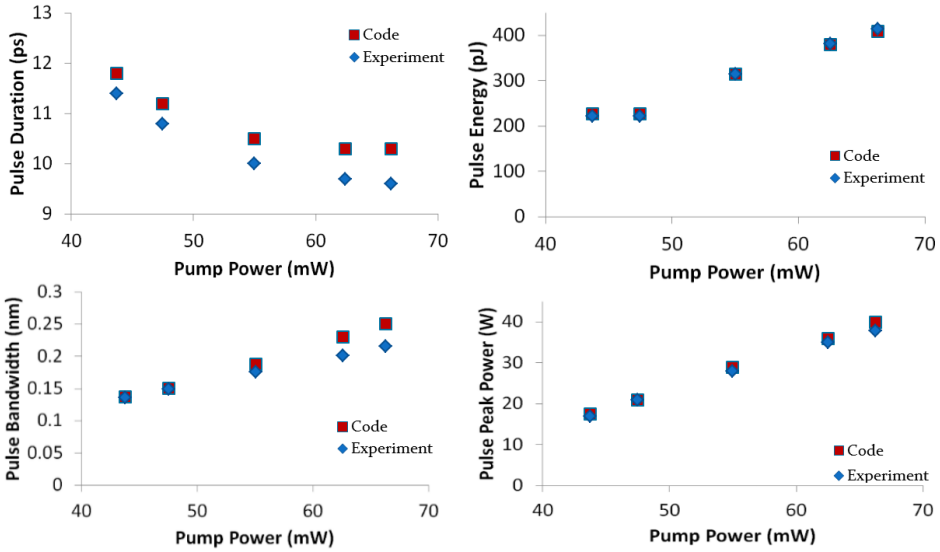

Figure 5.4.1 Comparison of simulation output with measured Fianium cavities for different pulse energies. The code was set up to get a pulse energy as close to the measured value as possible then the other parameters were compared.

mode-locked fibre lasers. Figure 5.4.1 show comparisons of measured pulse parameters of a known Fianium laser with the output pulse parameters of the same laser simulated with this code. Overall the code showed reliably good correlation with in existing laser cavity and was repeatable for different pulse durations and repetition rates.

5.5 Pulse variation within the cavity

The pulse variation through a cavity round trip is not something easily measured but can be shown in numerical simulations. Figure 5.5.1 shows the pulse at each stage through simple linear mode-locked laser cavity consisting of a gain fibre and passive delay fibre bound between a CFBG and a SESAM as used in chapter 6. The pulse is expected to broaden at the CFBG, as anomalous dispersion is applied to it, and to narrow at the SESAM. This is what is found in this set but with only a 4% fluctuation in pulse duration around the whole cavity. The same was found for this

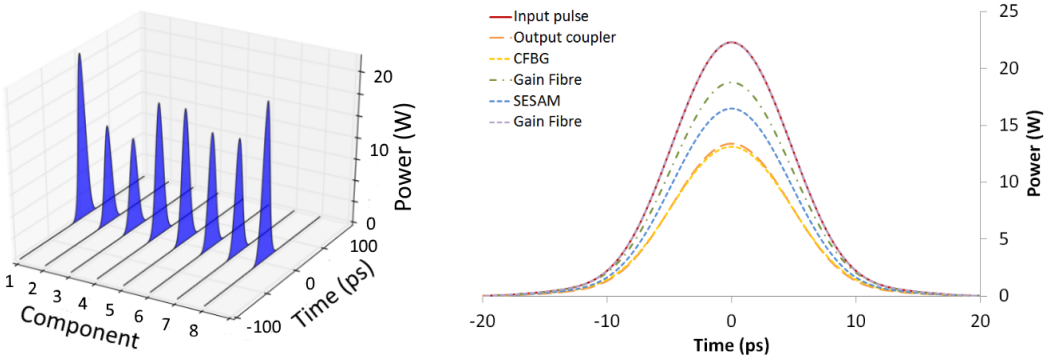

Figure 5.5.1 Temporal pulse as it travels through one loop of the cavity shown after each component in one cavity round trip. The measured pulse duration varied by approximately 4%.

laser cavity set up with different lengths of delay fibre assuming negligible dispersion in the delay fibre. Little change of the pulse parameters during propagation of the pulse through the cavity indicated stable, quasi-soliton behaviour.

5.6 Applicability of the simulation

The simulations described here provide good comparison to well known laser systems. In practice there are many unknowns within an experimental laser cavity, for example, the precise polarisation evolution through non-PM fibre or fluctuations in SESAM temporal response from manufacturing methods. This can cause difference in values such as mode-locking threshold which is usually lower in an idealised simulation which is not subject to temperature, polarisation or power fluctuations of a real world scenario. The simulations were useful in designing laser cavities and would give an indication of whether a laser cavity would mode-lock and the ideal pulse produced by such a cavity. This provided a useful starting point to an experiment even if the precise values differed from the experimental laser cavity results given in chapters 6 and 7. The simulations were proved useful for modelling a single pass through a fibre and provided a good comparison for the gas filled hollow core fibre results given in chapter 8.

5.7 Conclusion

This chapter has outlined the numerical tools used in this thesis for designing and analysing mode-locked laser cavities. The numerical model was tested in comparison with existing mode-locked fibre lasers and found good agreement. The numerical model was then used to confirm the expected existence of fundamental mode-locking in the cavities tested in chapter 6 and 7. The accuracy of the predictions by this numerical model did not cover modal or polarisation effects within a cavity so gave a more qualitative reference of laser performance when compared to lasers with strong polarisation dependent effects.

The same numerical model covered nonlinear and dispersive effects within a fibre and was used to quantify the effects of a pulse in a single pass of gas filled hollow core fibre that were studied in chapter 8.

Chapter 6

Mode-locked fibre laser with large mode area fibre

6.1 Introduction

This chapter covers the work conducted utilising large mode area (LMA) fibres as a means to reduce the pulse repetition rate of a mode-locked fibre laser. The sections in this chapter cover the motivation behind this work in the introduction. The fibres used are covered in section 6.1.1. The laser cavity design used is covered section 6.2. The representative results found with these lasers cavities are presented in section 6.3 before concluding with a discussion of this work and possible future directions for this work.

As discussed in section 4.7, the main limitation on low repetition rate is the nonlinear phase shift accumulated per round trip which increases with cavity length. To reach longer length cavities, the nonlinearity can be reduced to minimise the nonlinear phase shift. This chapter focuses on increasing the mode area of the delay fibre within the laser cavity to reduce the intensity and thus the nonlinear response of the fibre as discussed in chapter 2. The nonlinear coefficient is given by:

$$\gamma = \frac{2\pi n_2}{\lambda A_{eff}} \tag{6.1.1}$$

where n_2 is the nonlinear refractive index, λ is the light wavelength and A_{eff} is the effective mode area within the fibre. From this, increasing the effective mode area A_{eff} will reduce γ.

However there are draw backs to increasing the mode area. For step index fibres, increasing the mode size can be accomplished by increasing the core size. A larger core will support multiple spatial modes as discussed in section 2.3.1. Having multiple modes propagating through the cavity is disadvantageous as the presence of higher order modes disrupts mode-locking as each mode will have its own propagation constant and travel at different speeds through the cavity. The other disadvantage is that higher order modes will experience different losses compared to the fundamental mode and may be attenuated by single mode fibre pigtails or other cavity components designed to operate with the fundamental mode. This acts as a loss mechanism and increases the total cavity losses which also adversely affect the laser performance.

Some precautions can be made to minimise the excitation of higher order modes in the multi mode fibres. This can be done by tapering the regions on either end of the LMA section of fibre. With a gradual change in diameter along the fibre length the transition is adiabatic. Higher order modes can also be excited in a multi-mode fibre if there is a discontinuity such as a splice or a bend that would transfer energy to the higher order mode. As such care needs to be taken not to tightly wind the fibre and ensure any splices in the LMA sections are of sufficiently high quality.

6.1.1 LMA tapered fibre

The tapered fibre fabricated for this project had a core diameter of 20 µm at the widest part. The tapered ends were created during fibre fabrication by adjusting the draw speed of the fibre as is exits the furnace. This results in relatively long taper lengths. The LMA fibre was tapered down to a mode field diameter of 6 µm at each end to allow for splicing to the laser cavity. The taper and thin section of the tower tapers was approximately 5 m in length on each side.

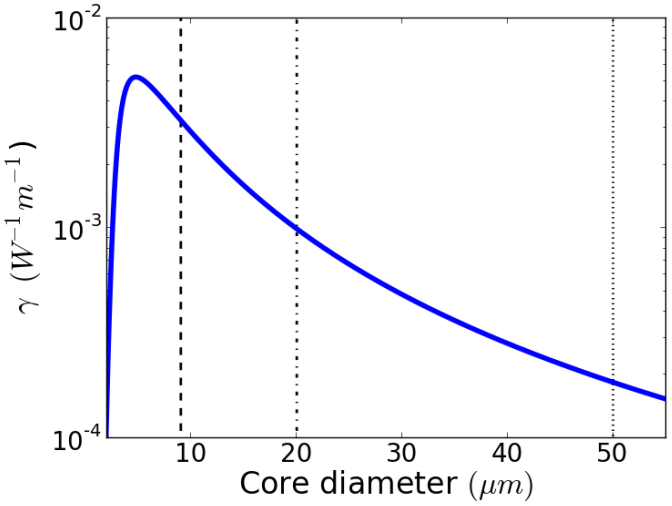

Figure 6.1.1 The calculated nonlinear coefficient for a fibre with an NA of 0.14 and n_2 of $2.6 \times 10^{-20}\,\mathrm{m}^2/\mathrm{W}$ for 1064 nm. The calculation used equation 6.1.1 and the Marcuse equation to calculate the effective mode area.[71]

The calculated nonlinear coefficients are shown in figure 6.1.1 which shows the nonlinear coefficient γ is reduced for the 20 µm core fibre compared to the 9 µm core fibre. This used the calculated mode field diameters for a step index fibre with a numerical aperture (NA) of 0.14 and a nonlinear coefficient (n_2) of $2.6\times10^{-20}\,\mathrm{m}^2/\mathrm{W}$ at a wavelength of 1064 nm. Two lengths of LMA were used in these experiments of 10 m and 20 m, the length of the tapered regions of the fibre were in addition to these lengths.

6.2 Laser cavity design

The laser cavity used for this work was of a linear cavity design. The advantages of this design is the double pass of the delay fibre and the gain fibre. The double pass of the delay fibre allows for a lower repetition rate to be achieved compared to a single pass of the extension fibre. Double pass of the gain allows for more efficient amplification of the pulse.

A diagram of the cavity design used is shown in figure 6.2.1. The cavity is defined by the reflective SESAM and CFBG. The spot size on the SESAM is defined by the mode area of the butt coupled commercially available fibre (SMF28). The SMF28 is spliced to a delay fibre, the length of which is used to control the cavity length and thus the repetition rate. The delay fibre is the fibre under test and exchanged with different lengths of fabricated fibre. The delay fibre is connected to the gain fibre via a passive fibre pigtail with a 6 µm mode field diameter. 65 cm of gain fibre was used (CorActive YB 401), the length of which was determined through simulation and experimental tests.

The CFBG transmitted 60% and reflected 40%. The CFBG applied approximately 10 ps / nm chirp to the reflected pulse, which dominates the cavity dispersion as the fibre dispersion is small in comparison, this defines the pulse duration as approximately 4 ps . A wavelength division multiplexer (WDM) couples the 980 nm pump light to the cavity fibre. The output isolator prevents reflections from entering the cavity and provides a monitoring tap of 5% of the output light. All of the cavity pigtails are 6 µm mode field diameter non-polarisation maintaining step index fibre. The isolator is polarisation sensitive so a polarisation controller was used to align the polarisation out of the cavity to the highest transmission through the isolator. The entire cavity was kept on a temperature controlled cooling plate to stabilise the polarisation state within the cavity.

The monitoring tap is connected to a photo diode and oscilloscope to monitor the pulse train. An oscilloscope does not have a fast enough response to display a 4 ps pulse but does show the stability of the pulse train and clearly shows harmonic multi-pulsing behaviour. The main output was connected to an optical spectrum analyser (OSA) to record the pulse spectra or to an autocorrelator to measure the temporal duration as needed. An amplifier was introduced after the laser output to provide enough signal for a clear autocorrelation consisting of a 60 cm section of ytterbium doped fibre pumped by another 980 nm laser diode. This was only used for autocorrelation measurements and was confirmed to not alter the pulse duration.

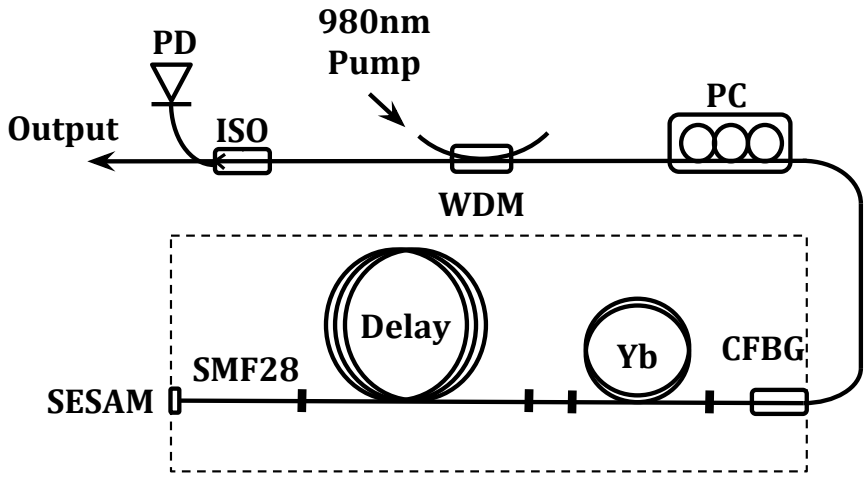

Figure 6.2.1 Diagram of laser for testing LMA fibre, the laser oscillator is in the dashed rectangle. The SESAM is connected through SMF28 spliced to the delay fibre. SMF28 is spliced to the delay fibre. The delay fibre is connected to the the gain fibre (Yb) via a fibre pigtail. The CFBG acts as the output coupler and applied dispersion. The output is controlled by a polarisation controller (PC). The pump light is coupled to the cavity through a WDM. An isolator (ISO) is used to prevent reflections returning to the cavity with a tap to a monitor photo diode (PD).

6.3 Experimental results

6.3.1 Reference cavity

A laser cavity was constructed similar to operational lasers produced by Fianium ltd. to provide a known starting point. This was a reference cavity with 3.5 m delay fibre with a 9 µm core diameter. The total cavity length was 5 m corresponding to 10 m round trip distance for double pass.

The reference cavity had a pulse repetition rate of 20 MHz . Figure 6.3.1 shows the spectrum for different pump power in the fundamental and multi-pulsed mode-locking region. The cavity starts mode-locking with a pump power of 39 mW measured after the WDM. This pulse shows Kelly side bands indicating soliton like behaviour.

As the pump power is increased the pulse spectrally broadens and the amplitude of the Kelly side bands increases. The broadening continues with pump power until 53 mW . At this power the pulse breaks up and the spectrum narrows again. Some interference fringes can be seen on the spectrum at this power as the two pulses interfere. At higher powers, the spectrum looks similar to a single soliton in the fundamental mode-locking region as the multiple pulses in the cavity are more separated in time. This similarity between fundamental and multi-pulsing behaviour means care needs to be taken in identifying multi-pulsing behaviour. The spectra of the reference cavity for different pump powers are presented as a heat map in figure 6.3.2. Here the spectral broadening and subsequent narrowing at 53mW is clear. Further pulse break up at higher powers was also visible in the heat map and eventually the fine features of the spectra become blurred as the OSA averages many pulses within the cavity. The single pulse regime was identified using the oscilloscope pulse train, the spectral evolution with pump power and autocorrelations. Summaries of the pulse width and output energies are given later in figure 6.3.5.

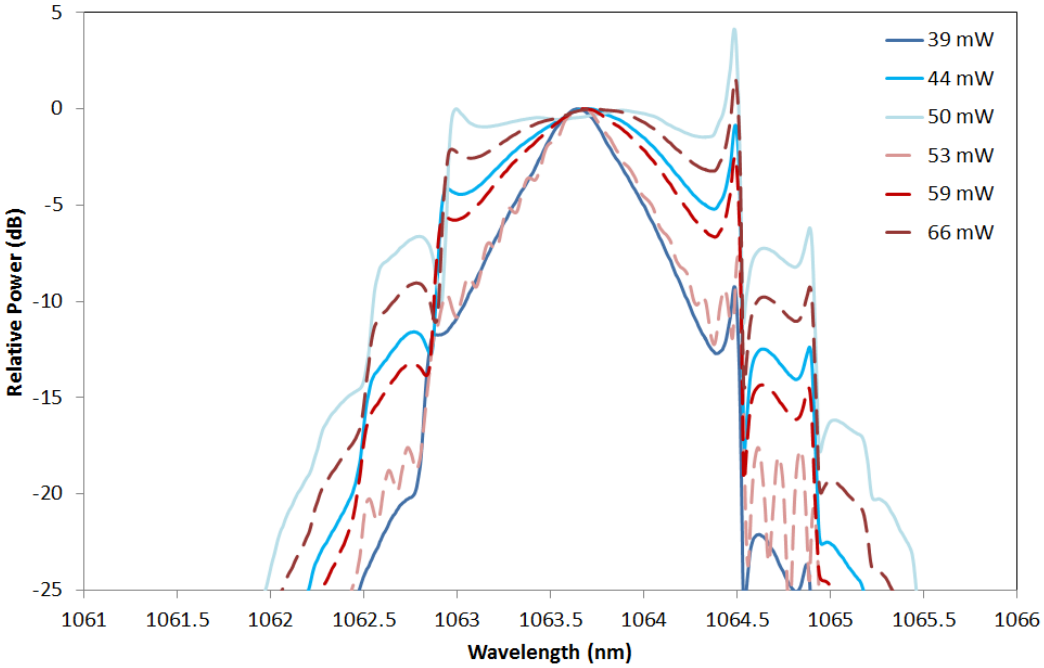

Figure 6.3.1 Comparison of the pulse spectrum of the reference 20 MHz laser output pulse in the fundamental mode-locking regime (blue) and in the multi-pulsing regime (red dashed).

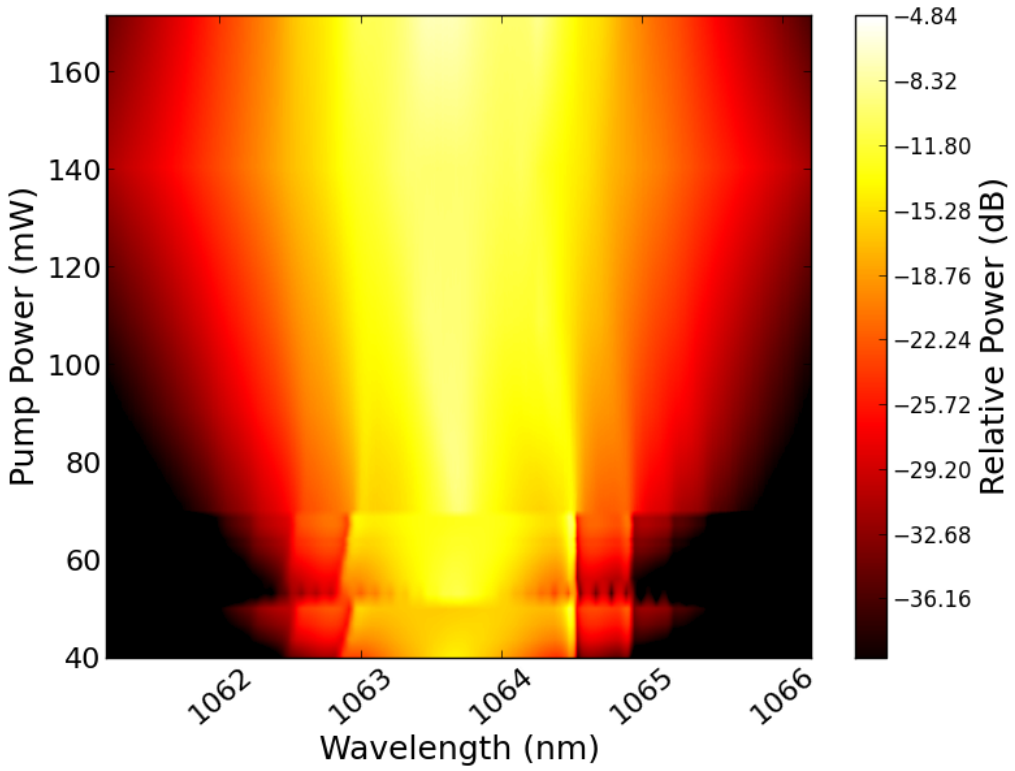

Figure 6.3.2 The spectral evolution of the 20 MHz reference cavity with pump power.

6.3.2 LMA fibre results

Two lengths of LMA fibre with tapered down ends were spliced into the laser cavity replacing the 3.5 m of 9 µm core fibre. The two lengths of tapered fibre (10 m and 20 m) produced repetition rates of 7.6 MHz and 3.6 MHz . The spectral results for these cavities are shown in figure 6.3.3. Spectral heatmaps were used to analyse the cavity behaviour at different pump power levels.

The cavity with 10 m of tapered fibre (7.6 MHz) does show Kelly side bands at low power. These are shown more clearly in figure 6.3.3b. The laser mode-locked at a pump power of 35.7 mW and broadened until 36.4mW before collapsing. This is characteristic of fundamental mode operation and is predicted to be fundamental

operation at these powers. However, the spectrum at 35.7 mW shows a fringe pattern across it indicative of interference from another pulse. This pattern could be from multiple pulses operating in the bunched pulse regime or could be from modal interference. It is unclear which as the autocorrelation for this cavity, figure 6.3.4a, and pulse train showed no sign of multi-pulsing. If the cavity was operating in the fundamental mode it was observed to be definitely multi-pulsing above 36.4 mW of pump power. This is a very small window of operation which would limit the robustness of the laser. This laser was stable over a few hours on a temperature controlled plate set at 21 °C but was not always reproducible if the fibre was removed and respliced into the cavity.

The results for the cavity with 20 m of tapered fibre (3.6 MHz repetition rate) show worse performance than the shorter 7.6 MHz cavity as expected. This cavity did not exhibit Kelly side bands or show characteristic fundamental mode-locked behaviour. Figure 6.3.3c shows the pulse spectral evolution with pump power. In this figure there is negligible change in pulse width and the pulse exhibits spectra similar to that of the higher order multi-pulsing regimes seen in the reference cavity in figure 6.3.2. Closer inspection of these pulse spectra in figure 6.3.3d confirm these were not fundamental mode-locking pulses. The autocorrelations of the 3.6 MHz cavity in figure 6.3.4b show much noise and a triangular shape which indicates it is detecting many pulses. These results indicate that there is no observable fundamental mode-locking operation in the cavity with this delay fibre.

The absence of an observed fundamental mode-locking region can be explained by the long taper lengths that arise from tapering fibres directly from the fibre tower. The length of these tapers (e.g. 5 m total for the 20 m LMA tapered fibre) adds a considerable nonlinear phase shift as these will have lengths of small mode area fibre with high intensity. Using a post processing technique, the taper lengths can be reduced to a few centimetres which would remove the phase shift of the long taper and allow for more controlled testing of the LMA as a delay fibre.

The pulse duration was found to be fairly consistent between laser cavities as

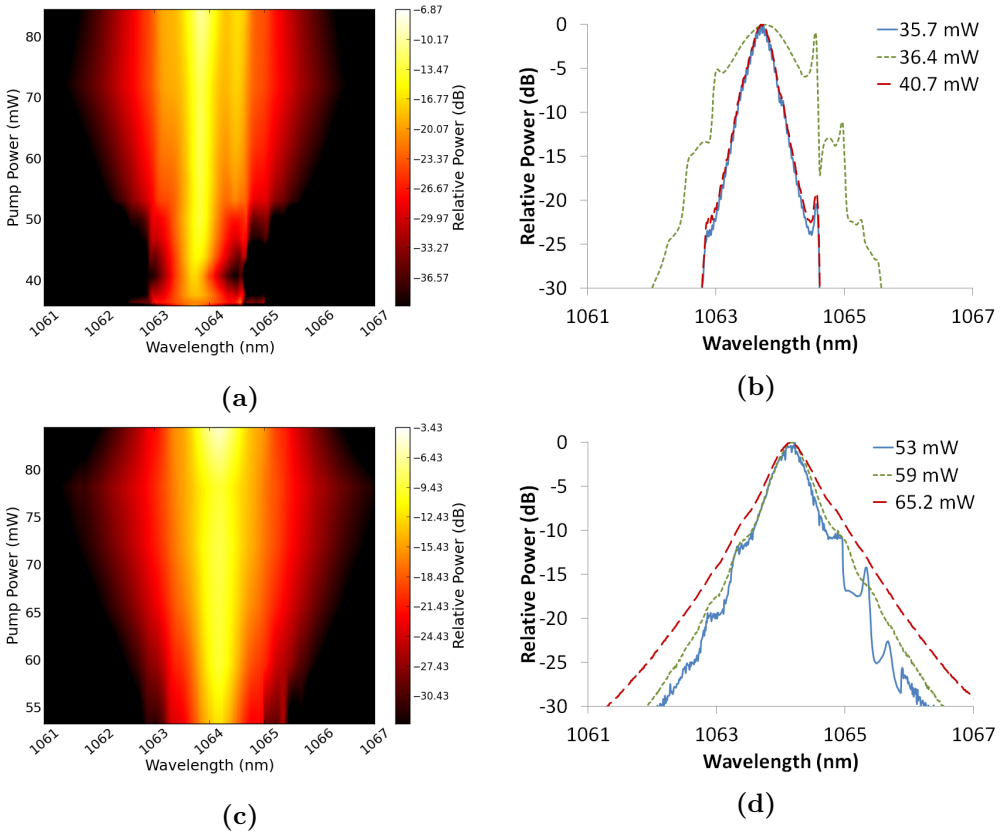

Figure 6.3.3 (a) & (b) - Spectra of the cavity with 10 m of LMA fibre (7.6 MHz). (c) & (d) - Spectra of the cavity with 20 m of LMA fibre (3.6 MHz).

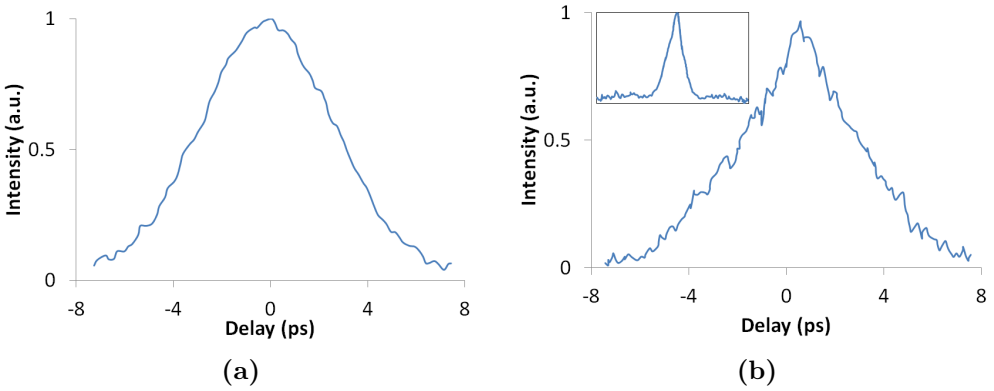

Figure 6.3.4 Autocorrelation traces for (a) the cavity with 10 m (7.6 MHz) and (b) the cavity with 20 m (3.6 MHz). The inset shows the 3.6 MHz cavity autocorrelation across a 50 ps window. All autocorrelations were taken just above the mode-locking threshold.

shown in figure 6.3.5. The output pulse energies also match between the laser cavities. These indicate that the overall behaviour is not significantly impeded by the introduction of the large mode area tapered fibre. The pulses were the expected pulse widths and energies. However, the multi-pulsing and spectral properties were impaired by the introduction of the tapered fibre. Improving the mode properties of the laser cavity, i.e. filtering out higher order modes, would determine if the LMA fibre cavities can actually be used to extend the cavity length in a useful manner.

The mode quality of the laser can be improved by implementing mode filters at the ends of the tapered LMA. This involves putting an additional taper in the fibre to reduce the mode area to a width that is definitely single moded. This could create some loss as higher order modes are filtered out but could improve the performance and prevent higher order modes from being excited in the LMA.

The multi-pulsing threshold can be further increased by using even larger mode area fibre. As shown in figure 6.1.1 the nonlinearity can be greatly reduced going to a 50 µm core diameter. With control of the mode properties within the cavity this should produce a reasonable fundamental mode-locking region.

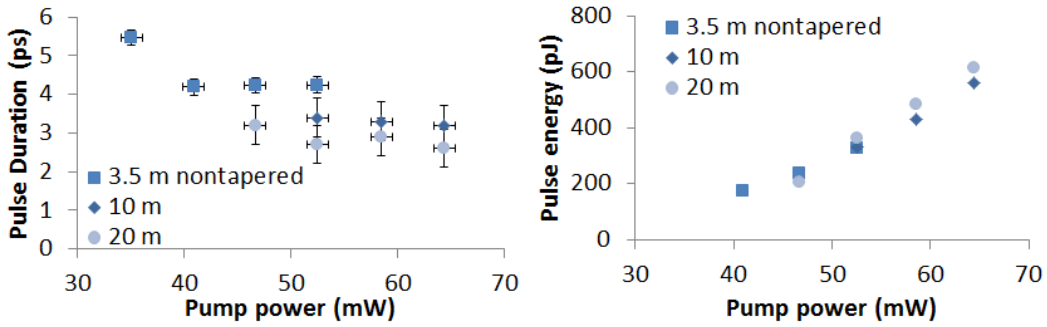

Figure 6.3.5 Results for the laser with 3.5 m of 9 µm core diameter fibre (20.2 MHz) with no taper, 10 m (4.2 MHz) tapered and 20 m (3.57 MHz) tapered fibres placed in the cavity. Only the data points for the fundamental mode-locking regime are shown.

6.4 Conclusion and outlook

Three representative mode-locked laser cavities were compared in this chapter showing the performance differences between a 20 MHz reference cavity and laser cavities with either 10 m (7.6 MHz) or 20 m (3.6 MHz) of tapered large mode area fibres. Both laser cavities successfully mode-locked and produced pulses of the expected duration and pulse energies. The 7.6 MHz cavity exhibited features similar to that of the reference cavity but did not conclusively show fundamental mode-locking. The 3.6 MHz cavity did not show any signs of fundamental mode-locking and appeared to start mode-locking in multi-pulsing regime. The lower multi-pulsing threshold is believed to arise from the extra lengths of small core fibre in the long taper length. The behaviour of the 7.6 MHz cavity was promising but could be further improved by reducing the taper length, improving the mode-filtering either end of the LMA and by increasing the mode area further.

This work became part of a collaborative project with Fianium ltd. funded by the Technology Strategy Board (now Innovate UK) and the project was further progressed beyond what has been described here by Ben Cemlyn. The work further expanded to fibres up to 50 µm in diameter core LMA fibres with post-processed tapers and mode filters on the end. The tapered fibre mode-locked fibre laser design

was then used as a supercontinuum source in Fianium ltd. The results of which have not yet been published and are omitted from this thesis as they are outside of its remit.

Chapter 7

Mode-locked fibre laser with hollow core fibre

7.1 Introduction

This chapter covers the work conducted using hollow core fibre as a delay fibre in a mode-locked laser cavity. Initial tests with a ring laser cavity were conducted with a hollow core, photonic band gap PCF covered in section 7.4. Subsequent experiments covered in section 7.5 were conducted using negative curvature hollow core fibre (NCF).

Hollow core fibres provide access to the low nonlinearity of air with the advantages of guiding in fibre. The nonlinear refractive index of air is approximately three orders of magnitude smaller than that of silica being approximately $10^{-23}\mathrm{m}^2/\mathrm{W}$ compared to $10^{-20}\mathrm{m}^2/\mathrm{W}$ for silica. The low nonlinearity is a promising means to overcome the nonlinear phase shift limits of mode-locked fibre lasers as discussed in chapter 4. However, care needs to be taken with the integration of hollow core fibres in to a solid fibre cavity. Fibre lasers with all solid fibre are traditionally spliced to form an all fibre cavity that is robust to environmental conditions. As mode-locked fibre lasers are sensitive to reflections within the laser cavity. The interface between a hollow core and a solid core fibre naturally has Fresnel reflections between the

silica and air boundary. To overcome this a free space coupling system with angle cleaves on the solid fibres was employed to minimise reflections at this boundary. The free space integration also allows for the testing of different hollow core fibres with minimal change to the laser cavity.

7.2 Ring laser cavity Design

The introduction of free space coupling stages meant certain cavity design considerations had to be taken into account. Having free space components meant the cavity could be incomplete if not fully aligned or the free space beam was blocked. This is different from an all spliced fibre laser where the cavity is always complete and will produce stimulated emission keeping the upper states of the gain fibre depleted. In the event that the cavity is interrupted the gain fibre stores energy in the excited state without stimulated emission to deplete it. If this occurs, any sudden reflected light reaching the gain fibre will trigger a large Q-switched pulse. This pulse can be energetic enough to damage cavity components so care had to be taken to isolate the gain fibre from the free space coupling stage. As such, a ring cavity design was employed with a circulator directing any reflected light away from the gain fibre.

The cavity design used for the experiments in this section is shown in figure 7.2. The cavity was designed with the aid of numerical simulations as discussed in chapter 5. The ring design means light is primarily travelling in one direction around the cavity. The components used in this laser are the same as the previous chapter with the addition of two circulators. The reflective chirped fibre Bragg grating (CFBG) and the saturable absorber mirror (SESAM) are connected via circulators to the main ring. The gain fibre and pump light are located on the SESAM arm of the cavity. Having the gain fibre located here allows for a double pass of the gain medium giving more efficient gain and also isolates the gain fibre from the free space components. The CFBG used had a transmission of 60% and a dispersion of $10\text{ps}\,\text{nm}^{-1}$ applied to the reflected 40% of the light. The CFBG dispersion is large with respect to the fibre dispersion and so is the main contributor to the pulse du-

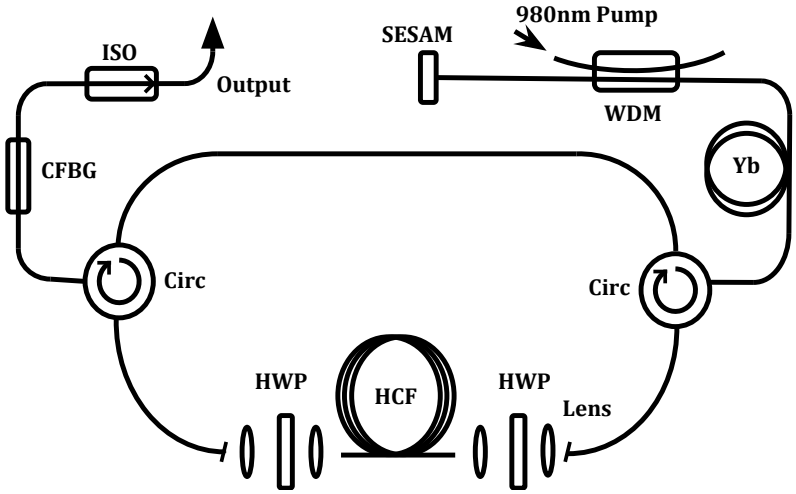

Figure 7.2.1 Layout of ring based laser cavity with two reflective arms. The SESAM is the mode-locking element and mirror to the right arm. Yb is the ytterbium doped gain fibre pumped through a wavelength division multiplexer (WDM) from a 980 nm laser diode. The solid fibre pigtails were angle polished and the hollow core fibre (HCF) is coupled in using a lens pair on motion stages. Half wave plates (HWP) were used to align the polarisation angle of the solid and hollow core polarisation axes. The chirped fibre Bragg grating (CFBG) was an output coupler and applied anomalous dispersion to the reflected light. The isolator (ISO) protected the cavity from back reflections.

ration. Transmission through the output isolator and splices reduced the measured output power from 60% to 40% of the pulse power that was incident on the CFBG. Approximately 65 cm of core pumped ytterbium doped gain fibre with a mode field diameter of 6 µm was used (CorActive YB 401-PM). The length was experimentally found to be the optimum length to get the highest gain before saturation effects became significant as discussed in chapter 4. The hollow core fibre under test was flat cleaved and coupled to angle polished pigtails through a free space coupling stage consisting of two lenses and an half wave plate to fine align the polarisation state. All solid fibre pigtails used in the laser cavity are polarisation maintaining (PM), solid core fibres totalling a length of 5.4 m . The entire cavity was kept on a temperature controlled plate set at 20 °C.

The output isolator has a 5% tap (not shown) that connects to a photodiode and oscilloscope to measure the pulse repetition rate and monitor the pulse train. The main output is then connected to an OSA or to an autocorrelator via an amplifier as described in the previous chapter.

7.3 Reference cavity

The reference cavity output pulse characteristics used for these experiments are as shown in figure 7.3.1. These cavities were constructed with only one free space coupling stage and no hollow core fibre. These cavities identified the behaviour of the cavity without the fibre under test but also with the free space component. A half wave plate was still used in the free space coupling stage to fine align the polarisation axis of the light from the angle cleaved pigtails. Qualitatively, the reference cavity was slightly more unstable than an all-spliced cavity and sometimes needed to be perturbed to start mode-locking at lower powers.

A main note at this point is the difference in cavity behaviour with different SESAMs. All the SESAMs used had the same specifications but manufacturing methods means there is a variation in the actual parameters of individual SESAMs which can impact the performance of the laser. Figure 7.3.1 shows the heat maps of

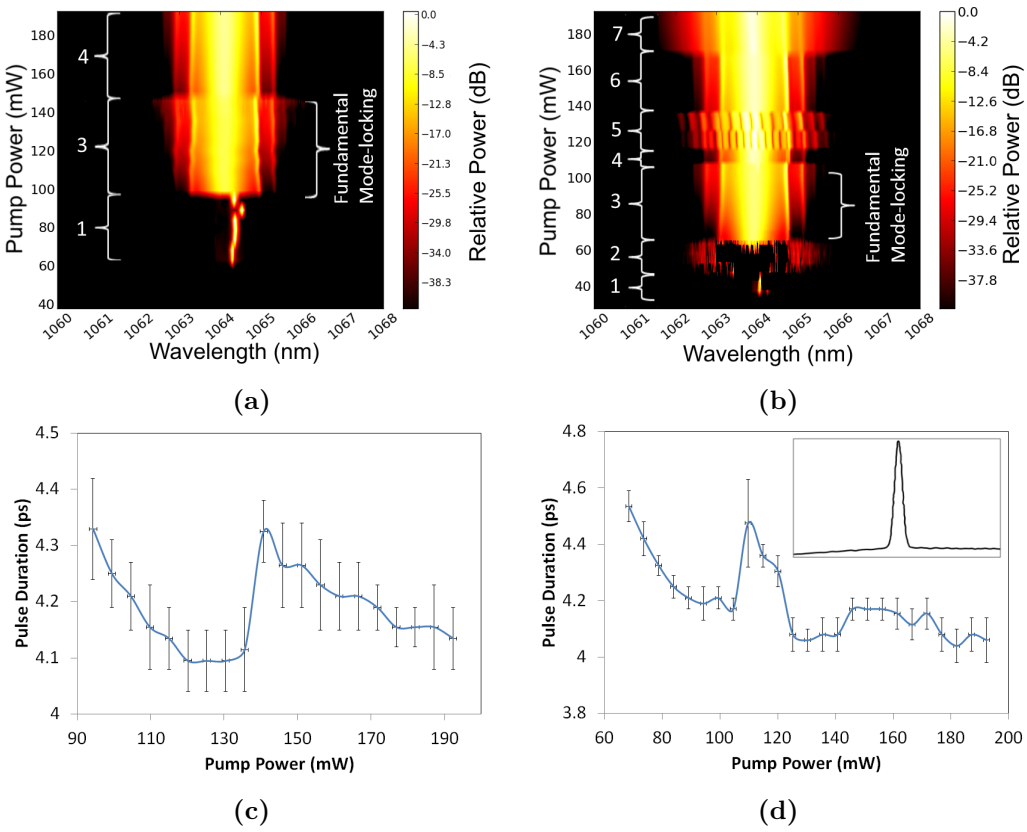

Figure 7.3.1 a) Spectral evolution of reference cavity-a with a free space coupling stage without hollow core fibre. b) Spectral evolution of reference cavity-b, the same laser cavity with a different SESAM and slightly larger spot size on the SESAM. Labels correspond to 1) CW operation, 2) Q-switched mode-locking, 3) fundamental mode-locking, 4 & 6) Harmonic mode-locking, 5) Bunched pulse mode-locking and 7) Higher order multi-pulsing.
c) Measured $1/e^2$ pulse duration of reference cavity-a. d)Measured $1/e^2$ pulse duration of reference cavity-b, inset shows autocorrelation trace across a 150 ps time window.

the output pulse spectra and measured pulse durations for two identical reference cavities with different SESAMs of the same specification. Reference cavity-a and reference cavity-b used fibre pigtails with a mode field of 6.5 µm and 7.8 µm respectively which were butt-coupled to the SESAM.

Both reference cavities produce pulses of approximately 4.2 ps with some fluctuation with pump power. The duration of a pulse decreases slightly with increasing pump power but will sharply increase in duration when the pulse breaks into multiple pulses. This increase in pulse duration corresponds to the decrease in bandwidth as expected. Both cavities show clear Kelly side bands and have a broad fundamental mode-locking region of operation. The maximum output pulse energy produced in the fundamental mode-locking region was 325 pJ (11.6mW average power) for reference cavity-a and 180 pJ (6.6 mW average power) for reference cavity-b. Reference cavity-b does show a Q-switch mode-locking region at low pump powers (region 2) and an interference pattern from bunched pulse regime (region 5) in figure 7.3.1b. The results presented with hollow core PCF in section 7.4 use reference cavity-a while the results in section 7.5 with the NCF use reference cavity-b. Both reference cavities had a repetition rate of approximately 37 MHz .

7.4 Hollow core PCF in ring cavity

Initial tests with hollow core fibre as a delay fibre used hollow core PCF (HC-PCF) shown in inset in figure 7.4.1. The HC-PCF was fabricated in house prior to this project with a design wavelength of 1060 nm . The attenuation spectrum is shown in figure 7.4.1 which was obtained from a total cut back of 140 m to 5 m and averaged over several measurements. The attenuation at the operational wavelength of 1064 nm is 96 dB km^{-1}.

7.4.1 1.5 m HC-PCF delay fibre

A laser cavity with 1.5 m of HC-PCF produced mode-locked pulses at a repetition rate of 27 MHz . The pulses were similar to that of reference cavity-a in duration

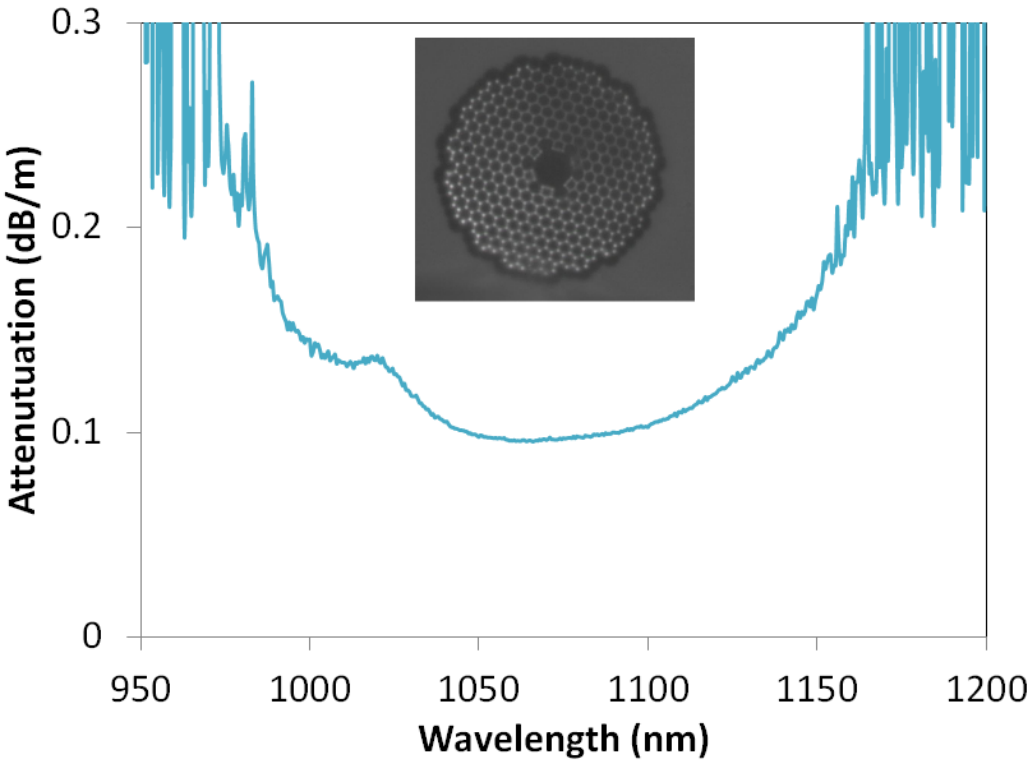

Figure 7.4.1 Attenuation spectrum of the HC-PCF. Attenuation at 1064 nm was measured to be 96 dB km^{-1} from cut back measurements. Inset: Micrograph of Hollow core PCF structure. Core diameter was measured as 9.2 µm and mode field diameter of 5.6 µm .

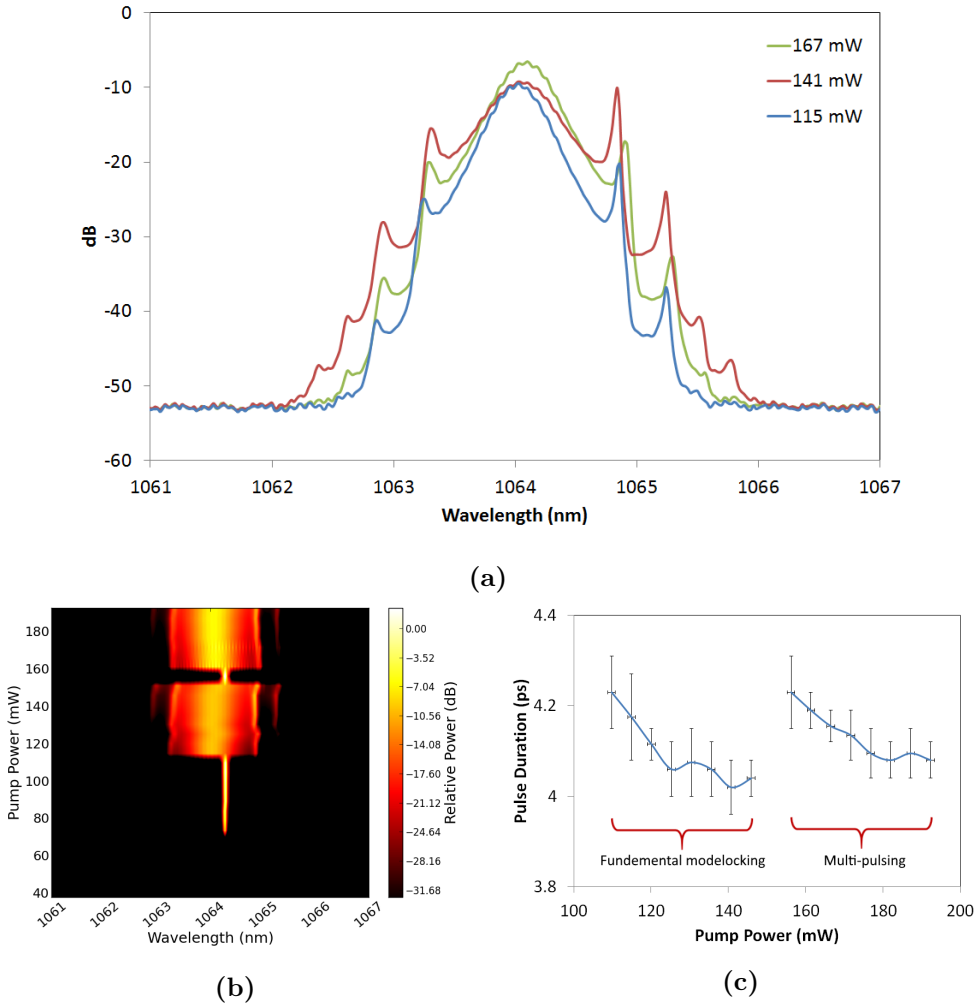

Figure 7.4.2 a) Measured spectra at three different pump powers, 115 mW and 141 mW are at the lower and upper boundaries of the fundamental model-locking regime and 167 mW is harmonic mode-locking. b) Spectral heat map of cavity with 1.5 m of HC-PCF. c)Measured pulse duration from autocorrelations for laser cavity with 1.5 m of HC-PCF.

and spectra. Figure 7.4.2 shows the measured spectral evolution and measured pulse durations. The mode-locking threshold increased to 120 mW pump power as a result of added loss within the cavity from fibre attenuation and additional coupling losses. The 1.5 m of fibre transmitted 74% of the input light including an estimated coupling efficiency of 80%. However, unlike the reference cavity this was not self starting and required physical perturbation of the fibre to produce pulses. Once mode-locked, the fundamental mode-locking regime was stable and pump power could be adjusted within this region and the pulse train remained robust. At the multi-pulsing threshold of 150 mW the cavity became unstable and would not self start or hold pulses at this power level. But in the multi-pulsing region of 160 mW pump power and above the cavity was self-starting and stable.

The quality of the pulses produced indicate that this is a useful means to reduce the repetition rate but the degradation to the cavity stability and self-starting reduced the usefulness of the laser.

7.4.2 25 m HC-PCF delay fibre

Tests with 25 m of HC-PCF produced a repetition rate of 8.6 MHz . This section of fibre is from the same fibre as the 1.5 m fibre. However, the laser performance was unstable and not self starting at any pump power. The pump power required for mode-locking was also higher than expected at 160 mW of pump power. The fibre loss resulted in 50% transmission of light through the HC-PCF which should produce a cavity mode-locking at <135 mW based on the reference cavity mode-locking at 68 mW. The spectrum did not have the characteristic Kelly side bands of the reference cavity as shown in figure 7.4.3. This additional loss is believe to impede the self starting of the laser.

There was also a repeating pattern across the spectrum in figure 7.4.3 that could be manipulated with half wave plates in the free space coupling stages. This structure arises from the interaction of the polarisation state in the cavity with the circulators. As the circulators are polarisation state dependent, they act as polaris-

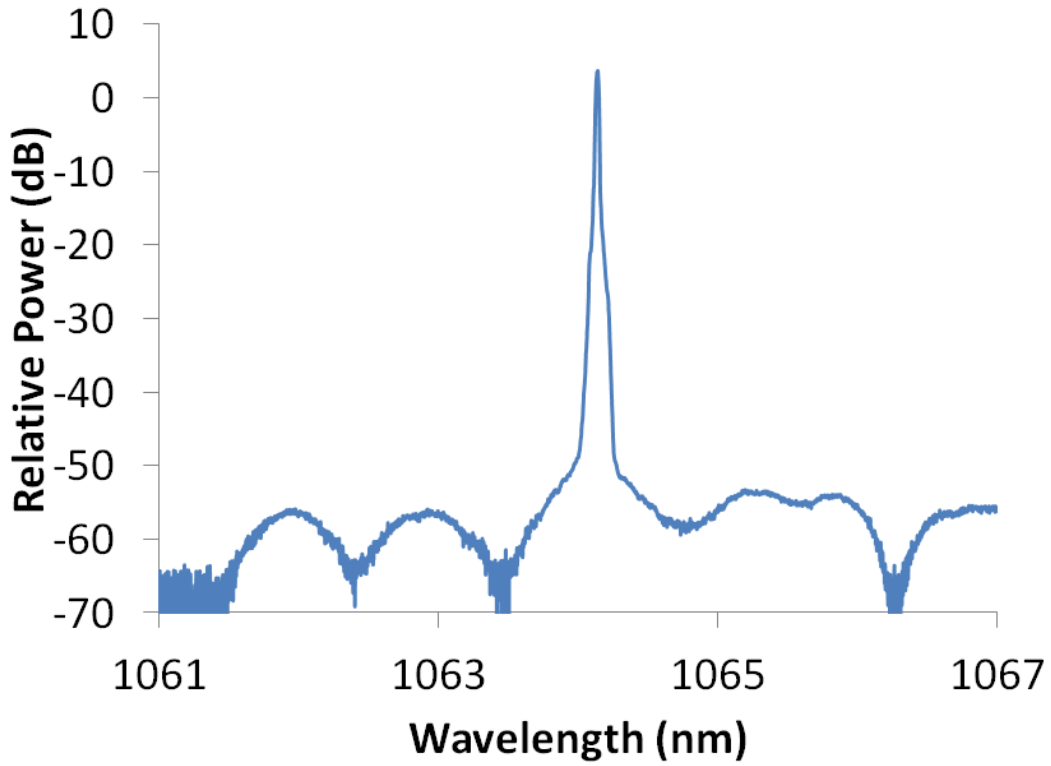

Figure 7.4.3 Spectrum of cavity with 25 m of HC-PCF as a delay fibre. Spectrum recorded at the mode-locking threshold at 160 mW.

ers and the spectrum can show the polarisation beat length $L_b = \Delta\lambda L/\lambda$ where L is the length of a fibre and $\Delta\lambda/\lambda$ is the wavelength interval between peaks divided by the wavelength.[72] The fringes observed correspond to a polarisation beat length of 2.4 cm . The PM pigtails used in constructing the cavity have a beat length of approximately 2 mm so this observed beating is believed to arise from the HC-PCF itself. This fibre is not designed to be polarisation maintaining but asymmetries in the structure can create some birefringence. Further investigation into the polarisation properties of the fibre revealed that the fibre was also depolarising the linearly polarised input. This depolarisation was investigated qualitatively by coupling linearly polarised light into the fibre and using a polariser to attenuate the output light after a single pass of the fibre. The depolarisation of light through the fibre is

thought to further destabilise the cavity as it interacts with the polarisation state dependent components such as the circulators.

7.4.3 130 m HC-PCF delay fibre

A longer piece of 130 m of HC-PCF was also tested. The longer length was calculated to bring the pump power needed to reach the mode-locking threshold down by approximately 90% compared to the reference cavity as the mode-locking threshold is cavity length dependent as discussed in section 4.5. However, the increased fibre length also increases the cavity loss by 95% from fibre attenuation requiring more pump power to compensate. Thus, the resulting theoretical mode-locking threshold was similar to the reference cavity. Experimentally this was not the case as no mode-locking was found with this cavity. The linear polarisation was found to be severely depolarised on the output of the fibre after this length and so the extra losses from extinction in the polarisation dependent cavity components was believed to prevent the laser from reaching the mode-locking threshold.

7.5 Negative curvature hollow core fibre in a ring cavity

The majority of low repetition rate mode-locked laser work has been conducted using anti-resonant negative curvature hollow core fibre (NCF) as described in section 3.3. This fibre has been developed more recently than the HC-PCF and all fibre used was fabricated for this work, with the exception of an existing 8 m long fibre. The low nonlinearity of the air core and low group velocity dispersion of a few $\mathrm{ps\,nm^{-1}\,km^{-1}}$ allowed for pulse transmission with little disturbance.[73]

The NCF has a different guiding mechanism from the HC-PCF and different polarisation properties. Tests found negligible depolarisation after a single pass through 50 m of NCF, thus it was not subject to the same laser cavity performance issues as the HC-PCF.

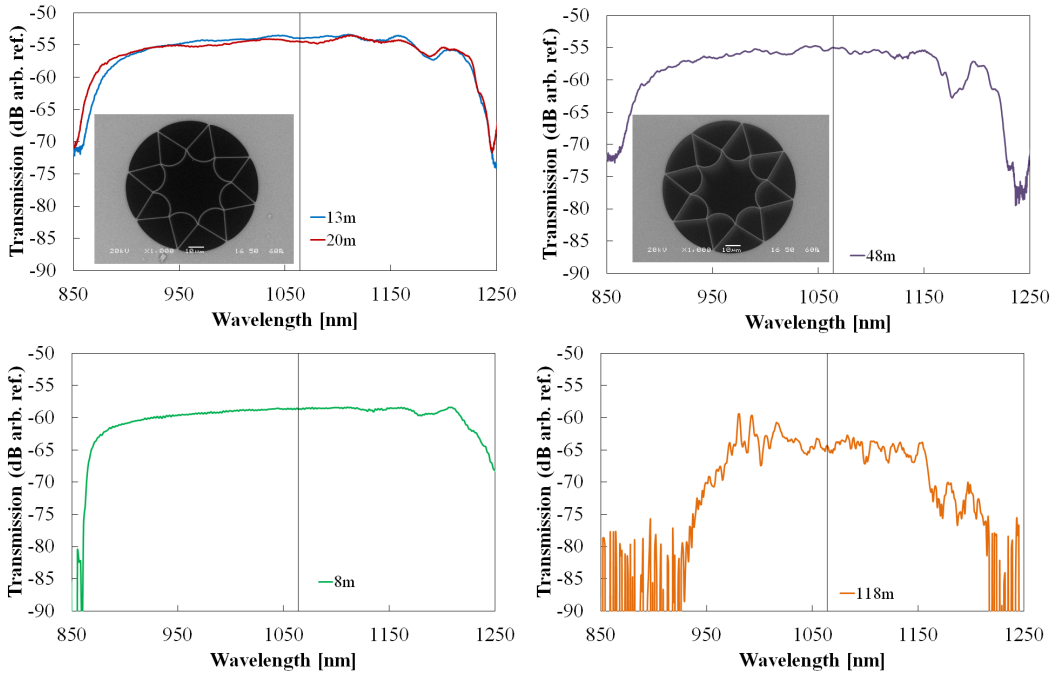

Figure 7.5.1 Transmission curves of different fabrications of NCF taken at an arbitrary reference power measured using a broadband xenon bulb as a white light source. The black vertical line is the operational wavelength 1064 nm. The inset shows an SEM image of the fibre end of the 48.

7.5.1 NCF fibre specifications

The NCF fibre used had an eight capillary cladding structure as shown in the inset in figure 7.5.1. The transmission spectra of a selection of NCF fabricated for this project are shown in figure 7.5.1. The fibres had a core diameter of $32 \pm 2\,\mu m$. The 13 m and 20 m lengths shown are from the same fibre draw, the rest of the NCF fibres are from separate draws and preforms. Apart from the 118 m fibre, the main transmission bands were flat, spanned approximately 400 nm and found to have an attenuation of $< 40\,dB\,km^{-1}$ at 1064 nm. The fibre attenuation was estimated from the measured proportion of light through the fundamental mode of the fibres with estimated coupling efficiency achieved. The 118 m fibre was found to have an attenuation of $< 100\,dB\,km^{-1}$.

The 118 m length was the longest fibre fabricated for the operational wavelength of 1064 nm in this work. This was pushing the limits of what could be feasibly fabricated in a continuous piece and also was one of the NCF designs that did not have a fluorine doped silica outer jacket. Both of which are thought to limit the consistency fibre along its length. A cavity was tested with this fibre and reviewed in section 7.5.3.

7.5.2 Main results

The lengths of NCF covered in this section are 8 m , 13 m , 20 m , 33 m and 48 m to give a representative sample of cavity lengths. These delay fibre lengths correspond to respective pulse repetition rates of 18.2 MHz , 14.2 MHz , 10.8 MHz , 7.4 MHz and 5.4 MHz .

The spectral heat maps of a sample of these cavities is shown in figure 7.5.2. The cavity with 8 m of NCF (18.2 MHz), shown in figure 7.5.2a, shows similar behaviour to the reference cavity exhibiting Q-switched mode-locking, fundamental mode-locking and a mixture of harmonic and bunched pulse mode-locking at higher pump powers. However, compared to the reference cavity both the mode-locking and the multi-pulsing thresholds are reduced, along with the range of pump power in the fundamental mode-locking region, as expected from extending the cavity length. The cavity with 20 m (10.8 MHz) in figure 7.5.2b shows further reduction of the fundamental mode-locking region as well as reduction in both the mode-locking and multi-pulsing thresholds. This cavity did not have a Q-switched mode-locking region, going from CW operation to full mode-locking at a pump power of 40 mW . Figure 7.5.2c shows the cavity with 48 m of NCF (5.4 MHz), which has the smallest region of fundamental mode-locking, where the mode-locking threshold matches the lasing threshold of the cavity.

An important comparison to make is the pulse bandwidth and the position of the Kelly side bands with increased cavity length. Figure 7.5.2d shows a comparison of the spectra of each cavity produced in the middle of the fundamental mode-locking

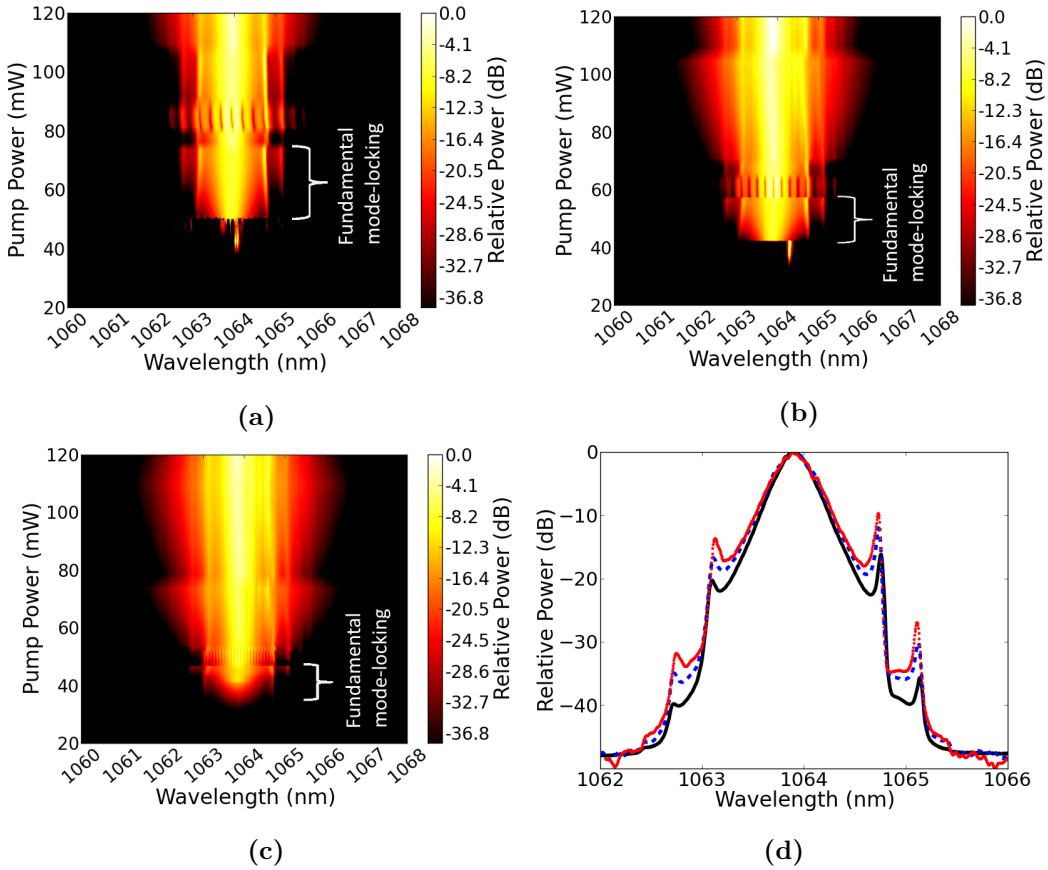

Figure 7.5.2 a), b) and c) are the output spectra with pump power for cavities with 8 m , 20 m and 48 m respectively. d) Comparison of spectra at comparable cavity powers for the reference cavity-b (black solid line), the cavity with 20 m of NCF (Blue dashed line) and with 48 m of NCF (Red dotted line).

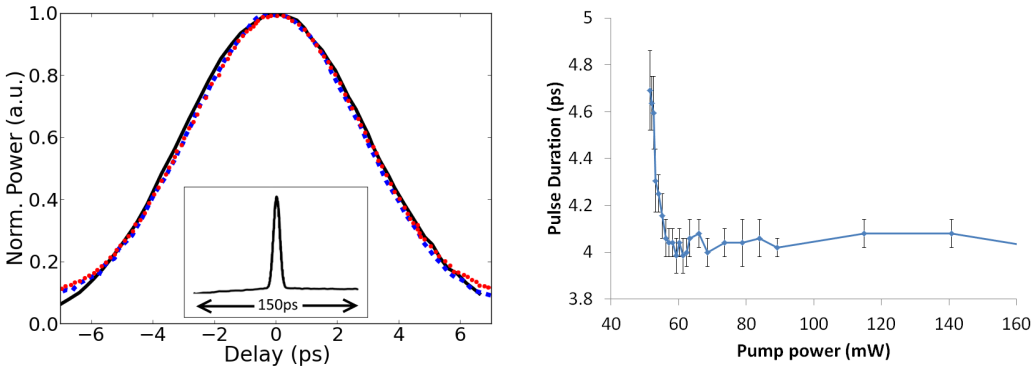

(a) (b)

Figure 7.5.3 a) Autocorrelations of the laser output for the reference cavity-b (solid black line), the cavity with 20 m of NCF (blue dashed line) and for the cavity with 48 m of NCF (red dotted line). Autocorrelations taken at comparable points in the fundamental mode-locking region. b) Pulse duration of the 5.4 MHz cavity with 48 m of NCF with pump power.

region where the cavity is most stable. The spectra shown in this figure are the reference cavity, the cavity with 20 m and the cavity with 48 m , which covers a change from 37 MHz to 5.4 MHz . There is negligible change in spectral bandwidth between these measurements and the Kelly side bands appear at the same wavelengths for each laser cavity. As the Kelly side bands are dependent on the net group velocity dispersion in the cavity it can be shown that the NCF contributes negligible dispersion to the system, allowing for a longer cavity without altering the pulse duration.

A comparison of the autocorrelations of the pulses from different cavities is shown in figure 7.5.3a. These traces are measured from the same cavities as figure 7.5.2d and at similar power levels. These autocorrelation measurements, assuming a sech^2 shape, have a pulse duration of 4.2 ps and did not change with cavity length. There was also no noticeable pedestal on the trace when viewed on a wider time-scale as shown in the inset of figure 7.5.3a. The pulse durations for each cavity fluctuated slightly with pump power as seen in the reference cavity. This variation is shown

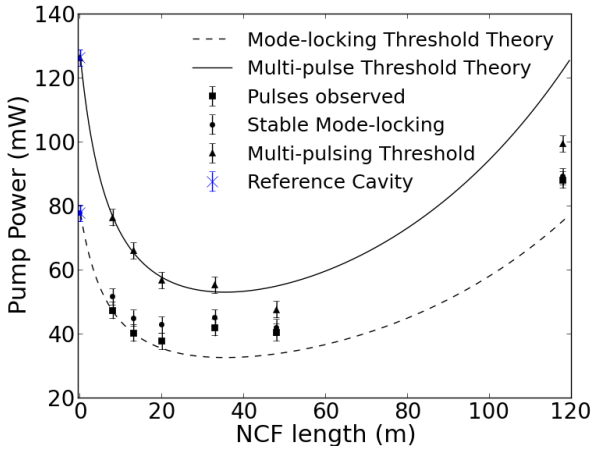

Figure 7.5.4 The mode-locking and multi-pulsing thresholds of reference cavity-b in blue points. The dotted and solid lines are the theoretical mode-locking and multi-pulsing thresholds projected from the measured reference cavity values. The black points correspond to measured laser cavities. The minimum pump power needed to observe pulses is recorded along with the pump power where those pulses became stable. Included, for comparison, are the results from a cavity with 118 m of NCF which will be discussed in section 7.5.6.

in figure 7.5.3b for the cavity with 48 m . The pulse duration starts at 4.8 ps at the mode-locking threshold and drops to 4 ps at higher pump powers and remains at this duration in the multi-pulsing regime. The change in pulse duration and bandwidth resulted in a fluctuation of the time-bandwidth product between the values of 0.35 at the mode-locking threshold to 0.5 at higher pump powers. These values are close to the theoretical minimum for pulses with a sech^2 shape which is 0.315 meaning the pulses were close to transform limited exhibiting little chirp.

The measured properties of the NCF cavities have shown they not only were soliton like, but produced identical pulses at different repetition rates. This demonstrates the robustness of the NCF as a passive delay fibre that does not add unwanted nonlinearity or dispersion to these types of lasers.

The mode-locking and multi-pulsing thresholds did change with addition of extra NCF. Both of these thresholds were calculated and projected from known fibre

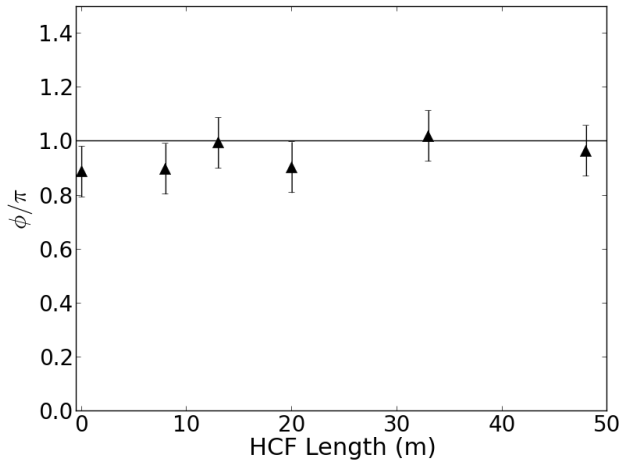

Figure 7.5.5 The total cavity phase shift of the highest power fundamental mode-locked pulses prior to pulse break up. Phase shift is calculated from measured output characteristics and known cavity component parameters.

losses and cavity length and shown in figure 7.5.4. This was done by starting with the measured reference cavity-b thresholds and calculating how these will change only from increased length and cavity loss from fibre attenuation. These are the theoretical thresholds in the absence of additional nonlinearity or dispersion. The measured thresholds of a selection of constructed lasers are shown and agree well with the theoretical lines of mode-locking and multi-pulsing thresholds. There is some deviation in the results with 33 m and 48 m of NCF as the 33 m experiment used a 13 m and 20 m fibre butt-coupled together and so had higher loses and the 48 m length of NCF had a lower than average fibre attenuation of $<30\,\mathrm{dB\,km^{-1}}$.

The cavities constructed were repeatable and produced similar results if the NCF was replaced and recoupled. Each cavity was monitored for stability over several hours. At low pump powers close to the mode-locking threshold the cavities were not self starting and could be unstable with pulse trains only lasting a few seconds or minutes. At slightly higher pump powers the pulses became stable and self-starting, maintaining operation across the monitored time. The pump powers where the cavities were stable are shown in figure 7.5.4. The region between the stable

fundamental mode-locking pump powers and the multi-pulsing threshold are the practical working ranges of these lasers which does decrease with length. However, this region was thought to exist in longer cavities than 48 m. Tests with longer fibres have been conducted and will be discussed in section 7.5.3.

The multi-pulsing threshold is defined by the nonlinear phase shift as discussed in chapter 4. For a laser to operate at full range the fundamental pulses should reach that threshold before breaking up. Figure 7.5.5 shows the calculated phase shift of several cavities calculated from the measured output power and pulse duration taking into account known cavity component parameters. The cavities tested all reach approximately π phase shift before pulse breaking. This demonstrates that the cavities were working at the theoretical maximum peak power in the fundamental mode-locking regime and there were not any unexpected effects disrupting the pulses in the cavities. The output peak power at the multi-pulsing threshold was approximately 40 W producing output pulse energies of 179 pJ to 240 pJ.

7.5.3 118 m NCF results

Fabricating long continuous pieces of NCF proved challenging due to the small draw down ratio and high pressure needed to create the negative curvature structure for this wavelength as discussed in chapter 3. The maximum fibre length achieved in a continuous draw was 118 m. This length produced pulses with a repetition rate of 2.4 MHz which was the lowest repetition rate achieved with NCF in this work. However, the laser produced pulses with a longer duration which drifted between 8 ps and 12 ps each time it was switched on. An autocorrelation trace is shown in figure 7.5.6b, which has a lot of noise, a large pedestal and was unstable. The spectra of this cavity are shown in figure 7.5.6a, which is much narrower than previously measured cavities and corresponds to a longer pulse duration. The spectrum also did not have any Kelly side bands and was highly structured meaning the pulses produced were not an ideal soliton like pulse.

A notable difference between the longer fibres drawn and the NCF previously

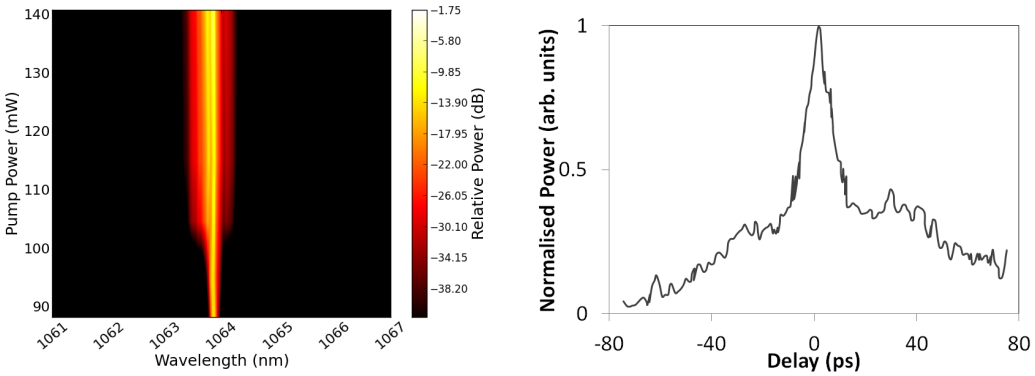

(a) (b)

Figure 7.5.6 a) The spectrum of the 2.4 MHz cavity with 118 m of NCF. b) Autocorrelation of the 2.4 MHz repetition cavity with 118 m of NCF.

reported in this chapter is the absence of a fluorine doped silica outer jacket. Fibre fabrication techniques of drawing fibre without the fluorine doped outer tube were being developed at the time of the long NCFs were fabricated. Cut back measurements of an identical 110 m fibre revealed an average attenuation of 100 dB km^{-1} at 1064 nm which is higher than the attenuation of the other fibres used. Subsequent testing found shorter pieces of this fibre were of variable transmission quality. As a result of this, imperfections occurring during fibre fabrication is believed to be the main cause of the mode-locked laser performance issues at long length.

7.6 Conclusion and outlook

Hollow core fibres have been inserted into a mode-locked laser cavity as a delay fibre to decrease the repetition rate without the introduction of nonlinearity. Two types of hollow core fibre were tested, photonic bandgap fibre and negative curvature anti-resonant fibre.

A repetition rate of 37 MHz was reduced to 8.6 MHz with little change to the pulse duration or spectrum using PCF. The introduction of PCF to the cavity did noticeably decrease the self starting properties of the cavity and the pulse stability.

The limits of using this PCF as a delay fibre in a mode-locked cavity were found to be the high fibre attenuation of $100\,\mathrm{dB\,km^{-1}}$ and the depolarisation of the light within the delay fibre disrupting the mode-locking.

NCF proved to be a more robust delay fibre and reached a pulse repetition rate 5.4 MHz using 48 m of NCF with no detriment to the near transform limited pulses or the cavity stability. The polarisation state was preserved well through the fibre and low losses of $40\,\mathrm{dB\,km^{-1}}$ enabled the successful extension of the cavity length. Longer lengths of NCF have been tested with 118 m of NCF producing a 2.4 MHz pulse train but with an increased pulse duration of $10 \pm 2\,\mathrm{ps}$ from 4.2 ps and decreased stability. The 2.4 MHz also did not exhibit Kelly side-bands normally associated with a useful soliton-like pulse. The cause of this is believed to be imperfections in the fibre caused by fabrication limitations.

Overall this work has successfully shown that hollow core fibre can be used as a delay fibre to reduce mode-locked pulse repetition rates. The work with the PCF could potentially be taken further by developing a non-PM laser cavity to test but overall the NCF has proved to be the more suitable fibre out the two types tested. The NCF laser cavities could be extended further by improving fabrication techniques to engineer longer fibres with low loss. Eventually the robustness of the laser cavity can be improved with the development of angle splices to directly connect the hollow core fibre to the solid core cavity fibre without unwanted reflections. This may also require tapering of fibre ends to improve the mode matching between the fibres, which was done here with a lens pair in the free space coupling stages.

Chapter 8

Pulse Propagation in Gas-Filled Hollow Core Fibre

8.1 Introduction

Hollow core fibres offer the possibility to look at pulse propagation in a medium other than traditional solid, silica fibres allowing for the use and analysis of different materials.

Previously in this thesis, negative curvature hollow core fibres (NCFs) have been used to minimise the nonlinear phase shift applied to a pulse within a laser cavity. At the peak power levels studied of a few Watts, air has been a sufficient medium having a relatively low nonlinear refractive index. However, when studying higher power pulses (a few MW peak power) the nonlinear phase shift in air becomes significant. Using NCF allows for both the transmission of high power pulses as well as inducing nonlinear effects such as self-phase modulation (SPM) in an appropriate medium.

Generating clean SPM is a task of academic interest as well as having applications in pulse compression. It can be a useful tool that spectrally broadens the pulse, acquiring chirp, which can be used to compress a pulse using a linear compression technique such a grating pair.[74] Effective pulse compression is a means to achieve high peak power pulses either by itself or in conjunction with low repetition rate

lasers explored previously to create ultra short, high peak power pulses.

The high power transmission and resultant nonlinear effects were explored initially in air at atmospheric pressure with results shown in the next section. Section 8.3 covers similar experiments using NCF filled with argon. Different pressures of argon were tested as nonlinear refractive index, n_2, of argon varies with pressure.[75] The values of the nonlinear refractive index of argon reported in literature has a significant variance and are summarised in Börzsönyi et al.[75] ranging from 0.98 to 19.4 m^2/W at 1 bar . The range of methods used to measure n_2 in these papers vary considerably and each is subject to different experimental errors. The measured n_2 can depend on the polarisation state of light being measured or the Kerr nonlinearity being mixed with other nonlinear effects that distort the results. Also for optical fibres, any overlap of the light with the guiding structure can result in a net measurement of the n_2 of the core material and the cladding. The pulse duration also has an impact on which nonlinear effects are observed. These are discussed in Nibbering et al.[76] The excited atoms in experiments with CW or nanosecond pulses can be considered to be thermally stable across the pulse duration but are subject to inter-atomic collisions occurring during the pulse. The mean collision time for the gases considered here are of the order 10 to 100 ps . Pulses shorter than this can be considered to be collision free. However, femtosecond pulses have a broad bandwidth which is more likely to overlap with wavelength specific effects such as material excitation bands. SPM is one of the instantaneous nonlinear responses discussed in section 2.6 which arises from light interactions with electrons. Ideally to exploit the purely electronic nonlinear effects in a material, a short pulse is required with a bandwidth that does not excite competing nonlinear effects. To excite only the electronic nonlinear response to generate SPM a pulse of ≈10 ps or shorter and a gas with rotational and vibrational symmetry, i.e. a noble gas such as argon or xenon should be used.

Early work looking at the nonlinear optical properties of gases was conducted in gas filled capillaries as in Nibbering et al.[76] This allowed for high powers to

be explored with large beam diameters, though these were conducted with collimated beams in rigid tubes which limits the practical interaction length that can be explored. Flexible capillaries would be lossy but provide guidance. With the advent of hollow core fibre, long lengths of flexible tubes with good guidance have been achieved. The induced SPM and subsequent pulse compression have been conducted in helium (900 fs to 300 fs at 100 µJ),[77] xenon (1 ps to 250 fs with 0.7 µJ of pulse energy at 1030 nm)[78] and argon (740 fs to 88 fs at 1030 nm)[79] filled Kagome fibres. The majority of this work appears to be in Kagome style fibres as outlined in[12] and use femtosecond pulses in the input. Xenon has attracted much interest in this field as it has been shown to reach nonlinear refractive indices higher than fused silica at pressures above the critical pressure (58 bar) at room temperature where the xenon is in a supercritical fluid state.[80] Argon has a lower nonlinear refractive index than xenon and the critical pressure (48 bar) does not have as much of an impact on the n_2 value. Although xenon does have a higher nonlinear refractive index than argon, there is further experimentation that can be done with argon which is a cheaper alternative to xenon.

This chapter covers initial results taken with hollow core anti-resonant negative curvature fibres (NCF) filled with air at atmospheric pressure and temperature. Results are presented in section 8.3 from experiments conducted with fibres filled with zero grade argon and pressured up to 40 bar . The fibre dispersion regime in the argon experiments was found to have a large impact on the ability to generate clean SPM. The two cases of anomalous and normal dispersion regimes have been separated into two sections and will be discussed separately.

All experiments in this section used a 1064 nm Fianium Hylase system with a pulse duration of 10 ps , a spectral bandwidth of 0.2 nm and a linearly polarised output. The fibres used were of a set of anomalous dispersion fibres engineered to have a central wavelength of 1064 nm in the main transmission band and were of lengths: 48 m , 20 m , 13 m (later 7 m) and 9 m . An 18 m length of normal dispersion fibre was also tested which had a transmission band centred at 1200 nm . All of

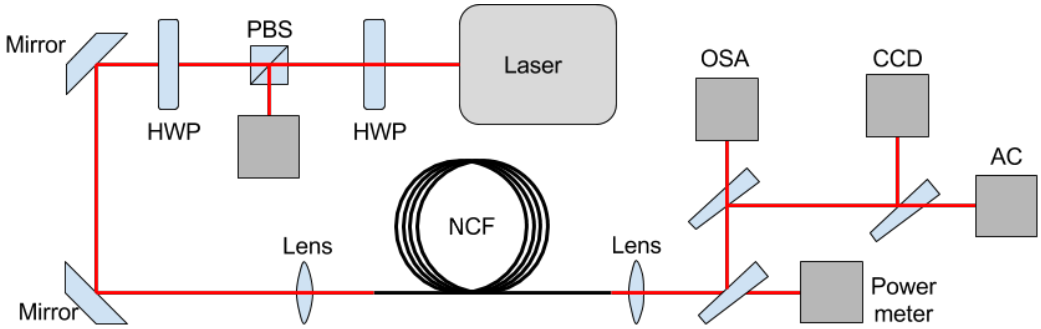

Figure 8.1.1 Experimental set up of atmospheric hollow-core negative curvature fibre (NCF). The laser is a Fianium Hylase-25 10 ps set at 200 kHz. Power control was provided by half wave plate (HWP) and polarizing beam splitter (PBS). The light was coupled into the fibre using translation stages and lenses. The output beam was split between a power meter, a Yokogawa optical spectral analyser (OSA), a CCD camera and an autocorrelator (AC).

these fibres have a core diameter of 34 ± 2 µm measured from the shortest distance between opposing curves in the structure.

8.2 Pulse transmission in air

Preliminary experiments were conducted using NCF fibres in air at atmospheric pressures using a Fianium Hylase system. The experiment was set up as shown in figure 8.1.1. The power incident on the fibre was controlled with a polarising beam splitter cube and half-wave plate. The output from the fibre was divided using wedges to the relevant monitoring equipment. The coupling efficiency was monitored with a power meter on the output. The beam profile was monitored with a CCD camera. A typical profile is shown in figure 8.2.1. The profile is mostly the fundamental mode of the core with a small portion of LP_{11} mode present, which was observed as distortions to the beam profile when perturbing the fibre.

At 200 kHz the laser had a maximum average power of 20 W corresponding to a pulse energy of 100 µJ and an 8.8 MW peak power. Using the theory of self-phase modulation described in section 2.6; a 20 m fibre with a core diameter of 28 µm and

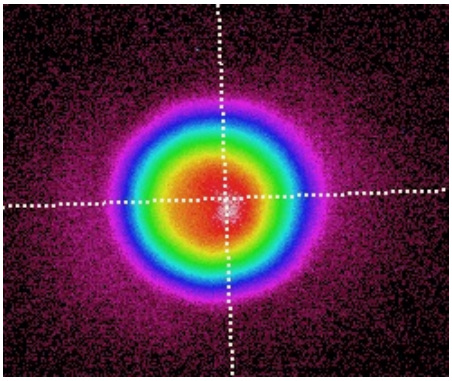

Figure 8.2.1 Near field image of the output of the 48 m NCF imaged with CCD camera.

the nonlinear refractive index of air being approximately 1×10^{-23} m^2/W, would produce a maximum SPM phase shift of $\phi \approx 5.4\pi$ using the equation 2.6.5.

The SPM manifests as a series of peaks in the pulse spectrum as discussed in section 2.6. The number of peaks, M, is related to the nonlinear phase shift such that $\phi \approx (M + \frac{1}{2})\pi$. The example given above should therefore result in a maximum of 5 SPM peaks. In practice, there are losses in coupling and interference from higher order modes and other nonlinear effects within the fibre. A total of four lengths of fibre were used for this experiment: 48 m, 20 m, 13 m and 0.5 m (0.5 m was taken from the 48 m length). With these lengths a range of spectral broadening should in principle be observable.

The shortest length of 0.5 m fibre was enough to observe small amounts of SPM as shown in figure 8.2.2a. This length had a much higher optical throughput than the other fibres tested as this length is not sufficient to extinguish cladding modes from the light not coupled directly to the core.

Two clear SPM peaks were observed using the 13 m fibre, as shown in figure 8.2.2b, which is expected from equation 2.6.6 given an optical throughput of 55%. Some asymmetry in the peaks is also visible in this experiment.

For a pulse energy of 100 µJ in a 20 m fibre with an optical throughput of 65%, approximately four peaks should be visible. However, this is not reflected in the

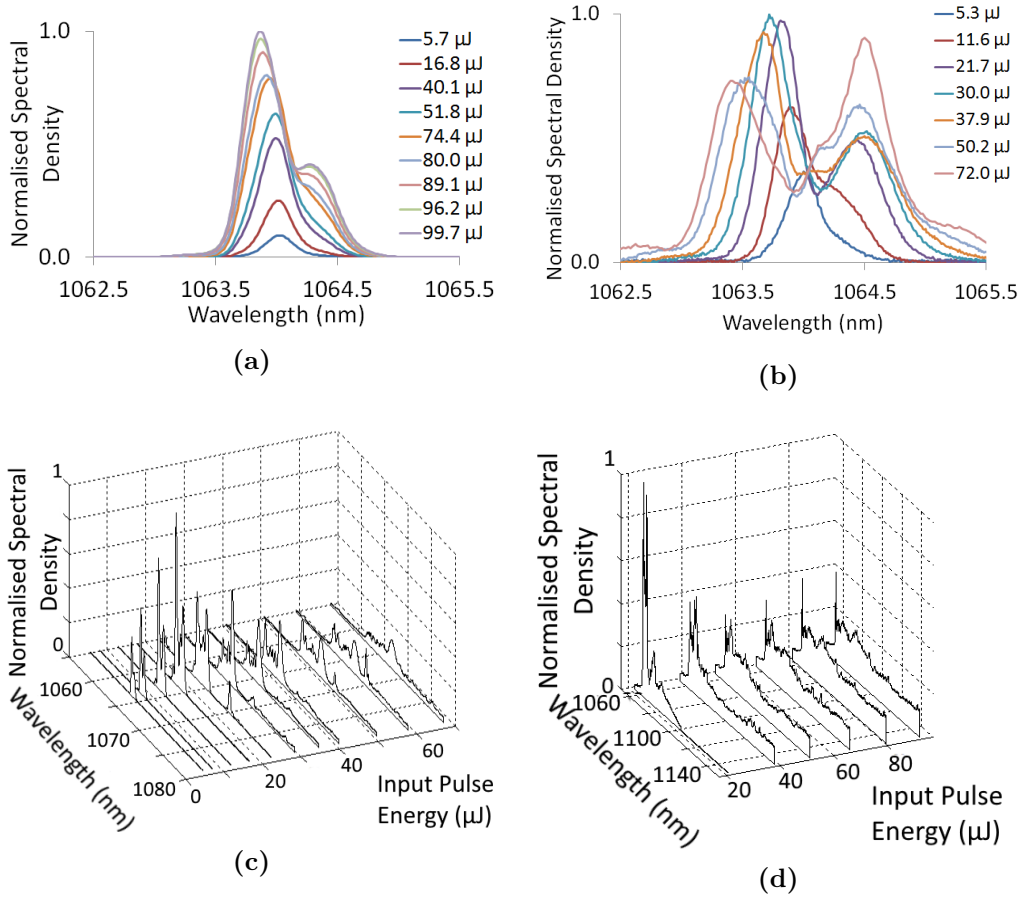

Figure 8.2.2 Spectra of output pulses from 0.5 m , 13 m , 20 m and 48 m of NCF exposed to air for differing pulse energies incident on the fibre end shown. Light throughput through fibre was $\approx$ 75%, 55%, 65% and 50% respectively.

experimental results as the spectrum is heavily structured (figure 8.2.2c). This distortion can be attributed to two main causes. The first is the increased interaction length with the silica cladding structure. Although the overlap of core mode and cladding structure is small, the cumulative interaction in longer fibres could introduce interference from other nonlinear effects in the silica. Secondly, the increased interaction length of the air itself which has a Raman response from the nitrogen and oxygen components as discussed in section 2.6.

The 48 m length in figure 8.2.2d again showed strong distortion with large por-

tions of the energy shifting to longer wavelengths. This length should provide the largest SPM broadening of the pulse but is also subject to other nonlinear effects. This spectrum would prove difficult to compress but demonstrates the broadening capabilities of air in this fibre.

The experiments using ambient air have shown that SPM is present in this set up. However, it is in small amounts and is largely dominated by other effects from the air or from cladding interaction. The fibre also has a small portion of higher order transverse modes present in the core which could cause further interference.

There were also limits imposed by the coupling efficiency achieved in this set up. The attenuation of these fibres were ≈ 30 to 40 $\mathrm{dB\,km^{-1}}$ as discussed in chapter 3, which means significant coupling losses were present in this set up. This could be improved by carefully selecting the coupling lenses used to find the ideal focal length with low aberrations. There were also limits in the amount of power that could be coupled into the fibre. The end face of the fibre began to degrade with an incident pulse energy of $\approx 90\,\mu\mathrm{J}$ in this experiment. The damage threshold of the fibre is dependent on the coupling efficiency and the beam quality incident on the fibre as light not coupled directly to the core is interacting with the silica guiding structure at the end face.

To further explore the possible application of this fibre to generate clean SPM for pulse compression, the spectral structure caused by cladding interaction needed to be isolated from the structure introduced from pulse-air interaction. The use of a Raman-free medium, such as argon, was needed to ascertain if the spectral structure observed at longer lengths was from increased interaction with air or with the fibre itself.

8.3 Argon filled NCF

Argon is a noble gas which has no Raman response. It has nonlinear refractive index of the same order of magnitude as air. Using argon in the NCF was expected to induce self-phase modulation without the distortions arising from Raman effects as

seen in the previous section with air filled fibre. This section explored the broadening achieved with different values of nonlinear refractive index controlled by using different pressures of argon. The different dispersion regimes of the fibre are explored. In the anomalous dispersion regime, modulation instability is observed which is used to characterise the precise dispersion of the fibre. The normal dispersion regime exhibited clean SPM without the onset of soliton dynamics. This is then compressed using a grating pair going from ≈10 ps to 420 fs .

8.3.1 Set up

The set up for the argon filled NCF experiment is similar to the previous air filled experiment, shown in figure 8.3.1, with the exception of gas cells on either end of the NCF. The gas cells each had an anti-reflection coated fused silica window 5 mm thick to allow light to be coupled into the fibre. The gas cells had a maximum pressure of ≈ 40 bar and had a 5 µm particulate filter on the gas input. The workable distance from the lens to the fibre end face through the window was approximate 15 mm . This did limit the focal length of the coupling lens used to couple light into and out of the fibre. The beam from the Hylase system had a diameter of 1.2 mm which needed to be focused to a mode field diameter of ≈ 28 µm at the fibre end. After testing with a range of focal lengths of lenses available, a 20 mm lens was chosen as it provided the best coupling efficiency during testing: 73% light incident on the fibre was measured at the output from the fibre core, through 48 m fibre at maximum with no gas present. The distance between the window and the fibre end face also ensured the beam was still relatively large when it passed through the window resulting in low nonlinear interactions with the windows and minimised damage to the window. The nonlinear phase shift contribution of the windows was found to be negligible in comparison to the expected phase shift from the fibre. For this experiment, measurements were taken immediately after the output coupling lens. A mirror was used to steer the beam into an autocorrelator for temporal readings. An integrating sphere connected to a Yokogawa OSA was used to collect the spectra

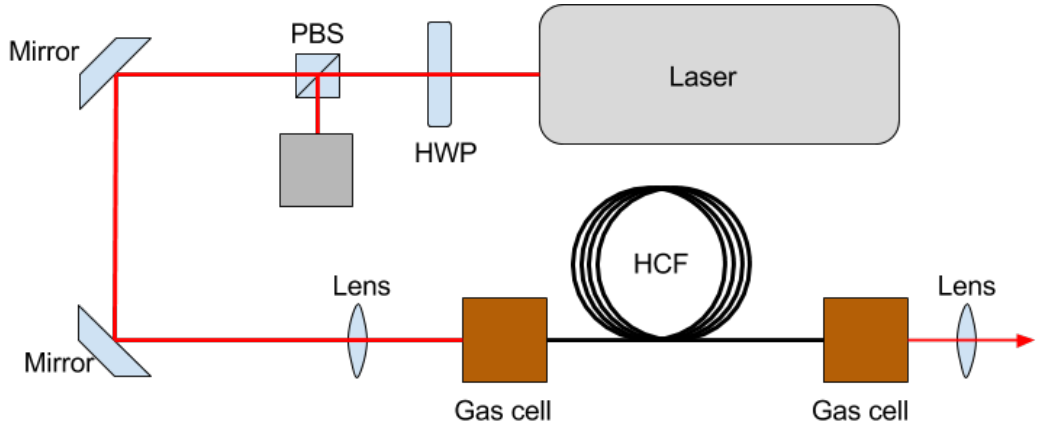

Figure 8.3.1 Experimental set up of gas filled hollow-core negative curvature fibre (HCF) and grating pair pulse compressor. The laser is a Fianium Hylase-25 10 ps pulse picked laser. Power control was provided by half wave plate (HWP) and polarizing beam splitter (PBS).

and output power was monitored with a thermal power meter. A CCD camera was used to image the beam profile on the output end face of the fibre. Each piece of measurement equipment was put in place as needed.

Prior to each experiment the NCF was flushed with argon to remove any residual air in the fibre or gas cells. The fibre was then pressurised and left for 20 - 30 minutes to equilibrate. Filling time for this fibre was calculated to be less than two minutes but longer was given to allow any particulates in the gas cells to settle prior to switching on the laser to ensure they are not pushed into the fibre. A slight pressure gradient was placed across the fibre of <0.5 bar from the output end to the input end to ensure glass fragments did not enter the fibre in the event of end face damage.

8.3.2 Anomalous dispersion fibres and modulation instability in Argon

The fibres used in this section are those used in the previous section with the exception of the 13 m fibre which was shortened to a 7 m piece used in these experiments and an additional 9 m piece was tested. These were all designed to have a central

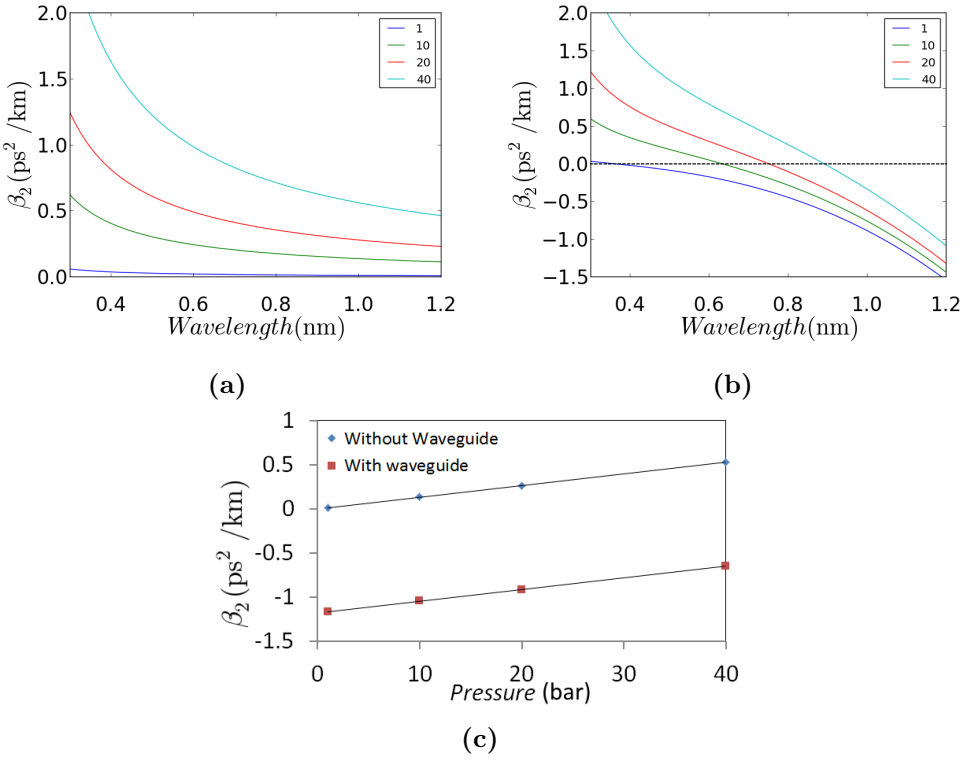

Figure 8.3.2 a) Group velocity dispersion of argon at different pressures, b) dispersion of argon with waveguide dispersion of a capillary of 34 µm in diameter. Legend is pressure of argon in bar. c) Estimation of the total group velocity dispersion at a wavelength of 1064 nm.

wavelength of 1064 nm in the main transmission band. Working at 1064 nm the dispersion is close to the zero dispersion point of the fibre but is slightly anomalous from the waveguide dispersion as discussed in chapter 2.4. Argon has a normal material dispersion that varies with pressure. This is estimated from the Sellmeier coefficients of argon[7] and shown in figure 8.3.2a. The group velocity dispersion in a NCF is similar to that of a capillary,[27] the combination of material and waveguide dispersion is shown in figure 8.3.2b. The dispersion expected at 1064 nm in these fibres at different pressures is shown in figure 8.3.2c.

In these experiments, the fibre was tested at a repetition rate of 100 kHz . The laser had a maximum output of 3.5 W corresponding to a pulse energy of 35 µJ at 100 kHz . The end face was observed to damage more easily with increasing argon pressure, thus the maximum power recorded in each experiment is adjusted accordingly. There was some variance from initial coupling efficiency and drift over time, quality of end cleave and in fibre structure; the threshold typically varied from > 3.5 W at 1 bar , to approximately 2.5 W at 10 bar and to 1 W at 40 bar .

The results of spectral broadening with pressure were recorded with a 7 m length of fibre, from the 13 m section mentioned previously in this thesis, and are shown in figure 8.3.3. At 1 bar there is evidence of spectral broadening but no clear SPM peaks are visible at 3 W (22 µJ pulse energy coupled into the fibre core). At 10 bar two SPM peaks become visible at 0.5 W (4 µJ in fibre core), this then increases to three and then four at 1.6 W (12 µJ). Fibre pressurised to 25 bar reached six SPM peaks in the spectrum at 1.4 W , but was distorted at higher powers. This was not due to fibre damage as the fibre was still intact after 2 W of average power was incident on the fibre. A comparison of the spectra for 1 W and 1.7 W of incident power on the fibre pressurised to 25 bar is also shown in figure 8.3.3. Even at low incident power the spectrum showed some asymmetry with more power in the shorter wavelengths. At higher powers of 1.7 W the spectrum became more structured indicating there is something affecting the pulse beside SPM.

The spectral broadening increased with power and pressure as expected. The

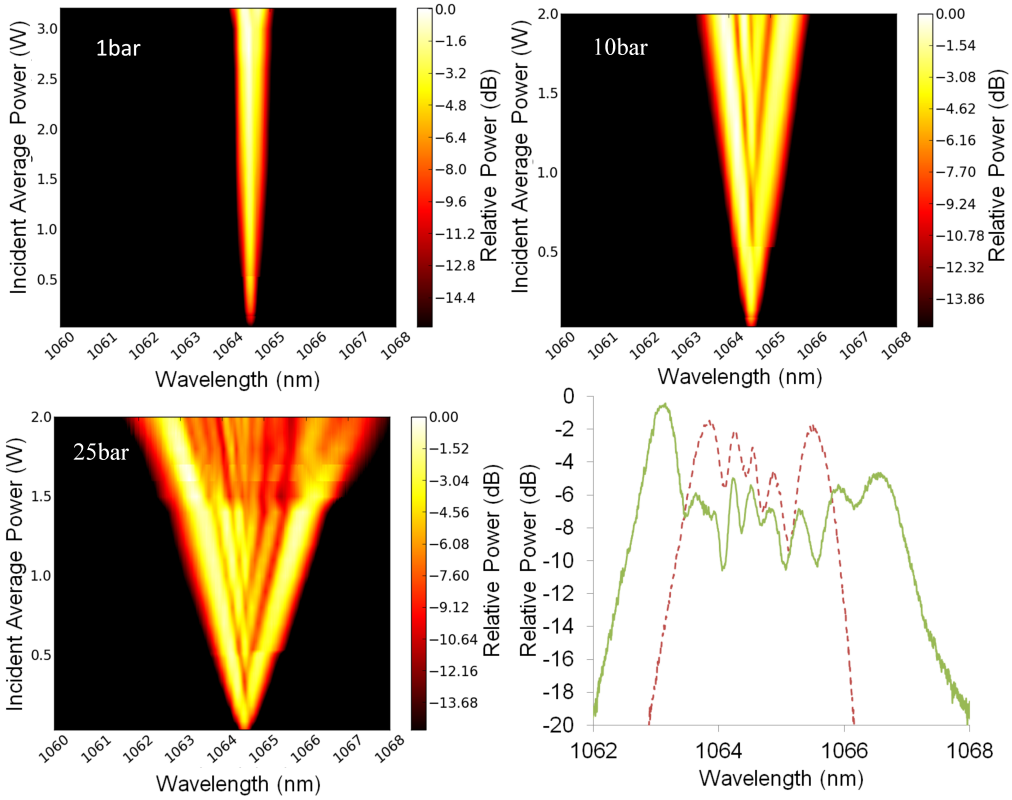

Figure 8.3.3 Pulse spectra with incident average power which is controlled by rotating the HWP on the output of the laser. The repetition rate was 100 kHz and pressures of argon are given for the respective heat maps. A slight discontinuity is observed at 0.5 W due to changing the amplification regime of the laser itself. Fibre loss is estimated as 0.04 dB/m. Initial coupling efficiency to the core was 73%, 75% 74% for 1, 15 and 25 bar respectively. Bottom right figure shows the spectrum from the fibre pressurised to 25 bar at 1 W (red dashed line) and 1.7 W (green solid line).

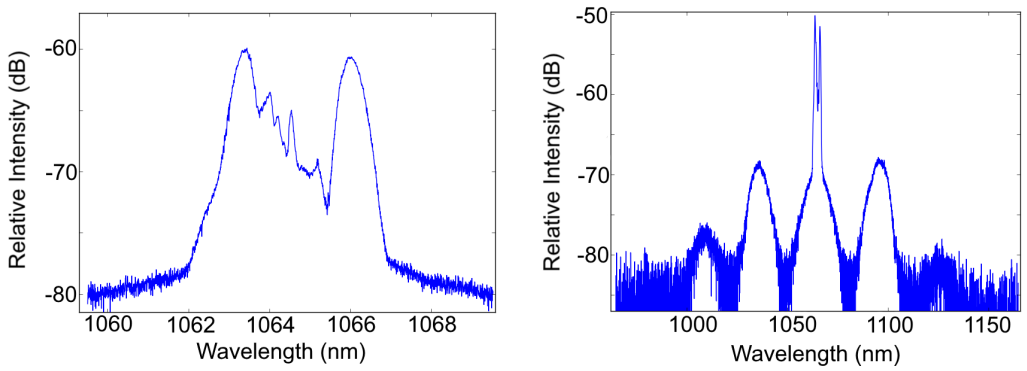

Figure 8.3.4 a) Pulse spectra taken at 1.7 W of incident average power (12 µJ pulse energy coupled into the core) in the 9 m length of fibre pressurised to 25 bar . b) Wider wavelength window showing the onset of modulation instability.

fibre was pressurised up to 40 bar but only survived to 0.9 W before end face damage started occurring. The practical working pressure of this experiment was considered to be 25 bar to obtain reliable results without fibre damage. The amount of SPM allowed for the nonlinear refractive index of argon at different pressures to be calculated. This is summarised later with the results from the normal dispersion fibre in figure 8.3.10.

An identical fibre of 9 m was also tested that had the same design but from a different fibre draw. This fibre exhibited similar behaviour but with more structure in the spectra. There is also a consistent asymmetry with more power being in the shorter wavelength side of the spectra which is indicative of self steepening as discussed in chapter 2.6. This is visible in figure 8.3.4a showing the spectra at 1.7 W of average power (12 µJ pulse energy in the fibre core) from the 25 bar results. There is similar structure visible in all spectra at higher powers and gas pressures. Figure 8.3.4b shows a wider spectral window of the same pulse shown in figure 8.3.4a. In this window clear side lobes are visible either side of the main pulse spectrum. These are caused by modulation instability (MI) of the pulse which was discussed in chapter 2.6. The position of these lobes gives information on the fibre dispersion as

the peaks of the side lobes are given by the angular frequency shift from the main pulse $\Omega_{\max}$ from equation 2.6.8:

$$\Omega_{\max} = \pm\left(\frac{2\gamma P_0}{|\beta_2|}\right)^{1/2}, \tag{8.3.1}$$

where γ is the nonlinear coefficient, P_0 is the peak power and β_2 is the group velocity dispersion. Both γ and P_0 are reasonably well known from experimental conditions but can also be verified from the SPM results of the fibre as the SPM is related to the phase shift $\phi = \gamma P_0 L_{\text{eff}}$. From this β_2 can be calculated. The MI of the 9 m and 20 m fibres was measured for different input powers and at five different pressures in the 9 m fibre and two in the 20 m fibre. Assuming the lowest average power has the least pulse distortion the dispersion can be estimated using the MI side lobe position at the MI threshold power. The corresponding β_2 value was then calculated and plotted in figure 8.3.5. Using the known group velocity dispersion of argon given in figure 8.3.2a and the measured nonlinear phase shift from the SPM observed, the waveguide dispersion of the fibre was then calculated to be 0.99 ± 0.05 ps^2/km for this wavelength. This is in good agreement with the approximated dispersion estimated from a capillary waveguide.[27]

One main discrepancy between the experimental results and the theoretical gain curves is that the position of the side lobes should vary with pulse peak power as indicated in equation 8.3.1. The peak of the MI side lobes was found in the same position for each input average power available from the MI threshold to the point of fibre damage. An example plot of the 9 m results taken at 20 bar is shown in figure 8.3.6 along with the corresponding theoretical gain curve. Simulations of the modulation instability in this experimental set up were conducted using the Python code discussed in chapter 5 and confirmed with Fiberdesk pulse propagation software. The simulations used the group velocity dispersion values corresponding to those in figure 8.3.5 and the corresponding coupled pulse energy from the experimental results. The position of the MI side lobes matched for the lowest power, i.e. at

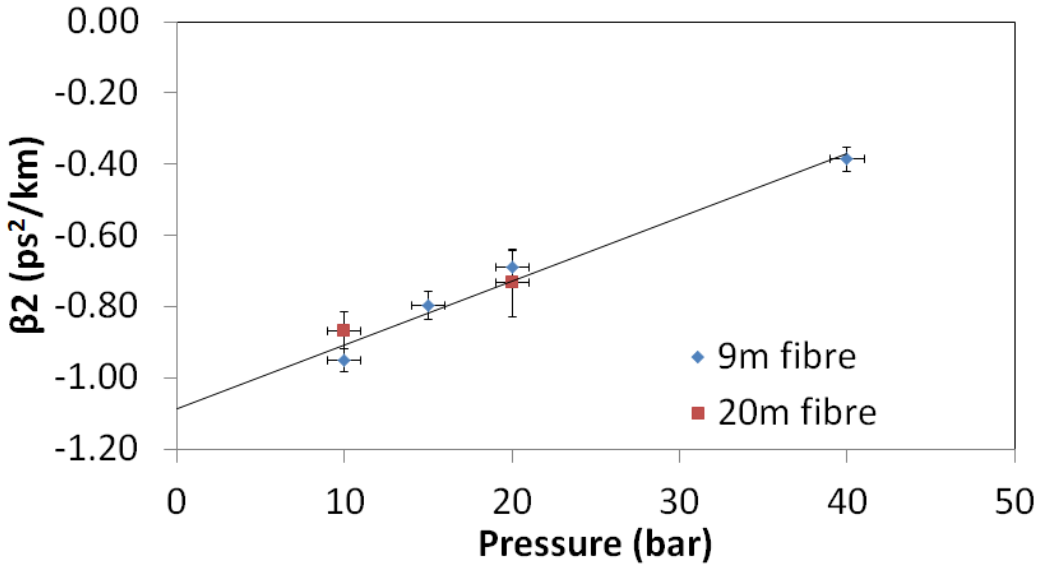

Figure 8.3.5 Measured group velocity dispersion for argon filled NCF fibre for different applied pressures of argon with a line of best fit.

the MI threshold, but still moved outward with increasing power as expected from theory with the peak shifting by approximately 6 nm at a pulse energy of 6.7 µJ, shown in figure 8.3.7. The simulations explored SPM effects, MI, self steepening, and third order dispersion without reproducing fixed MI side lobe positions. These effects were discussed in chapter 2. The MI was observed in three fibres and none of which showed a power dependence in the MI peak wavelength demonstrating this was not unique to one fibre.

The fact the side lobe positions do not change with average input power indicates that the peak power of the pulse is not scaling with the input average power within the fibre as expected. The peak power is dependent on the pulse energy and the shape of the pulse. The percentage of power transmitted through the fibre did not change with input power so it can be considered that the pulse shape must be changing or losing power to a dispersive wave. There is a difference of approximately 20dB between the peak of the main pulse and the peak of the side lobes so rela-

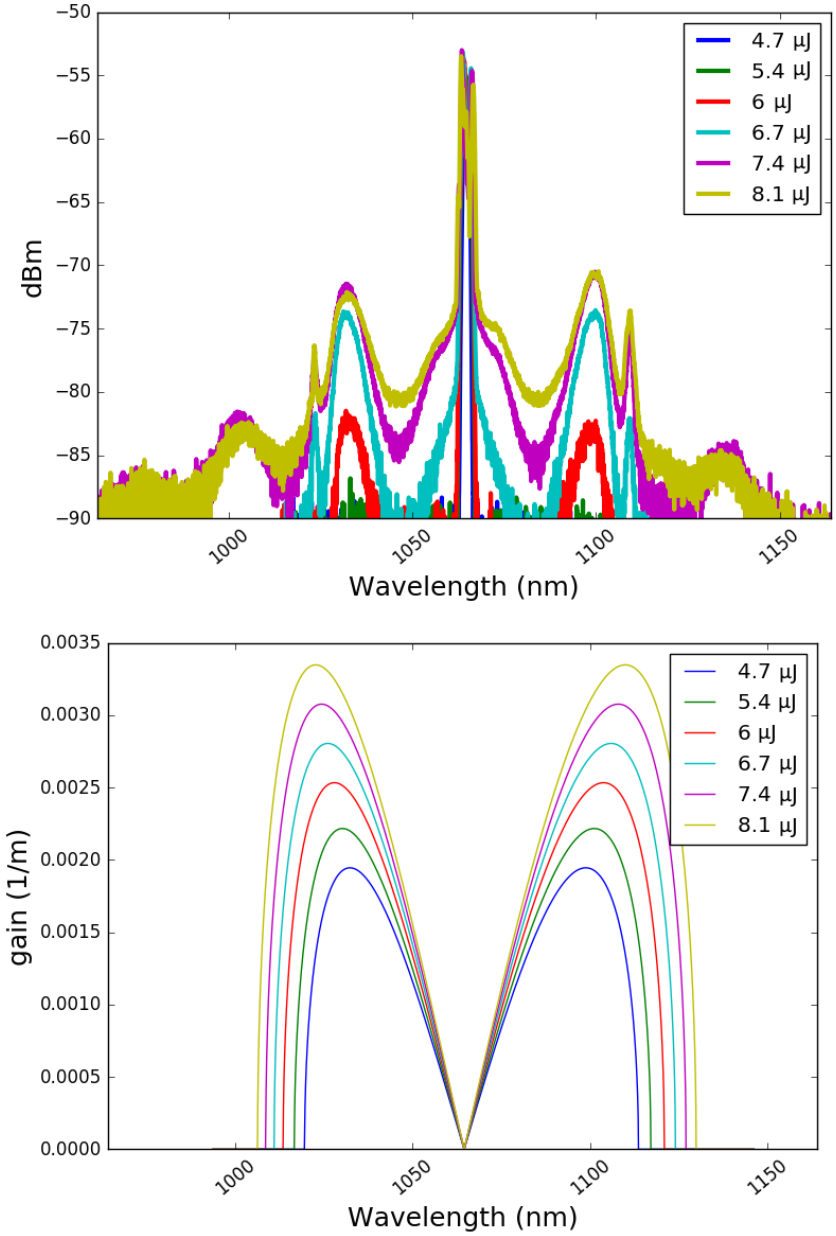

Figure 8.3.6 a) Modulation instability in 9 m fibre at 20 bar of argon for different incident average powers given in legend in mW. b) Theoretical modulation instability gain calculated for $\gamma = 2.5 \times 10^{-6}$ $\mathrm{W^{-1}m^{-1}}$, $\beta_2 = 1.2$ $\mathrm{ps^2/km}$ with pulse energies matching those coupled into the fibre the 20 bar, 9 m fibre experiment.

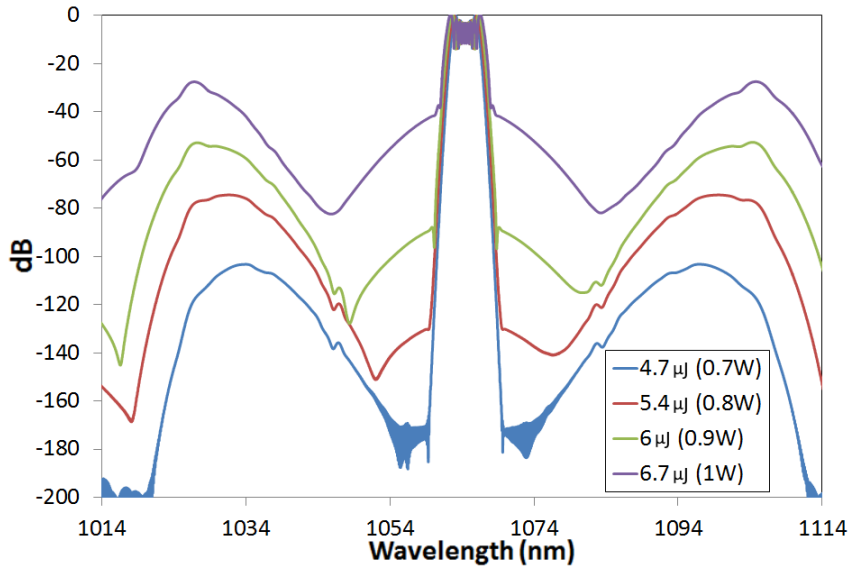

Figure 8.3.7 Fiberdesk simulation of modulation instability 9 m fibre using experimental parameters using a β_2 value of 1 ps^2/km.

tively little energy is being leached into the MI structure. Also if MI distortion was the main factor affecting the pulse peak power, the position of the MI side lobes would appear more random instead of clamped to one wavelength and would be reproducible in numerical simulations. The pulse peak power could also reduce if the pulse were getting broader as it propagated through the fibre. However, the pulse duration was measured from autocorrelations and was found to remain reasonably constant with some decrease in pulse duration with increasing pulse power. An example set of autocorrelations and MI spectra are shown in figures 8.3.8a and 8.3.8b. The measured FWHM duration of the pulse decreases slightly with increased incident average power but the shape is also changing in the autocorrelation trace. The changes are in the main shape of the pulse and in the appearance and then disappearance of side lobes with increasing power.

Clamping of the MI side lobes has been observed in previous work in fibre with pulsed light, such as the work by Wadsworth et al.[81] This was shown to happen in solid core silica fibre and exhibited a fixed MI side lobe position for different incident

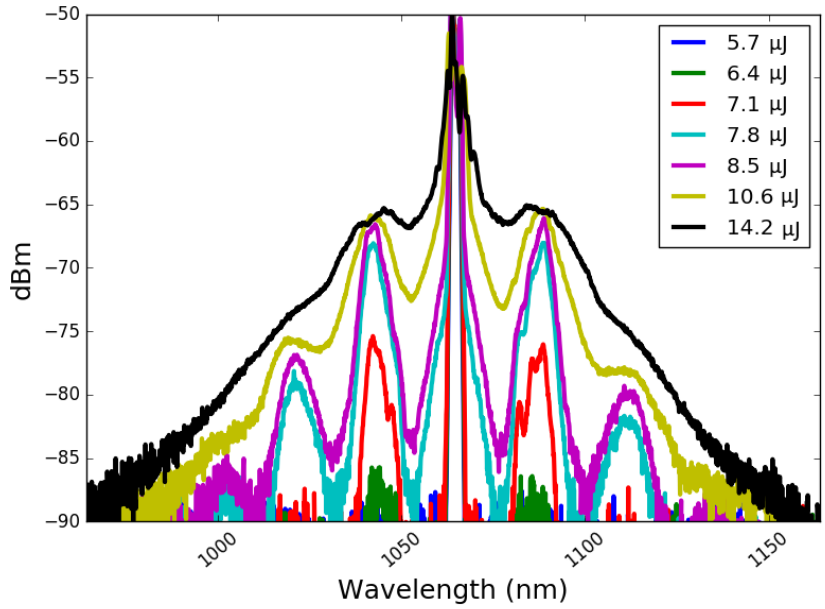

(a)

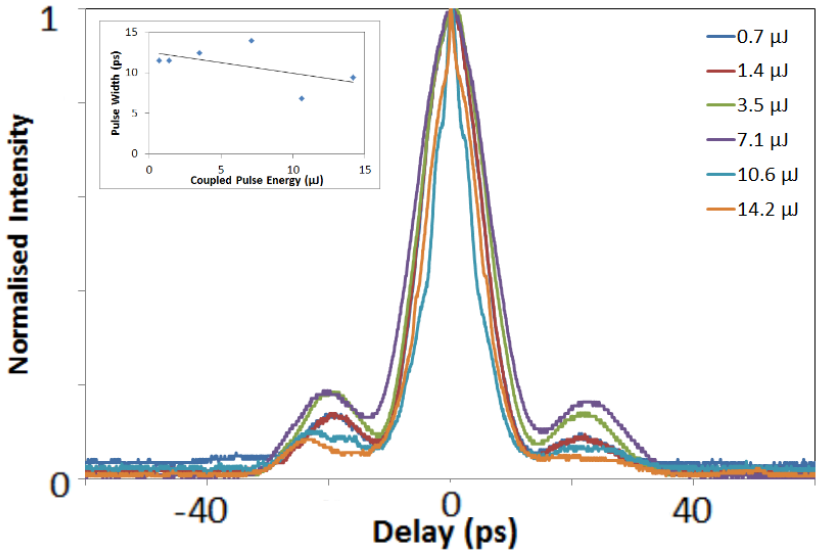

(b)

Figure 8.3.8 a) Pulse spectrum showing modulation instability side lobes for 20 m NCF at an argon pressure of 10 bar. b) Corresponding autocorrelations of the pulse, inset shows measured pulse duration. Legend shows the pulse energy coupled into the core calculated from the fibre measured throughput and the fibre loss.

powers. The position also varies with the length of the fibre in this paper but this was not reproduced with the argon filled NCF experiments. So far there is not a definitive explanation for this behaviour though it is possible that the modulation instability is being seeded by another effect. Though if another process is seeding the modulation instability it would invalidate the dispersion value for this fibre mentioned earlier.

In some of the spectra measured, narrow peaks at approximately 1023 nm and 1109 nm where observed as shown in figure 8.3.6. These are not present in every experiment and are not present in the results given in figure 8.3.8a. These peaks are always at the same wavelength and the behaviour is indicative of vector modulation instability arising from the small birefringence of the fibres slightly elliptical core. These peaks are only observed when light is coupled to both the fast and slow axis of the fibre. This was not controlled for during the experiments but is dependent on the fibre orientation in the gas cell. Future experiments could control the appearance of these peaks by controlling the input polarisation state with a half wave plate.

8.3.3 Normal dispersion fibres filled with argon

In contrast to the previous section, this section reports results of using a fibre with normal group velocity dispersion. The key difference in this is that scalar modulation instability is limited to the anomalous dispersion regime under normal circumstances. Although modulation instability gives a useful insight into the characteristics of this fibre, it does limit the SPM broadening needed for practical pulse compression. Operating in the normal dispersion regime in this case has the advantage of not supporting modulation instability or other soliton effects that would distort the pulse.

The same experimental set up was used as with the anomalous dispersion experiments shown in figure 8.3.1. The fibre used in this section was an 18 m length of NCF and had a central wavelength of 1200 nm with 1064 nm lying on the short wavelength edge of the main transmission window. From the Kramers-Kronig relations

the dispersion is known to be in the normal regime.[16] This fibre has an estimated loss of 0.12 $\mathrm{dB\,m^{-1}}$ deduced from observed transmission and coupling efficiencies achieved as no cut back has been performed on this fibre to preserve its length. The fibre also supported the $\mathrm{LP_{11}}$ as well as the fundamental mode, meaning that careful coupling was needed to ensure minimal interference from the higher order modes.

This fibre was also tested at different pressures of argon and at repetition rates of both 50 kHz and 100 kHz. A repetition rate of 50 kHz was favoured as higher peak powers could be reached with this fibre. For example, at 20 bar of argon pressure the fibre end face failed at an average incident power of 1.5 W at 50 kHz but at 100 kHz the end face failed at approximately 2.5 W of incident average power. This indicated that the fibre damage is not directly correlated to just peak power but is susceptible to high average power from the higher repetition rates. The spectral results for the 50 kHz experiments are shown in figure 8.3.9. These results were obtained by optimising the coupling for the purest fundamental mode by using a CCD camera to monitor the output mode pattern and check if the pattern distorts when perturbing the fibre. This was not always the highest throughput through the fibre but provided the cleanest SPM peaks. As expected, the SPM broadening increases with argon pressure. Up to 20 bar of pressure clean SPM peaks were observed with some distortion appearing at higher coupled pulse energies. At pressures of 25 bar and above the spectra had additional structure to the SPM peaks even at low powers as seen in figure 8.3.9. This structure on the spectrum would be detrimental to compression.

Some spectral distortion can be attributed to interference from higher order modes. Measurements were conducted to test the quality of the output beam from the fibre using the $\mathrm{M^2}$ technique. This was done through the gas cell at 20 bar of argon pressure. The beam was found to have an $\mathrm{M^2}$ value of 1.46. Using a polarising beam splitter cube the higher order mode could be removed after the fibre output and the beam $\mathrm{M^2}$ measurement improved to 1.26.

The broadest, clean SPM achieved was ≈ 10 nm with 15 peaks at 1.5 W at 20 bar of

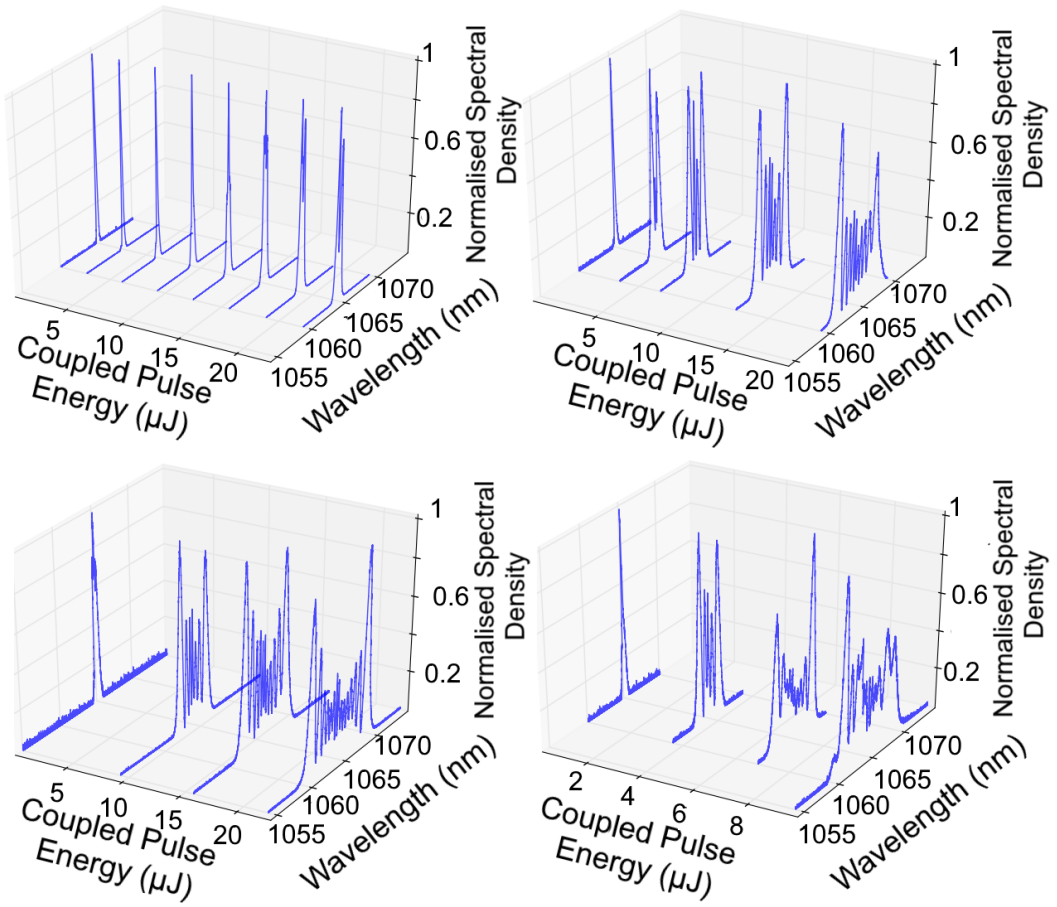

Figure 8.3.9 Spectra from the output of 18 m of NCF in the normal dispersion regime at a repetition rate of 50kHz. Top left is 1 bar , top right is 10 bar , bottom left is 20 bar and bottom right is 25 bar .

pressure shown in figure 8.3.9. The large number of SPM peaks observed in these experiments enabled a good estimation of the nonlinearity involved. Using equation 2.6.6 the nonlinear refractive index of argon was calculated for different pressures using both the anomalous and normal dispersion regime results. These are shown in figure 8.3.10. These figures were calculated using the estimated fibre attenuation of each fibre to get the effective fibre length, assuming a sech^2 temporal shape and the estimated coupling efficiency to calculate the peak power within the core, the mode-field was approximated as a Gaussian shape with a diameter of 28 µm. The nonlinear refractive index was calculated for each point by taking the gradient of the number of SPM peaks generated as a function of peak power for each pressure in each fibre. The anomalous regime results were taken from below the modulation instability threshold to ensure spectral distortion did not affect the nonlinear refractive index measurements.

The results show good agreement with the exception of the 9 m, 50 kHz results in figure 8.3.10 which read consistently higher for that set of experiments. The reason for this in unclear as the fibre showed agreement when measured at 100 kHz repetition rate and each pressure reading involved purging the system before the experiments, coupling the light to the core each time and were taken on different days so it is unlikely to be random experimental error.

These results indicate that the nonlinear refractive index of argon at 1 bar of pressure is $(1.5 \pm 0.4) \times 10^{-23}$ m^2/W with a pressure dependence of $(1.29 \pm 0.04) \times 10^{-23}$ $\text{m}^2/\text{W}/\,\text{bar}$. This value lies in the lower region of the values presented by Börzsönyi[75] in the literature summary. As there is little overlap of the light with the silica guiding structure there is little contamination from the nonlinear refractive index of silica in the measured n_2 here. Also, as the measurements were conducted at high pressures resulting in clear SPM peaks that could easily be counted there is little interference from other nonlinear effects that could affect a measurement of pulse broadening alone. The light through the fibre maintained a linear polarisation measured using the extinction ratio by a polariser and half wave plate on the fibre

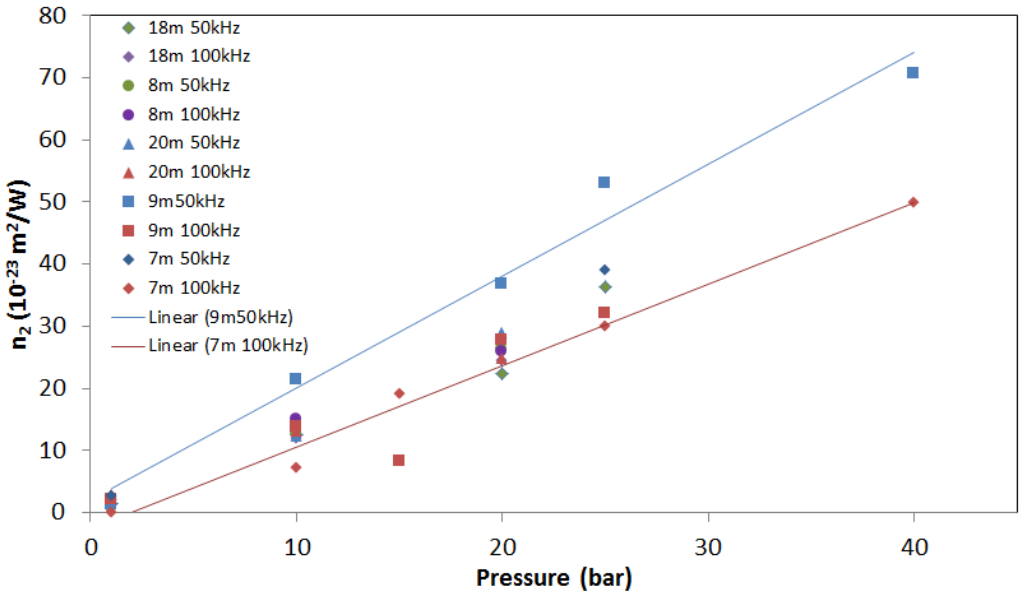

Figure 8.3.10 The calculated nonlinear refractive index of argon using the number of SPM peaks generated at different pressures of argon. Results are from normal dispersion fibre (18 m) and the rest are from anomalous dispersion fibre results. Two lines of best fit were used to highlight the difference between the 9 m, 50 kHz results and the result of the measurements.

output, although the orientation of the polarisation could be changed by moving the fibre. These factors indicate the n_2 results obtained here are reliable and can be applied to future work with nonlinear effects in argon.

8.3.4 Pulse compression

The results from studying the spectra at different incident power levels at different pressures found the optimum parameters to produce clean and broad SPM were a pressure of approximately 20 bar , an incident power of less than 1.5 W and a 50 kHz repetition rate. The set up for pulse compression used the same set up as shown in figure 8.3.1 with a double pass grating pair added to the output. The grating pair applies a dispersion of approximately 1 ps nm^{-1}. The output from the grating pair was then measured with an autocorrelator to obtain the compressed pulse duration. The precise amount of dispersion applied to the pulse was controlled by the grating separation which was adjusted to provide the optimal compression for a given pulse bandwidth.

The pulse compression was performed with 18 bar of pressure and the system was left to equilibrate. Coupling was optimised to minimise the presence of higher order modes reaching a coupling efficiency of approximately 80% at a repetition rate of 50 kHz . The coupling efficiency was estimated from the measured throughput through the core using a power meter on the input and output then factoring in the estimated fibre loss. Autocorrelations and spectra were taken for a range of input powers and the pulse compression was found to be optimum at an input average power of 1.2 W ($\approx$ 20 µJ pulse energy and a peak power of 1.7 MW coupled into the core). This power produced 7.6 nm of SPM broadening shown in figure 8.3.11 corresponding to a phase shift of 12.5π. The 10 ps pulse was compressed to 420 fs as shown in figure 8.3.12a. The output energy was $\approx$ 8 µJ after fibre and compressor loss.

Higher powers did produce further compression reaching 360 fs at an incident power of 1.4 W (22 µJ) coupled pulse energy. However, the autocorrelations showed

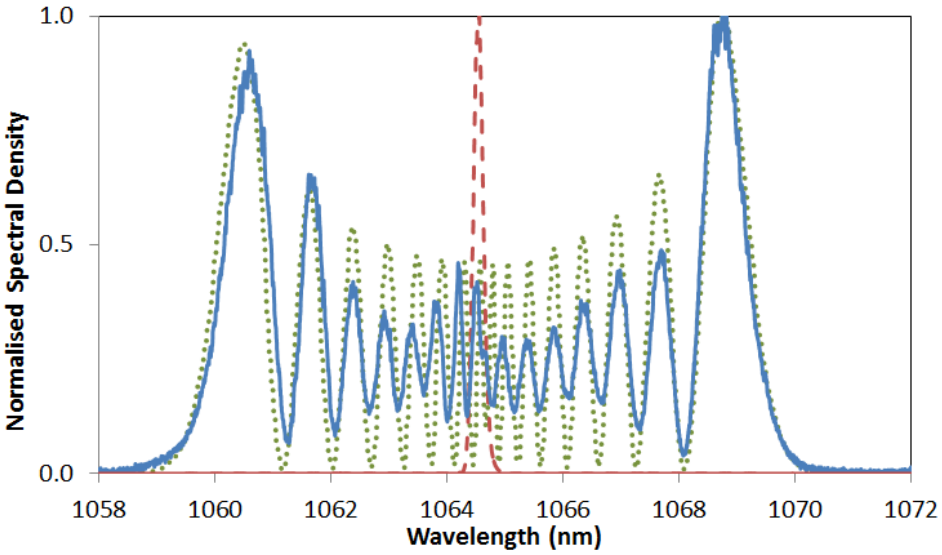

Figure 8.3.11 Pulse spectra of the input laser with 0.2 nm bandwidth (red dashed), spectra after propagating in fibre showing 7.6 nm FWHM bandwidth (blue solid) and simulated SPM spectra using experimental parameters (green dotted). The simulations were conducted with; $n_2 = 21 \times 10^{-23}\,\mathrm{m}^2/\mathrm{W}$, MFD = 30 µm and $\beta_2 = 2\,\mathrm{ps}^2/\mathrm{km}$.

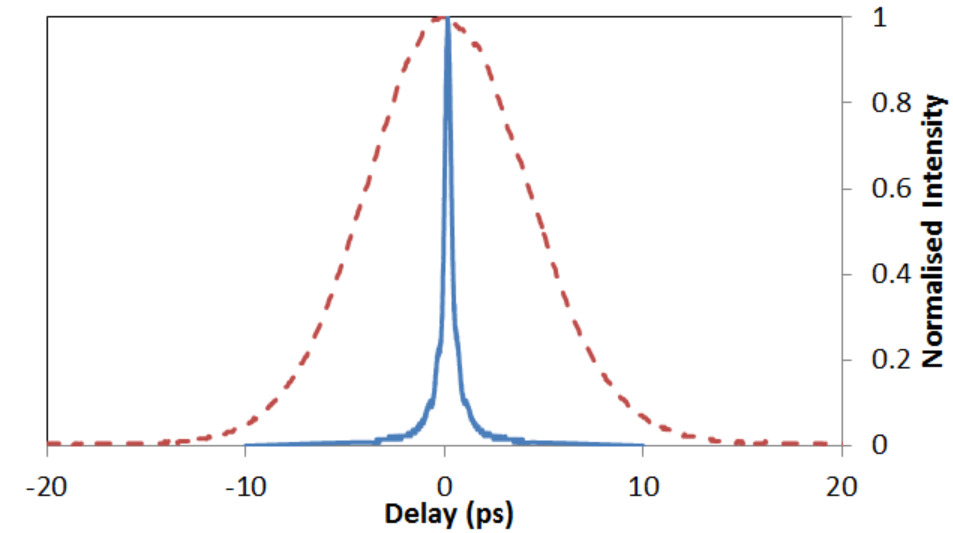

(a)

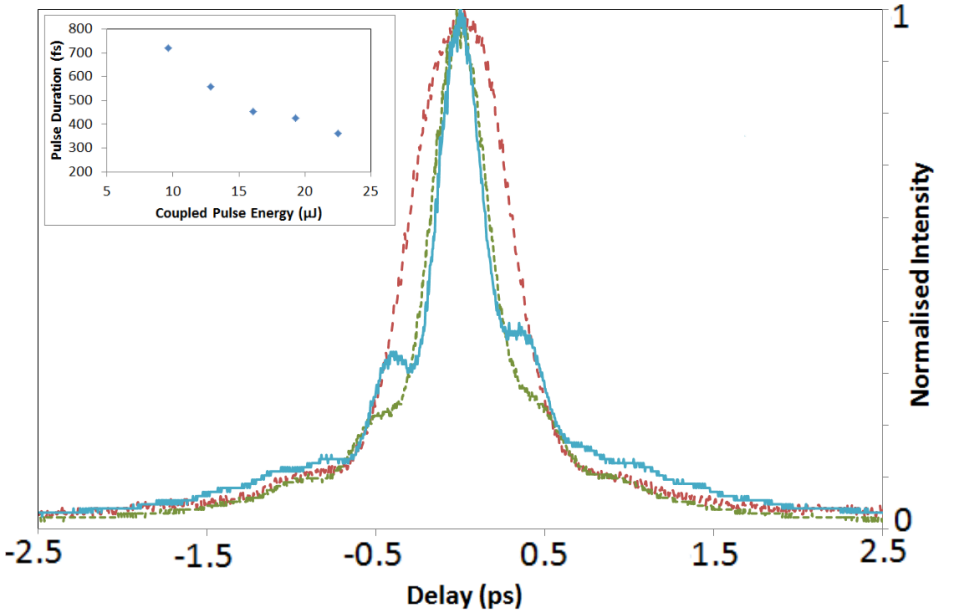

(b)

Figure 8.3.12 a) Autocorrelation traces from laser measuring 9.6 ps (red dashed) and after compression measuring 420 fs (blue solid). Results obtained with 18 bar of argon and input pulse energy of 24 µJ. b) Autocorrelation traces of the compressed pulse with a coupled pulse energy of 9.6 µJ (red dashed line), 19.3 µJ (green dotted line) and 22.5 µJ (blue solid line). Inset shows measured compressed pulse duration.

additional structure indicating pulse distortion. Comparisons of the autocorrelations and the pulse durations achieved in this work are shown in figure 8.3.12b. The power was not increased past this as this 1.5 W consistently ablated the fibre end face.

To reach further compression, an increase in the pulse bandwidth would be required. Increased spectral broadening could occur with greater nonlinearity. This can be done using higher pressures if the cause of the added spectral structure can be eliminated either by using shorter pulses to minimise inter-atomic collisions during excitation or in minimising interference from higher order modes. Creating an NCF that is single moded at this wavelength would be advantageous in eliminating distortion from higher order modes. Further increases in nonlinearity could be achieved with higher peak power but this would need to be done without damaging the fibre. Using an even lower repetition rate source to reduce the average power could achieve this as results showed that higher pulse energies could be tolerated by the fibre at lower repetition rates. The damage threshold could also be improved with better coupling efficiency into the core so less light is incident on the glass structure at the input end of the fibre. This could be done with higher quality lenses, redesign of the gas cell to allow a shorter coupling distance, and in improving the beam quality from the laser. An improved coupling system would also include reducing the drift in the coupling system with time as this drift also damages the fibre as the focus of the beam shifts from the centre of the core. An additional method to increase the nonlinearity in the fibre is to use a different gas with a higher nonlinear refractive index. There are gases with negligible Raman response that have a higher n_2 in the noble gas group such as xenon;[75] though these gases tend to be of higher price which could be detrimental in any industrial application settings.

8.4 Conclusion and outlook

This chapter has covered the spectral broadening induced by self-phase modulation in gas filled hollow core negative curvature fibre. The effects and limitations of air at atmospheric pressure were explored for a range of pulse powers and successfully

demonstrated SPM broadening in this fibre. The spectrum of pulses through air filled NCF was heavily structured by nonlinear effects other than the desired SPM.

Using multiple lengths of NCF pressurised with argon gas, the effects of SPM were observed and used to deduce the nonlinear refractive index of argon at different pressures. The nonlinear refractive index found was in the range of the values provided in literature.

In the anomalous regime, modulation instability was observed and used as a method to measure the dispersion of this fibre design with the waveguide dispersion measured to be -0.99 ± 0.05 ps^2/km at the design wavelength of 1064 nm .

In the normal dispersion regime, SPM was the dominant nonlinear effect in the workable power range of this fibre in these conditions. This produced sufficient clean pulse broadening to 8 nm from 0.2 nm allowing for a compression from the picosecond to the femtosecond pulse regime. This was demonstrated with a compression from 10 ps to 420 fs by using a grating pair after the fibre.[82]

Further work would include exploring this with different gases, preferably with no Raman response and a higher nonlinear refractive index to improve the pulse broadening. Developments in the fibre design can also potentially improve the results. Improvements can be made by fabricating a single mode NCF at the operational wavelength. This would negate interference from higher order modes and in increasing the power tolerance of the fibre.

Chapter 9

Conclusion

This thesis has investigated the theoretical and experimental methods of using different optical fibres for reducing the pulse repetition rate of a mode locked laser and the use of gas filled hollow core fibre as a means to create pulse spectral broadening.

The theory of the optical fibres considered in this thesis were presented which pertained to both fabrication of these fibres and their use in mode-locked fibre lasers. This was also modelled numerically in addition to the experimental results given.

Low repetition mode-locked lasers operating in the normal dispersion of silica were shown to be limited by the cumulative nonlinear phase shift acquired by the pulse in a round trip of the laser cavity. This sets an upper pump power limit where the pulse will break into multiple pulses if exceeded and this limit decreases with extra cavity length until no fundamental mode-locking can occur.

Investigations of low repetition mode-locked lasers cavities included the use of large mode area (LMA) fibres to reduce the intensity of the guided light and thus the nonlinear phase shift incurred. Experimentally, this method showed some promise with the reduction in pulse repetition rate from 20 MHz to 7.6 MHz of a 4 ps pulse at an operational wavelength of 1064 nm. The integration and design of the LMA fibres required careful consideration of the spatial mode behaviour within the laser cavity. This work then split into another project taken over by Ben Cemlyn and Fianium ltd.

The use of hollow core fibre provided a more drastic change in nonlinearity compared to increasing the mode area of the fibre as it changes the medium the light is propagating through. The use of hollow core fibre necessitates the consideration of effective integration of the hollow core fibre into the cavity while limiting unwanted reflections at the interface between fibre cores. A free space coupling stage with angle polished solid core pigtails in a ring configuration proved to be an adequate method of integration in this work. Further development is possible with creating an angle splice between the hollow and solid core fibres for a more robust and permanent integration of the hollow core fibre into a fibre laser cavity.

Initial mode-locked cavity experiments with hollow core fibre used hollow core photonic crystal fibres (PCFs) which were used to construct an operational mode-locked cavity at short lengths reaching a pulse repetition rate of 27 MHz reduced from 37 MHz for a 4 ps pulse at 1064 nm . However the introduction of longer lengths of PCF was limited by the high fibre loss and the depolarisation of the light within the PCF. This could be further explored with the development of a non-PM laser cavity but the experiments with negative curvature anti resonant fibre (NCF) proved not to suffer these same polarisation issues and so is the favoured fibre for this purpose.

The use of NCF proved to be an effective method to reduce the pulse repetition rate as a reduction from 37 MHz to 5.4 MHz was achieved with no detriment to the pulse duration or spectrum. The negligible nonlinearity and dispersion of the NCF makes it an appealing delay fibre. The current limitations of this work are in the constraints of fibre fabrication restricting the maximum lengths of good quality fibre that can be made. Improvements to the drawing methods that allow for longer lengths to be fabricated would allow for lower repetition rates to be achieved.

The NCF drawn was also used as a means to create clean and symmetric spectral broadening of a 10 ps pulse centred at 1064 nm in a single pass. The use of pressurised argon provided a sufficient nonlinear response to produce self-phase modulation without distortion from Raman effects that occur in air and in silica. The spectrally broadened pulse was then compressed to 420 fs with the use of a grating pair on the

fibre output. The analysis of the nonlinear effects in the argon filled fibre allowed for characterisation of the fibre dispersion in the anomalous regime and also provide an estimate of the pressure dependent nonlinear refractive index of argon at 1064 nm .

With further development of laser stability and robustness the low repetition lasers produced here could be an attractive seed laser with applications that require high pulse peak power, but not necessarily high average power such as machining or as a seed for supercontinuum generation. The compression of a pulse, like that achieved here with gas filled hollow core fibre and grating pair, to further increase the peak power is also applicable to these applications as well increasing the fundamental understanding of the physics of the optical fibres studied.

Appendix A

Publications

A.1 Papers corresponding to chapter 7

Harvey, C., Yu, F., Knight, J. C., Wadsworth, W., & Almeida, P. (2015). "Reducing Nonlinear Limitations of Ytterbium Mode-Locked Fibre Lasers with Hollow-Core Negative Curvature Fibre," Cleo: 2015 (p. STh1L.5), Optical Society of America. http://doi.org/10.1364/CLEO_SI.2015.STh1L.5

Harvey, C. M., Yu, F., Knight, J. C., Wadsworth, W. J., & Almeida, P. J. (2016). "Reduced Repetition Rate Yb3+ Mode-Locked Picosecond Fiber Laser With Hollow Core Fiber," IEEE Photonics Technology Letters. JOUR. http://doi.org/10.1109/LPT.2015.2504407

A.2 Paper corresponding to chapter 8

Harvey, C., Yu, F., Knight, J. C., Wadsworth, W., & Almeida, P. (2016). "Spectral Broadening and Pulse Compression Using Argon Filled Hollow-core Negative Curvature Fiber" Cleo: 2016(p. STu4P.3), Optical Society of America. http://doi.org/10.1364/CLEO_SI.2016.STu4P.3

Reducing Nonlinear Limitations of Ytterbium Mode-Locked Fibre Lasers with Hollow-Core Negative Curvature Fibre

C. M. Harvey[1]*, F. Yu[1], J. C. Knight[1], W. J. Wadsworth[1], P. Almeida[2]

[1]*Centre for Photonics and Photonic Materials, Department of Physics, University of Bath, Bath, BA2 7AY, UK*
[2]*Fianium ltd. 20 Compass Point, Ensign Way, Southampton SO31 4RA, UK*
**c.m.harvey@bath.ac.uk*

Abstract: Ultralow nonlinearity hollow-core negative curvature fibre is used in a mode-locked Ytterbium fibre laser to prevent the onset of pulse breakup at low repetition-rates. Identical pulse peak-power limit at 37MHz and 11MHz is experimentally demonstrated.

© 2014 Optical Society of America
OCIS codes: 140.3510, 140.3615, 140.4050

1. Introduction

Mode-locked fibre lasers are traditionally known for high repetition rates, typically 80MHz and above, and short (picosecond or below) pulse lengths. There are applications for which similarly short pulses at lower repetition rates are desirable, such as cold material processing. Mode-locked oscillators producing short pulses at a low repetition-rate can simplify laser system design by removing the need of additional amplification and pulse-picking. Lower repetition rates however require longer cavity lengths. For conventional soliton mode-locked fibre laser designs, longer cavity lengths and higher pulse energies both lead to an increase in nonlinear phase shift per round trip which leads to pulse break-up and undesirable mode-locking characteristics. The lowest repetition-rate reported for a mode-locked fibre laser is 37kHz, but it produced 10ns pulses due to the strong nonlinear evolution in the normal dispersion regime [1]. For a soliton mode-locked laser, the nonlinear phase shift, ϕ, which the pulse acquires in propagation through the cavity causes breakup at $\phi_{max} = \gamma L P_0 = \pi$ [2] where γL is the cavity nonlinearity, P_0 is the pulse peak power. Stable fundamental mode-locking occurs therefore in a finite range of pulse energies between the mode-locking threshold, where the pulse energy is sufficient to achieve stable pulses, and the multi-pulse threshold where the pulse breaks into harmonic or bunched pulse regimes. This paper experimentally demonstrates the possibility of using state-of-the-art hollow-core fibre as means to extend the cavity length of a 4ps soliton laser without adding nonlinear phase shift and distortion to the pulses.

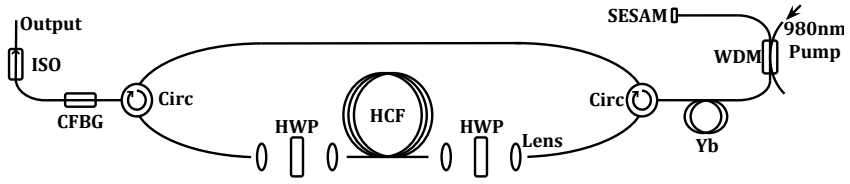

Fig. 1. Experimental setup of Yb mode-locked fibre laser based on ring cavity with hollow-core negative curvature fibre (HCF). ISO: optical isolator; HWP: half-wave plate; Circ: optical circulator; CFBG: chirped fibre Bragg grating; SESAM: semiconductor saturable absorber mirror.

2. Experiment

Our configuration is based on a polarisation maintaining ring cavity, Fig 1. The cavity comprises a SESAM mode-locking element and a chirped fibre Bragg grating (CFBG, used to periodically apply anomalous dispersion) incorporated via circulators. The Ytterbium gain fibre was pumped with a 980nm laser diode. A half waveplate was used to align the polarisation angles. We establish baseline data using a reference cavity with no hollow-core fibre and a free space coupling stage. After characterising the reference cavity we introduced different lengths of hollow-core fibre (HCF), 8m, 13m and 20m. The HCF is based on the negative curvature design with a core diameter of 34μm [3].

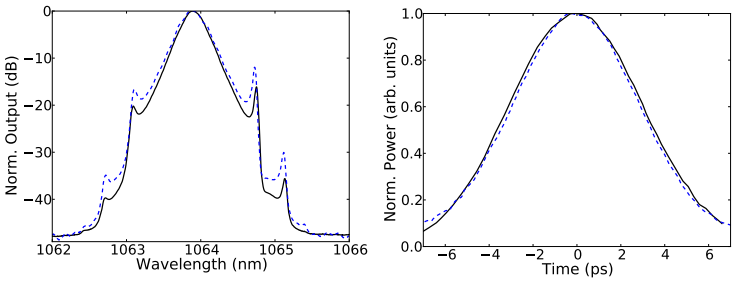

Fig. 2. Measured mode-locked pulses with (dashed line) and without (solid line) 20m of HCF. Left: Pulse Spectrum. Right: Autocorrelation.

3. Results

The reference cavity contained 5.4m of conventional solid-core fibre (in total) and oscillated at 37MHz. As the pump power was increased the laser evolved through operational states: CW, Q-switched mode-locking, desirable fundamental mode-locking then multi-pulsed mode-locking. Cavities with added HCF also showed this behaviour with similar pulses. Fig. 2 compares pulses from the reference cavity and a cavity with 20m of HCF oscillating at 11MHz.

Increasing the cavity length reduces the pump power needed for mode-locking, however the fibre attenuation introduced will increase the pump power needed. Using these effects and the reference cavity data, the mode-locking and multi-pulsing thresholds were calculated assuming a fibre attenuation of 0.04dBm^{-1} (Fig. 3(a)). The mode-locking and multi-pulsing thresholds were determined by examining the pulse spectra, oscilloscope and autocorrelation traces.

The mode-locking threshold shown corresponds to stable oscillations (although pulses were observed at lower pump powers). The stable mode-locking threshold can be affected by additional instabilities in the system from mode interference, polarisation effects within the hollow-core fibre and in the free space coupling. The multi-pulsing thresholds in Fig. 3(a) agrees well with the prediction indicating there is no additional nonlinearity in the cavity. This is reinforced by Fig. 3(b) which shows the calculated peak power for the reference cavity that would correspond to $\phi_{max} = \pi$.

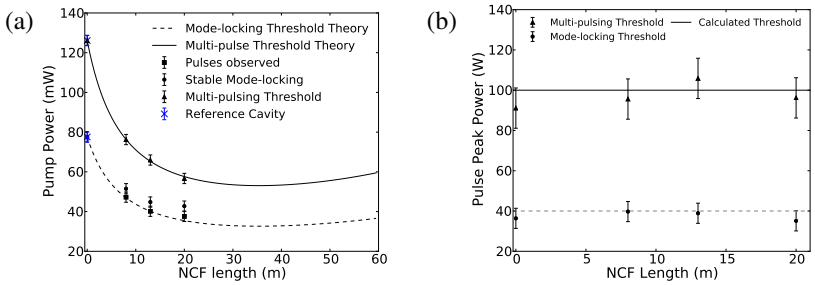

Fig. 3. (a) Predicted mode-locked ranges based on the measured reference cavity with experimental results. (b) Calculated peak pulse power corresponding to $\phi_{max} = \pi$ with measured intra-cavity pulse peak powers at lower and higher points of fundamental mode-locking.

4. Conclusion

Up to 20m of HCF has been added to an Yb^{3+} mode-locked fibre laser and shown not to introduce additional nonlinearity to the cavity. The results show that HCF can be used to extend short pulse Yb mode-locked laser length with minimum detriment to the pulses and could be a viable means to achieve low repetition rates. Further work can explore longer lengths of additional HCF and also the effect of different pulse lengths.

This work is supported by EPSRC industrial CASE award EP/K504245, TSB project TP101503, and Fianium Ltd.

References

1. Kobtsev, S.M. and Kukarin, S.V. and Smirnov, S.V. *Laser Physics* **20** (2010) pp. 375-378
2. Renninger, W.H. and Wise, F.W. *IEEE Journal of Selected Topics in Quantum Electronics* **21**, (2015) pp. 1-8
3. Yu, F and Knight, J.C. *Opt. Express* **21** (2013) pp. 21466-21471

Reduced Repetition Rate Yb^{3+} Mode-Locked Picosecond Fiber Laser With Hollow Core Fiber

C. M. Harvey, F. Yu, J. C. Knight, W. J. Wadsworth, and P. J. Almeida

***Abstract*— Anti-resonant guiding negative curvature hollow core fiber operating at a wavelength of 1064 nm is used in the cavity of an ytterbium (Yb^{3+}) mode-locked fiber laser to increase cavity length without increasing the nonlinear phase shift. Repetition rates from 37 to 5.4 MHz are demonstrated using lengths of hollow core fiber up to 48 m in length. Each constructed cavity produced coherent 4-ps 1/e2 duration soliton-like pulses, with no degradation of the pulse peak power or pulse shape at lower repetition rates. Both the spectral distributions and the autocorrelations of output pulses are compared along with the mode-locking and multi-pulse power thresholds.**

***Index Terms*— Fiber lasers, fiber nonlinear optics, laser mode-locking, ultrafast optics.**

I. Introduction

MODE-LOCKED fiber lasers are becoming an increasingly common tool in many areas of industry and scientific research. They are typically known for producing short pulses of picosecond length or shorter at repetition rates of 80 MHz and above while being robust and compact in nature compared to their solid state counterparts. Many applications of such lasers however require coherent short pulses at lower repetition rates including ultrafast laser material processing where high peak intensity pulses can ablate a material without collateral damage [1], and stimulated emission depletion microscopy with a supercontinuum laser where high peak power pulses at low repetition-rate are required to reduce photobleaching effects [2]. Ideally, pulses from a low repetition-rate oscillator can be directly amplified to high pulse energy without need of complex pulse picking circuitry. Short picosecond pulses can be directly amplified to high pulse energy using a hybrid laser architecture based on a fiber mode-locked oscillator followed by a chain of bulk solid-state amplifiers [3]. As the nonlinear effects in the crystal amplifiers are negligible with the pulse peak power only limited by the critical self-focusing limit, this avoids the need to use pulse compression after amplification, which for industrial use could require active stabilization.

To achieve lower repetition rates a longer cavity length is required. However, introducing more fiber into a cavity increases the cumulative nonlinear phase shift of the pulse per cavity round trip. Excessive phase shift can lead to pulse break up [4].

As Ytterbium fiber lasers operate in the normal dispersion regime of standard silica fiber, soliton propagation is not possible. Soliton compression is necessary to generate short picosecond pulses directly from a mode-locked laser cavity without use of external compression. To induce soliton-like behavior at these wavelengths the dispersion can be managed across a cavity round trip in order to achieve net anomalous dispersion. However, for long cavities the total nonlinearity must also be controlled to preserve the pulse and avoid the onset of pulse break up.

The lowest reported repetition rate for an Ytterbium doped mode-locked fiber laser is 37 kHz [5] with pulse duration of 10ns. This is operating in a different regime to the short pulse durations considered in this work. For shorter pulse durations the nonlinearity places increasing limits on the pulse. For <10ps FWHM pulse the lowest reported repetition rate is 5.96MHz [6].

Traditional silica fibers have a nonlinear refractive index (n_2) of approximately $2.6 \times 10^{-20}\mathrm{m^2W^{-1}}$ which determines the nonlinear phase shift [7]:

$$\phi_{NL} = \frac{2\pi n_2(\lambda)}{\lambda A_{eff}} P_0 L \tag{1}$$

P_0 is the pulse peak power; L is the fiber length, $n_2(\lambda)$ is the nonlinear refractive index at wavelength λ and A_{eff} is the effective mode area of the fiber or free space beam. Pulse break up for soliton laser occurs when the cumulative nonlinear phase shift of the pulse in one cavity round trip is $\phi_{NL} = \pi$ [4].

The overall phase shift can be reduced by propagating in a mode with a larger area, a lower peak power or by using a medium with a lower n_2. Propagating through air with n_2 of the order $10^{-23}\mathrm{m^2W^{-1}}$ causes a reduced nonlinear phase shift compared to silica fiber.

Hollow core fibers (HCF) enable the propagation of light in air with the guiding capabilities and robustness suitable for integration into a fiber laser. The most common form of HCF is photonic bandgap fiber but other leaky mode fiber

Manuscript received September 3, 2015; revised October 29, 2015; accepted November 19, 2015. Date of publication December 1, 2015; date of current version February 18, 2016. This work was supported in part by the Engineering and Physical Sciences Research Council through the International Council of Associations for Science Education under Grant EP/K504245, in part by the Technology Strategy Board under Grant TP101503, and in part by Fianium Ltd.

C. M. Harvey, F. Yu, J. C. Knight, and W. J. Wadsworth are with the Centre for Photonics and Photonic Materials, Department of Physics, University of Bath, Bath BA2 7AY, U.K. (e-mail: c.m.harvey@bath.ac.uk; f.yu@bath.ac.uk; j.c.knight@bath.ac.uk; w.j.wadsworth@bath.ac.uk).

P. J. Almeida is with Fianium Ltd., Southampton SO31 4RA, U.K. (e-mail: paulo.almeida@fianium.com).

Color versions of one or more of the figures in this letter are available online at http://ieeexplore.ieee.org.

Digital Object Identifier 10.1109/LPT.2015.2504407

1041-1135 © 2015 IEEE. Personal use is permitted, but republication/redistribution requires IEEE permission.
See http://www.ieee.org/publications_standards/publications/rights/index.html for more information.

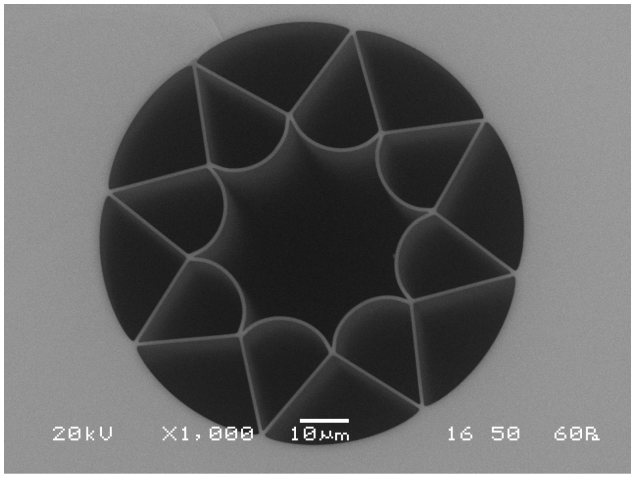

Fig. 1. Scanning electron micrograph of negative curvature, anti-resonant HCF (48m fiber sample).

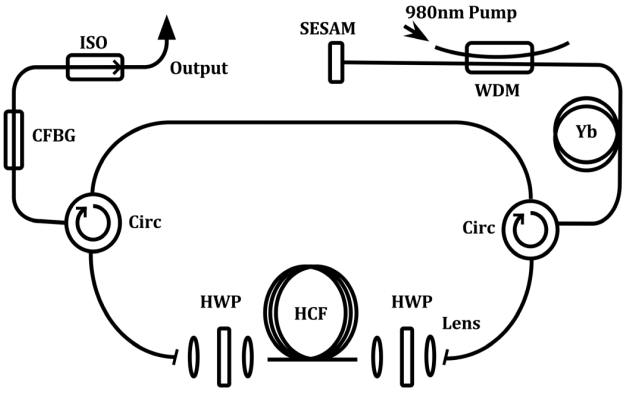

Fig. 2. Experimental setup of Yb mode-locked fiber laser based on ring cavity with hollow-core negative curvature fiber (HCF). ISO: optical isolator; HWP: half-wave plate; Circ: optical circulator; CFBG: chirped fiber Bragg grating; SESAM: semiconductor saturable absorber mirror.

designs also guide light. HCF can be filled with gas, liquid or evacuated. Hollow core fibers have benefits in transmitting high intensity light or light that would otherwise be subject to high material absorption due to low overlap with the glass structure [8]. Here we are interested in the low nonlinearity offered by transmitting through air and a hollow core, negative curvature, anti-resonant fiber was chosen for the experiment. The fiber structure fabricated for this experiment is shown in Fig. 1.

Negative curvature fiber has both low nonlinearity and anomalous group velocity dispersion of a few ps/nm/km at the design wavelength, due to large core size and propagation in air, allowing pulses to propagate with little disturbance [9]. We demonstrate this by extending a mode-locked laser cavity with up to 48m of negative curvature fiber while preserving the original pulse duration.

II. Experimental Details

The laser setup is a polarization maintaining ring cavity with two circulator arms to incorporate the reflective components: the SESAM mode-locking element and the chirped fiber Bragg grating (CFBG), as shown in Fig. 2. The SESAM is butt coupled to the fiber end. The CFBG has an anomalous dispersion of $+10$ps/nm and functions as an output coupler. The cavity gain is from a core-pumped ytterbium doped fiber amplifier with a length of 65cm, and pumped with a 980nm laser diode. All the pigtails consist of single mode, polarization maintaining, solid-core fiber totaling 5.4m. All of the components used are commercially available with the exception of the HCF which was fabricated in house.

A reference cavity was used as a baseline, characterized with no HCF and a single free space coupling stage with a repetition rate of 36.8MHz. Different lengths of HCF were then introduced, these included; 8m, 13m, 20m, 33m (20m and 13m coupled together), 48m. These corresponded to repetition rates of 18.2MHz, 14.2MHz, 10.8MHz, 7.4MHz and 5.4MHz respectively which were confirmed using oscilloscope traces of the pulse train. These fibers were all different fabrication iterations of the same structure with similar but not identical properties. Fiber attenuation was measured to be $>0.03\pm0.01$dB/m for each fiber. The HCF is flat cleaved and free space coupled to angle polished, solid-core pigtails using a lens pair and Thorlabs NanoMax stages. Angle polishes on the solid fibers were used to minimize detrimental Fresnel reflections. Two half-wave plates were used to align the polarization angle in and out of the HCF.

Each laser constructed was evaluated by taking the spectra and autocorrelation traces and by measuring the average output power for different pump powers. The spectra were measured on a Yokogawa optical spectrum analyzer, the autocorrelations taken with an APE PulseCheck autocorrelator and the power readings with a thermal power meter.

III. Results

A total of seven cavity lengths were assembled with different lengths of HCF. Many different mode-locking regimes were observed for different cavity pump powers. The evolution through these regimes with increasing pump power typically occurs as: amplified spontaneous emission operation at lowest powers; continuous wave operation once the lasing threshold is achieved; Q-switched mode-locking where pulses are observed but amplitude unstable; single pulse or fundamental mode-locking (which is the ideal regime in this case); and lastly multi-pulsing regimes. The multi-pulsing regimes consist of either harmonic mode-locking with pulses evenly spaced in time or in bunched pulse operation where the pulses are tightly bound and close in time, or a combination of both. All these pulse regimes have characteristic spectra, and the evolution with pump power can be observed as shown in Fig. 3.

The two main thresholds considered are the fundamental mode-locking threshold where stable pulses can be observed and the multi-pulse threshold where the pulse breaks up. The fundamental mode-locking threshold is dependent on pulse energy which is linked to the repetition rate of the cavity such that $E_p = P_{av}/F_{rep}$. Thus as the cavity length is increased, the pulse energy is also increased which reduces the mode-locking threshold. All the cavities were stable once started

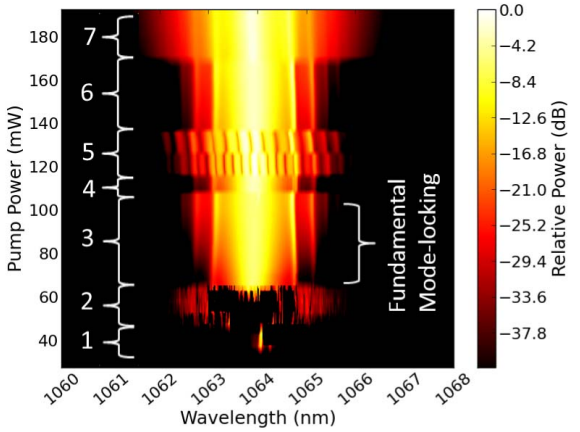

Fig. 3. Pulse spectral evolution with pump power for the reference cavity (36.8MHz) showing (1) CW lasing; (2) q-switched mode-locking; (3) fundamental CW mode-locking; (4,6) double pulse harmonic mode-locking; (5) bunched pulse multi-pulsing; (7) chaotic multi-pulsing. Scanning resolution was 0.02nm with spectrum recorded with pump power intervals varying between 1 and 5mW.

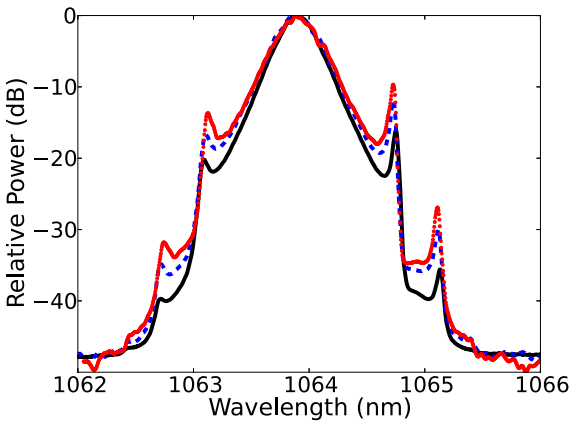

Fig. 4. Spectral comparison of cavity with 48m of HCF (red dotted line), with 20m of HCF (blue dashed line) and without HCF (solid line). Spectra taken at pump powers corresponding to the mid region of the fundamental mode-locking regime.

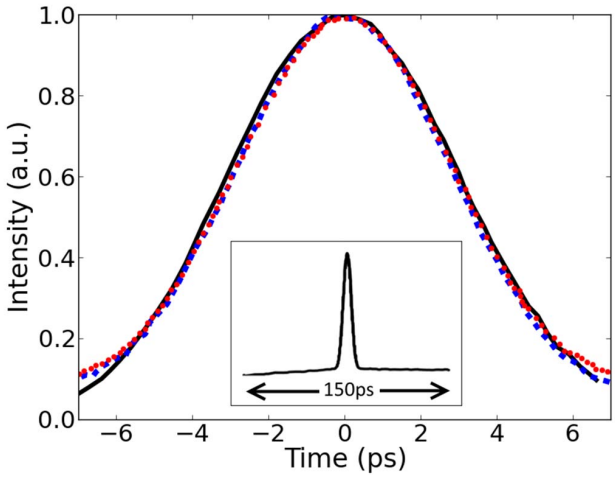

Fig. 5. Comparison of three autocorrelation traces with 48m of HCF (red dotted line), with 20m of HCF (blue dashed line) and reference cavity (solid line). Inset shows typical autocorrelation trace in a 150ps time span.

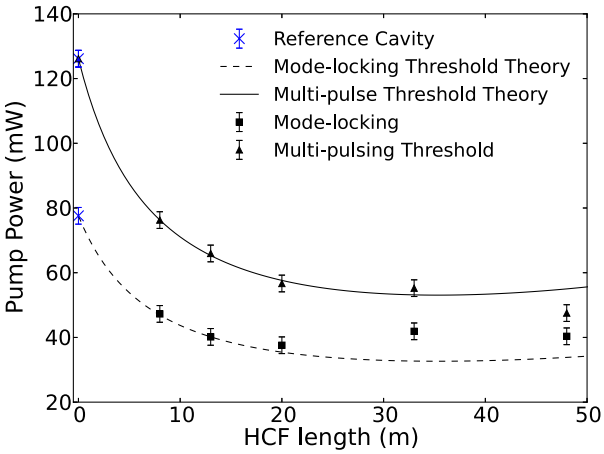

Fig. 6. Predicted mode-locked ranges based on the measured reference cavity with experimental results. 33m results are higher due to increased loss whereas 48m HCF results had lower than estimated fiber attenuation.

and measured over a few hours. All the cavities showed self-starting behavior for the majority of pump power in the fundamental mode-locking regime with the exception of low pump powers in the fundamental mode-locking regime.

The pulse spectra reliably showed the mode-locked state and were repeatable. Tracing the spectral evolution with pump power, Fig. 3, shows clear changes between the different pulsing regimes. Region 3 in Fig. 3 is the fundamental mode-locking regime defined by the mode-locking threshold at lower pump power and the multi-pulsing threshold at higher pump powers. These thresholds of pump power for each cavity are summarized later in Fig. 6.

Closer analysis of the pulse spectral shape shows a smooth shape with clear Kelly sidebands indicating a soliton-like pulse, Fig. 4. The shape of the pulse is preserved as the cavity length is increased. The position of the Kelly sidebands shows little change demonstrating there is negligible dispersion introduced by the extra lengths of HCF [10].

The measured autocorrelation traces for the different repetition-rate cavities showed similar shape and pulse width, shown in Fig. 5. At the lowest pump power in the fundamental mode-locking regime (shown in Fig. 6) the $1/e^2$ pulse width was measured as 4.8ps. With a few mW increase in pump power the pulse duration dropped to 4ps and had a time-bandwidth product of 0.35 in all cavities constructed. For further increases in pump power the pulse width was measured as 4.05ps $\pm$ 0.15ps but the time-bandwidth product increased to 0.5 at the multi-pulsing threshold in each cavity. The fundamental mode-locking region itself showed no autocorrelation coherence artifacts indicating full, coherent mode-locking was obtained without noise burst behavior. Increasing the cavity length reduces the pump power needed for mode-locking; however the fiber attenuation introduced will increase the pump power needed. Using these effects and the reference cavity data, an estimate of the mode-locking and multi-pulsing thresholds was obtained assuming a fiber

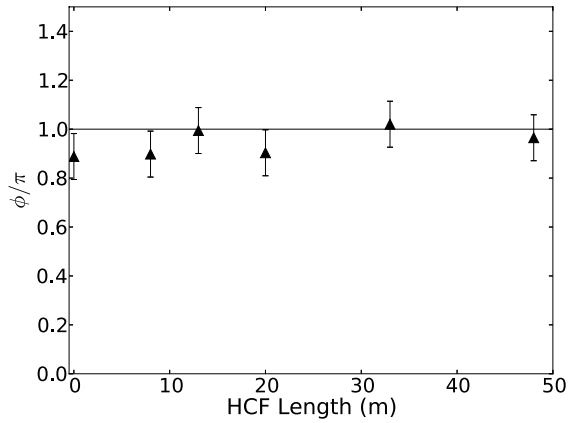

Fig. 7. Calculated nonlinear phase shift ϕ from measured intra-cavity pulse peak powers at lower and higher points of fundamental mode-locking.

attenuation of 0.04dBm^{-1} with no dispersion or nonlinearity, Fig. 6. The fundamental mode-locking and multi-pulsing thresholds for the different built cavities were determined by examining the experimental pulse spectra, oscilloscope and autocorrelation traces and plotted in Fig. 6.

The performance of each cavity is summarized in Fig. 7. The nonlinear phase shift, ϕ, was estimated by first calculating the pulse peak power from the average power, repetition rate and pulse width measured at the laser output. The pulse peak power at each point in the cavity was subsequently calculated taking into account the losses of the cavity components. The phase shift was calculated for each section of the cavity using Equation 1 with the pulse propagation with the HCF loss taken into account, and it was assumed nonlinear interaction only with air and no dispersion. The cumulative nonlinear phase shift was then obtained and each cavity is shown to reach the maximum phase shift of π with in error demonstrating the laser is reaching full performance. These points correspond to an output peak power of approximately 40W and output pulse energy of 179pJ in the reference cavity increasing to 240pJ in the 5.4MHz cavity.

Generally, the cavity performance showed some hysteresis in the threshold for multi-pulsing by approximately 5mW change of pump power. Starting in the single pulse regime and increasing power, the cavity remained single pulse to a higher pump power than starting in the multi-pulsing regime and decreasing power. For consistency, the threshold point was taken as the pump power where single pulse became multi-pulse when increasing pump power.

This measured threshold was also subject to drift over the course of several days. This was attributed to temperature fluctuations and mechanical drifts in coupling. These were minimized by use of a temperature controlled plate. This was incorporated into the errors in Fig. 6 and Fig. 7.

Further experiments have been conducted using a longer HCF piece, of 118m. However fibers at this length had considerably higher loss and produced a long pulse of approximately 50ps with no coherence artifacts observed in the autocorrelation trace. This is attributed to inadequate fiber manufacturing producing undesirable optical resonances in the fiber altering the dispersion profile of the fiber. Improved drawing techniques would produce better quality, long fibers.

A linear cavity laser with the HCF operating in double pass was also constructed and tested. The CFBG and SESAM used were similar to that used in the ring cavity. A HCF length of 1m in the linear cavity configuration produced pulses of approximately 6ps. The 48m piece of HCF tested in the linear cavity produced however 50ps pulses. The precise cause of this is yet to be confirmed.

IV. Conclusion

An Yb^{3+} mode-locked fiber laser has been extended with up to 48m of hollow core negative curvature fiber. The HCF did not introduce significant additional nonlinearity or dispersion to the cavity. Results show that HCF is a viable means to reduce the repetition rate of Yb mode-locked fiber lasers with minimum detriment to the pulse. Further reductions in repetition rate should be possible provided longer lengths of HCF of this type can be manufactured with sufficient quality.

Acknowledgment

Datasets DOI URL: http://dx.doi.org/10.15125/BATH00132

References

[1] A. Tünnermann, S. Nolte, and J. Limpert, "Femtosecond vs. picosecond laser material processing," *Laser Tech. J.*, vol. 7, no. 1, pp. 34–38, 2010.

[2] D. Wildanger, E. Rittweger, L. Kastrup, and S. W. Hell, "STED microscopy with a supercontinuum laser source," *Opt. Exp.*, vol. 16, pp. 9614–9621, 2008.

[3] A. Agnesi, L. Carra, F. Pirzio, R. Piccoli, and G. Reali, "Low repetition rate, hybrid fiber/solid-state, 1064 nm picosecond master oscillator power amplifier laser system," *J. Opt. Soc. Amer. B*, vol. 30, no. 11, pp. 2960–2965, 2013.

[4] W. H. Renninger and F. W. Wise, "Fundamental limits to mode-locked lasers: Toward terawatt peak powers," *IEEE J. Sel. Topics Quantum Electron.*, vol. 21, no. 1, Jan./Feb. 2015, Art. ID 1100208.

[5] S. M. Kobtsev, S. V. Kukarin, and S. V. Smirnov, "All-fiber high-energy supercontinuum pulse generator," *Laser Phys.*, vol. 20, no. 2, pp. 375–378, Feb. 2010.

[6] C. K. Nielsen and S. R. Keiding, "All-fiber mode-locked fiber laser," *Opt. Lett.*, vol. 32, no. 11, pp. 1474–1476, 2007.

[7] G. P. Agrawal, *Nonlinear Fiber Optics*. New York, NY, USA: Academic, 2013.

[8] F. Yu, W. J. Wadsworth, and J. C. Knight, "Low loss silica hollow core fibers for 3-4 μm spectral region," *Opt. Lett.*, vol. 20, no. 10, pp. 11153–11158, 2012.

[9] P. Jaworski *et al.*, "Picosecond and nanosecond pulse delivery through a hollow-core negative curvature fiber for micro-machining applications," *Opt. Exp.*, vol. 21, no. 19, pp. 22742–22753, 2013.

[10] M. L. Dennis and I. N. Duling, III, "Experimental study of sideband generation in femtosecond fiber lasers," *IEEE J. Quantum Electron.*, vol. 30, no. 6, pp. 1469–1477, Jun. 1994.

Spectral Broadening and Pulse Compression Using Argon Filled Hollow-core Negative Curvature Fiber

C. M. Harvey[1*], F. Yu[1], J. C. Knight[1], W. J. Wadsworth[1], P. J. Almeida[2]
[1]*Centre for Photonics and Photonic Materials, Department of Physics, University of Bath, Bath, BA2 7AY, UK*
[2]*Fianium ltd. 20 Compass Point, Ensign Way, Southampton SO31 4RA, UK*
[*]*c.m.harvey@bath.edu*

Abstract: We investigate self-phase modulation in 28m of negative curvature anti-resonant hollow-core fiber pressurized with argon. A 9.6ps pulse is spectrally broadened to 7.6nm, at 20bar of pressure, and compressed to 420fs with 8μJ output energy.
OCIS codes: 190.0190, 060.2390, 060.7140

1. Introduction

Low loss hollow-core fibers provide a means of using and studying different materials under distinctive conditions of optical intensity and long interaction lengths. By filling a hollow-core fiber with a fluid, material properties outside of the range of silica can be used to manipulate the propagating light. This work focuses on filling negative-curvature anti-resonant hollow-core fiber with argon gas with the aim of using Raman-free self-phase modulation (SPM) to spectrally broaden a pulse. The nonlinear refractive index of argon is pressure dependent allowing for scaling of the nonlinear effects in the fiber with applied pressure [1]. Previous work has been conducted using a mode-locked ytterbium laser with hollow-core fiber in the anomalous dispersion regime, which can be limited by the onset of modulation instability and soliton dynamics [2]. Here we investigated spectral broadening of pulses from an ultrafast laser operating at 1064 nm by propagating in the normal dispersion regime of a gas-filled hollow-core negative curvature fiber. In the normal dispersion regime, large spectral broadening associated with a linear frequency-chirp can be achieved, which allows for high quality pulse compression. In this paper, we demonstrate spectral broadening with nonlinear shift in excess of 12.5π, and subsequent low pedestal pulse compression.

2. Experiment

The experiment used a HYLASE-25 high-energy picosecond laser from Fianium with a pulse duration of about 10ps and pulse energy up to 125 μJ at 1064 nm, operating at a set pulse picked repetition-rate of 50 kHz at 1064 nm. The power incident on the fiber was controlled by a half wave plate and polarizing beam splitter. This was coupled into a length of hollow-core fiber housed between gas cells, as shown in Figure 1. Pulse spectra were measured at the output of the fiber prior to the grating pair pulse compressor. The fiber output collimated beam was then aligned into a double pass grating pair, applying approximately 1 ps/nm of dispersion. The fiber used was 28 m of negative curvature design [3] with a core diameter of 34 μm. This fiber was chosen so that the pulse at 1064.5 nm was at the short wavelength side of the transmission band where the fiber has normal dispersion. The fiber was pressurized with argon, which has minimal Raman response and a relatively high ionization threshold.

3. Results

Different pressures were tested and the spectrum was analyzed at varying input powers. The observed spectral broadening increased with pressure as expected. Output spectra are compared in Figure 2-a for a fixed input average power of 600 mW at 50 kHz (12 μJ). Below 25 bar regular spectral peaks can be observed and the pulse is

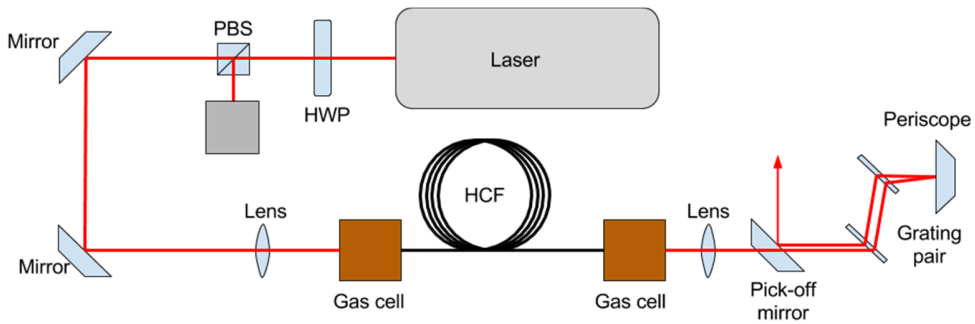

Figure 1, Experimental set up of gas filled hollow-core negative curvature fiber (HCF) and grating pair pulse compressor. Power control provided by half wave plate (HWP) and polarizing beam splitter (PBS).

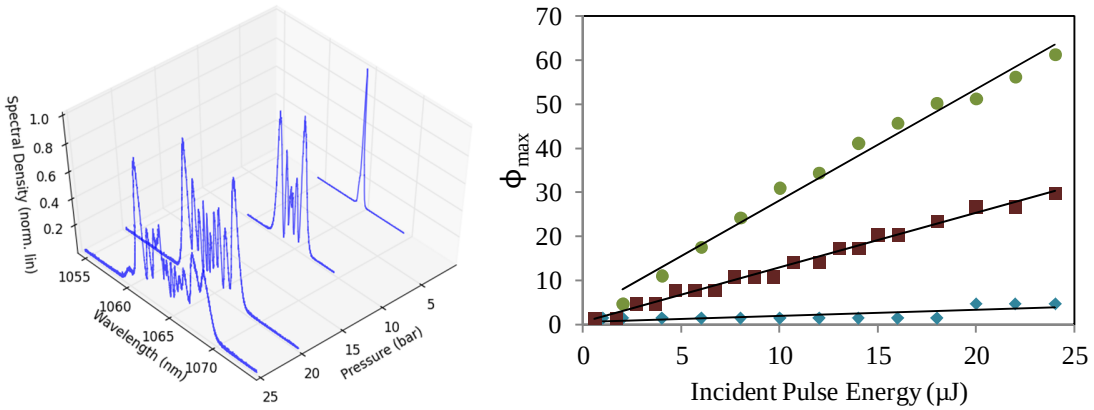

Figure 2, a) Pulse spectra at different pressures with fixed 12μJ pulse energy incident on fiber. b) Estimated nonlinear phase shift at different pulse energies for 1 bar (diamonds), 10 bar (squares) and 20 bar (circles). Both plots created using 28 m of HCF at 50 kHz.

compressible. Above 25 bar structure appears on top of the spectral oscillations from SPM limiting potential pulse compression. As a result 20 bar of pressure was chosen to proceed with pulse compression to provide the largest spectral broadening with least distortion. Figure 2-b shows the scaling of SPM induced phase shift with incident pulse energy for different pressures estimated using $\phi_{max} \approx \left(M - \frac{1}{2}\right)\pi$ where M is the number of SPM peaks [4].

The maximum structure free compression observed was at 50 kHz repetition rate, with 9.6 ps input pulse duration, 1.2 W average power giving a pulse energy of 24 μJ and a pre-compression estimated peak power of 2.2 MW. This produced a 7.6 nm bandwidth (FWHM) after propagation through the fiber, Figure 3. After compression the pulse was measured to be 420 fs FWHM and 8 μJ (estimated peak power of 10MW) after losses from fiber coupling and grating pair. Further SPM broadening was observed at higher powers up to 10.5 nm FWHM from 30 μJ pulse energy. However, the resulting autocorrelation trace displayed structure after compression.

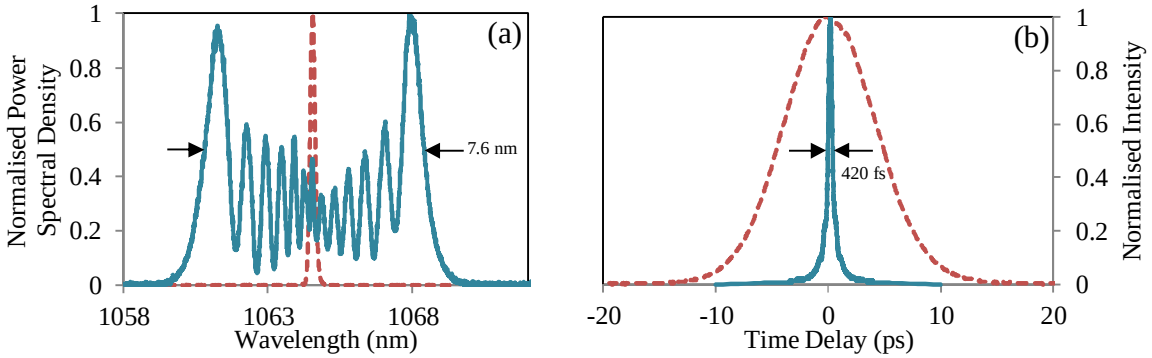

Figure 3, a) Pulse spectra of the input laser with 0.2 nm bandwidth (red dashed) and spectra after propagating in fiber showing 7.6 nm FWHM bandwidth (blue solid); b) Autocorrelation traces from laser measuring 9.6 ps (red dashed) and after compression measuring 420 fs (blue solid). Results obtained with 20 bar of argon and input pulse energy of 24 μJ.

4. Conclusions

The effect of pressure of argon on the produced self-phase modulation has been analyzed and a limit of <25bar has been found for this configuration. The self-phase modulation induced by different pressures of argon in negative curvature HCF has been recorded. An increase in spectral width from 0.2nm to 7.6nm was generated enabling a compression from 9.6ps to 420fs with no structure in the autocorrelation trace.

This work is supported by EPSRC iCASE award EP/K504245 and Fianium Ltd. Dataset: 10.15125/BATH-00171

5. References

[1] Á. Börzsönyi, et al. Opt. Express 18, 25847-25854 (2010)
[2] Florian Emaury, et al, Opt. Lett. 39, 6843-6846 (2014)
[3] Yu, F and Knight, J.C. Opt. Express 21, 21466-21471(2013)
[4] Govind Agrawal, *Nonlinear Fiber Optics* (Academic Press 2013)

Bibliography

[1] M. E. Fermann and I. Hartl, "Ultrafast fibre lasers," *Nat Photon*, vol. 7, no. 11, pp. 868–874, nov 2013.

[2] J. A. Buck, *Fundamentals of Optical Fibers*. Wiley, 2004.

[3] J. M. Fini, "Bend-resistant design of conventional and microstructure fibers with very large mode area," *Optics Express*, vol. 14, no. 1, pp. 69–81, 2006.

[4] E. Ding, S. Lefrancois, J. N. Kutz, and F. W. Wise, "Scaling Fiber Lasers to Large Mode Area: An Investigation of Passive Mode-Locking Using a Multi-Mode Fiber," *Quantum Electronics, IEEE Journal of*, vol. 47, no. 5, pp. 597–606, 2011.

[5] W. Belardi and J. C. Knight, "Effect of core boundary curvature on the confinement losses of hollow antiresonant fibers," *Optics Express*, vol. 21, no. 19, pp. 21 912–21 917, 2013.

[6] I. H. Malitson, "Interspecimen Comparison of the Refractive Index of Fused Silica," *J. Opt. Soc. Am.*, vol. 55, no. 10, pp. 1205–1209, oct 1965.

[7] A. Börzsönyi, Z. Heiner, M. P. Kalashnikov, A. P. Kovács, and K. Osvay, "Dispersion measurement of inert gases and gas mixtures at 800 nm," *Applied Optics*, vol. 47, no. 27, pp. 4856–4863, 2008.

[8] E. A. J. Marcatili and R. A. Schmeltzer, "Hollow metallic and dielectric waveg-

uides for long distance optical transmission and lasers," *Bell Syst. Tech. J.*, vol. 43, no. 4, pp. 1783–1809, 1964.

[9] G. P. Agrawal, *Nonlinear Fiber Optics*. Academic Press, 2013.

[10] W. M. Tolles, J. W. Nibler, J. R. McDonald, and A. B. Harvey, "A Review of the Theory and Application of Coherent Anti-Stokes Raman Spectroscopy (CARS)," *Applied Spectroscopy*, vol. 31, no. 4, pp. 253–271, 1977.

[11] H. A. Haus and M. Nakazawa, "Theory of the fiber Raman soliton laser," *Journal of the Optical Society of America B*, vol. 4, no. 5, pp. 652–660, 1987.

[12] J. C. Travers, W. Chang, J. Nold, N. Y. Joly, and P. S. J. Russell, "Ultrafast nonlinear optics in gas-filled hollow-core photonic crystal fibers [Invited]," *J. Opt. Soc. Am. B*, vol. 28, no. 12, pp. A11–A26, dec 2011.

[13] J. A. C. Weideman and B. M. Herbst, "Split-Step Methods for the Solution of the Nonlinear Schrodinger Equation," *SIAM Journal on Numerical Analysis*, vol. 23, no. 3, pp. 485–507, 1986.

[14] D. J. Korteweg and G. de Vries, "XLI. On the change of form of long waves advancing in a rectangular canal, and on a new type of long stationary waves," *Philosophical Magazine Series 5*, vol. 39, no. 240, pp. 422–443, may 1895.

[15] L. F. Mollenauer, R. H. Stolen, and J. P. Gordon, "Experimental Observation of Picosecond Pulse Narrowing and Solitons in Optical Fibers," *Phys. Rev. Lett.*, vol. 45, no. 13, pp. 1095–1098, sep 1980.

[16] D. C. Hutchings, M. Sheik-Bahae, D. J. Hagan, and E. W. Van Stryland, "Kramers-Krönig relations in nonlinear optics," *Optical and Quantum Electronics*, vol. 24, no. 1, pp. 1–30, 1992.

[17] T. A. Birks, P. J. Roberts, P. S. J. Russell, D. M. Atkin, and T. J. Shepherd, "Full 2-D photonic bandgaps in silica/air structures," *Electronics Letters*, vol. 31, no. 22, pp. 1941–1943, 1995.

[18] H. Yu, X. Wang, P. Zhou, X. Xu, and J. Chen, "High-Energy Square Pulses in a Mode-Locked Yb-Doped Fiber Laser Operating in DSR Region," *Photonics Technology Letters, IEEE*, vol. 27, no. 7, pp. 737–740, 2015.

[19] A. W. Snyder and J. Love, *Optical Waveguide Theory*, ser. Science paperbacks. Springer US, 1983.

[20] Y. Wang, F. Couny, P. J. Roberts, and F. Benabid, "Low Loss Broadband Transmission In Optimized Core-shape Kagome Hollow-core PCF," in *Conference on Lasers and Electro-Optics 2010*, ser. OSA Technical Digest (CD). San Jose, California: Optical Society of America, 2010, p. CPDB4.

[21] Y. Y. Wang, N. V. Wheeler, F. Couny, P. J. Roberts, and F. Benabid, "Low loss broadband transmission in hypocycloid-core Kagome hollow-core photonic crystal fiber," *Optics Letters*, vol. 36, no. 5, pp. 669–671, 2011.

[22] A. D. Pryamikov, A. S. Biriukov, A. F. Kosolapov, V. G. Plotnichenko, S. L. Semjonov, and E. M. Dianov, "Demonstration of a waveguide regime for a silica hollow - core microstructured optical fiber with a negative curvature of the core boundary in the spectral region > 3.5 μm," *Optics Express*, vol. 19, no. 2, pp. 1441–1448, 2011.

[23] F. Yu, W. J. Wadsworth, and J. C. Knight, "Low loss silica hollow core fibers for 3-4 μm spectral region," *Optics Express*, vol. 20, no. 10, pp. 11 153–11 158, 2012.

[24] F. Yu and J. C. Knight, "Negative Curvature Hollow-Core Optical Fiber," pp. 146–155, 2016.

[25] A. Bideau-Mehu, Y. Guern, R. Abjean, and A. Johannin-Gilles, "Measurement of refractive indices of neon, argon, krypton and xenon in the 253.7140.4 nm wavelength range. Dispersion relations and estimated oscillator strengths of the resonance lines," *Journal of Quantitative Spectroscopy and Radiative Transfer*, vol. 25, no. 5, pp. 395–402, 1981.

[26] F. Yu and J. C. Knight, "Spectral attenuation limits of silica hollow core negative curvature fiber," *Optics Express*, vol. 21, no. 18, pp. 21 466–21 471, 2013.

[27] P. S. J. Russell, P. Holzer, W. Chang, A. Abdolvand, and J. C. Travers, "Hollow-core photonic crystal fibres for gas-based nonlinear optics," *Nat Photon*, vol. 8, no. 4, pp. 278–286, apr 2014.

[28] R. Thomson, C. Leburn, and D. Reid, *Ultrafast Nonlinear Optics*, 1st ed. Springer International Publishing, 2013.

[29] A. Tuennermann, S. Nolte, and J. Limpert, "Femtosecond vs. Picosecond Laser Material Processing," *Laser Technik Journal*, vol. 7, no. 1, pp. 34–38, jan 2010.

[30] D. Wildanger, E. Rittweger, L. Kastrup, and S. W. Hell, "STED microscopy with a supercontinuum laser source," *Optics Express*, vol. 16, no. 13, pp. 9614–9621, 2008.

[31] R. Paschotta, "Ultrafast Laser Systems: Fiber or Bulk Solutions?" *Laser Technik Journal*, vol. 10, no. 3, pp. 51–55, 2013.

[32] K. Gürs and R. Müller, "Breitband-modulation durch steuerung der emission eines optischen masers (Auskoppelmodulation)," *Physics Letters*, vol. 5, no. 3, pp. 179–181, 1963.

[33] M. DiDomenico, "Small-Signal Analysis of Internal (Coupling-Type) Modulation of Lasers," *Journal of Applied Physics*, vol. 35, no. 10, pp. 2870–2876, 1964.

[34] L. E. Hargrove, R. L. Fork, and M. A. Pollack, "Locking of HeNe laser modes induced by synchronous intracavity modulation," *Applied Physics Letters*, vol. 5, no. 1, pp. 4–5, 1964.

[35] H. W. Mocker and R. J. Collins, "Mode Competition and Self-Locking Effects in a Q-Switched Ruby Laser," *Applied Physics Letters*, vol. 7, no. 10, pp. 270–273, 1965.

[36] E. P. Ippen, C. V. Shank, and A. Dienes, "Passive mode locking of the cw dye laser," *Applied Physics Letters*, vol. 21, no. 8, pp. 348–350, 1972.

[37] E. Snitzer, "Optical Maser Action of Nd^{+3} in a Barium Crown Glass," *Physical Review Letters*, vol. 7, no. 12, pp. 444–446, 1961.

[38] M. I. Dzhibladze, Z. G. Ésiashvili, T. É Sh, S. K. Isaev, and V. R. Sagaradze, "Mode locking in a fiber laser," *Soviet Journal of Quantum Electronics*, vol. 13, no. 2, p. 245, 1983.

[39] G. Geister and R. Ulrich, "Neodymium-fibre laser with integrated-optic mode locker," *Optics Communications*, vol. 68, no. 3, pp. 187–189, 1988.

[40] M. W. Phillips, A. I. Ferguson, and D. C. Hanna, "Frequency-modulation mode locking of a Nd3+-doped fiber laser," *Optics Letters*, vol. 14, no. 4, pp. 219–221, 1989.

[41] X. Zhou, D. Yoshitomi, Y. Kobayashi, and K. Torizuka, "Generation of 28-fs pulses from a mode-locked ytterbium fiber oscillator," *Optics Express*, vol. 16, no. 10, pp. 7055–7059, 2008.

[42] L. Krainer, R. Paschotta, S. Lecomte, M. Moser, K. J. Weingarten, and U. Keller, "Compact Nd:YVO₄ lasers with pulse repetition rates up to 160 GHz," *Quantum Electronics, IEEE Journal of*, vol. 38, no. 10, pp. 1331–1338, 2002.

[43] H. M. Pask, R. J. Carman, D. C. Hanna, A. C. Tropper, C. J. Mackechnie, P. R. Barber, and J. M. Dawes, "Ytterbium-doped silica fiber lasers: versatile sources for the 1-1.2 μm region," *Selected Topics in Quantum Electronics, IEEE Journal of*, vol. 1, no. 1, pp. 2–13, 1995.

[44] S. Hooker and C. Webb, *Laser Physics*. OUP Oxford, 2010.

[45] R. Paschotta, J. Nilsson, A. C. Tropper, and D. C. Hanna, "Ytterbium-doped fiber amplifiers," *Quantum Electronics, IEEE Journal of*, vol. 33, no. 7, pp. 1049–1056, 1997.

[46] Z. Sun, T. Hasan, F. Torrisi, D. Popa, G. Privitera, F. Wang, F. Bonaccorso, D. M. Basko, and A. C. Ferrari, "Graphene Mode-Locked Ultrafast Laser," *ACS Nano*, vol. 4, no. 2, pp. 803–810, feb 2010.

[47] S. Y. Set, H. Yaguchi, Y. Tanaka, and M. Jablonski, "Ultrafast fiber pulsed lasers incorporating carbon nanotubes," *Selected Topics in Quantum Electronics, IEEE Journal of*, vol. 10, no. 1, pp. 137–146, 2004.

[48] F. Salin, M. Piché, and J. Squier, "Mode locking of Ti:Al2O3 lasers and self-focusing: a Gaussian approximation," *Optics Letters*, vol. 16, no. 21, pp. 1674–1676, 1991.

[49] M. E. Fermann, M. L. Stock, M. J. Andrejco, and Y. Silberberg, "Passive mode locking by using nonlinear polarization evolution in a polarization-maintaining erbium-doped fiber," *Optics Letters*, vol. 18, no. 11, pp. 894–896, 1993.

[50] U. Keller, "Ultrafast solid-state laser oscillators: a success story for the last 20years with no end in sight," *Applied Physics B*, vol. 100, no. 1, pp. 15–28, 2010.

[51] H. A. Haus, "Theory of mode locking with a fast saturable absorber," *Journal of Applied Physics*, vol. 46, no. 7, p. 3049, 1975.

[52] M. Hercher, "An Analysis of Saturable Absorbers," *Applied Optics*, vol. 6, no. 5, pp. 947–954, 1967.

[53] C. Hönninger, R. Paschotta, F. Morier-Genoud, M. Moser, and U. Keller, "Q-switching stability limits of continuous-wave passive mode locking," *Journal of the Optical Society of America B*, vol. 16, no. 1, pp. 46–56, 1999.

[54] R. Paschotta, *Field Guide to Laser Pulse Generation*. Society of Photo Optical, 2008.

[55] S. M. J. Kelly, "Characteristic sideband instability of periodically amplified average soliton," *Electronics Letters*, vol. 28, no. 8, pp. 806–807, 1992.

[56] S. M. Kobtsev, S. V. Kukarin, and S. V. Smirnov, "All-fiber high-energy supercontinuum pulse generator," *Laser Physics*, vol. 20, no. 2, pp. 375–378, 2010.

[57] S. Kobtsev, S. Kukarin, and Y. Fedotov, "Ultra-low repetition rate mode-locked fiber laser with high-energy pulses," *Optics Express*, vol. 16, no. 26, pp. 21 936–21 941, 2008.

[58] X. Tian, M. Tang, X. Cheng, P. P. Shum, Y. Gong, and C. Lin, "High-energy wave-breaking-free pulse from allfibermode-locked laser system," *Optics Express*, vol. 17, no. 9, pp. 7222–7227, 2009.

[59] Z. Meng, C. Lingling, Z. Chun, C. Yue, and Z. Zhigang, "Ultra-low repetition rate all-normal-dispersion linear-cavity mode-locked fiber lasers," in *Lasers & Electro Optics & The Pacific Rim Conference on Lasers and Electro-Optics, 2009. CLEO/PACIFIC RIM '09. Conference on*, 2009, pp. 1–2.

[60] L. J. Kong, X. S. Xiao, and C. X. Yang, "Low-repetition-rate all-fiber all-normal-dispersion Yb-doped mode-locked fiber laser," *Laser Physics Letters*, vol. 7, no. 5, pp. 359–362, 2010.

[61] S. Rui, C. Hong-Wei, C. Sheng-Ping, H. Jing, and L. Qi-Sheng, "A SESAM passively mode-locked fiber laser with a long cavity including a band pass filter," *Journal of Optics*, vol. 13, no. 3, p. 35201, 2011.

[62] M. Baumgartl, J. Abreu-Afonso, A. Díez, M. Rothhardt, J. Limpert, and A. Tünnermann, "Environmentally stable picosecond Yb fiber laser with low repetition rate," *Applied Physics B*, vol. 111, no. 1, pp. 39–43, 2013.

[63] A. Agnesi, L. Carrá, F. Pirzio, R. Piccoli, and G. Reali, "Low repetition rate, hybrid fiber/solid-state, 1064 nm picosecond master oscillator power amplifier laser system," *Journal of the Optical Society of America B*, vol. 30, no. 11, pp. 2960–2965, 2013.

[64] S. Boivinet, J. B. Lecourt, Y. Hernandez, A. A. Fotiadi, M. Wuilpart, and P. Megret, "All-Fiber 1-um PM Mode-Lock Laser Delivering Picosecond Pulses at Sub-MHz Repetition Rate," *Photonics Technology Letters, IEEE*, vol. 26, no. 22, pp. 2256–2259, 2014.

[65] C. K. Nielsen and S. R. Keiding, "All-fiber mode-locked fiber laser," *Optics Letters*, vol. 32, no. 11, pp. 1474–1476, 2007.

[66] L. Chen, M. Zhang, C. Zhou, Y. Cai, L. Ren, and Z. Zhang, "Ultra-low repetition rate linear-cavity erbium-doped fibre laser modelocked with semiconductor saturable absorber mirror," *Electron. Lett.*, vol. 45, no. 14, pp. 731–733, 2009.

[67] B. N. Nyushkov, V. I. Denisov, S. M. Kobtsev, V. S. Pivtsov, N. A. Kolyada, A. V. Ivanenko, and S. K. Turitsyn, "Generation of 1.7-μJ pulses at 1.55 μm by a self-mode-locked all-fiber laser with a kilometers-long linear-ringcavity," *Laser Physics Letters*, vol. 7, no. 9, pp. 661–665, 2010.

[68] H. G. Rosa and E. A. Thoroh de Souza, "Pulse generation and propagation in dispersion-managed ultralong erbium-doped fiber lasers mode-locked by carbon nanotubes," *Optics Letters*, vol. 37, no. 24, pp. 5211–5213, 2012.

[69] N. Li, J. Xue, C. Ouyang, K. Wu, J. H. Wong, S. Aditya, and P. P. Shum, "Cavity-length optimization for high energy pulse generation in a long cavity passively mode-locked all-fiber ring laser," *Applied Optics*, vol. 51, no. 17, pp. 3726–3730, 2012.

[70] Y. Senoo, N. Nishizawa, Y. Sakakibara, K. Sumimura, E. Itoga, H. Kataura, and K. Itoh, "Ultralow-repetition-rate, high-energy, polarization-maintaining,

Er-doped, ultrashort-pulse fiber laser using single-wall-carbon-nanotube saturable absorber," *Optics Express*, vol. 18, no. 20, pp. 20 673–20 680, 2010.

[71] D. Marcuse, "Loss Analysis of Single-Mode Fiber Splices," *Bell Syst. Tech. J*, vol. 56, no. 5, pp. 703–718, 1977.

[72] M. Szczurowski, W. Urbanczyk, M. Napiorkowski, P. Hlubina, U. Hollenbach, H. Sieber, and J. Mohr, "Differential Rayleigh scattering method for measurement of polarization and intermodal beat length in optical waveguides and fibers," *Applied Optics*, vol. 50, no. 17, pp. 2594–2600, 2011.

[73] P. Jaworski, F. Yu, R. R. J. Maier, W. J. Wadsworth, J. C. Knight, J. D. Shephard, and D. P. Hand, "Picosecond and nanosecond pulse delivery through a hollow-core Negative Curvature Fiber for micro-machining applications," *Optics Express*, vol. 21, no. 19, pp. 22 742–22 753, 2013.

[74] E. Treacy, "Optical pulse compression with diffraction gratings," *IEEE J. Quant. Electron.*, vol. 5, no. 9, pp. 454–458, 1969.

[75] Á. Börzsönyi, Z. Heiner, A. P. Kovács, M. P. Kalashnikov, and K. Osvay, "Measurement of pressure dependent nonlinear refractive index of inert gases," *Optics Express*, vol. 18, no. 25, pp. 25 847–25 854, 2010.

[76] E. T. J. Nibbering, G. Grillon, M. A. Franco, B. S. Prade, and A. Mysyrowicz, "Determination of the inertial contribution to the nonlinear refractive index of air, N2, and O2 by use of unfocused high-intensity femtosecond laser pulses," *J. Opt. Soc. Am. B*, vol. 14, no. 3, pp. 650–660, 1997.

[77] Y. Y. Wang, X. Peng, M. Alharbi, C. F. Dutin, T. D. Bradley, F. Gérôme, M. Mielke, T. Booth, and F. Benabid, "Design and fabrication of hollow-core photonic crystal fibers for high-power ultrashort pulse transportation and pulse compression," *Optics Letters*, vol. 37, no. 15, pp. 3111–3113, aug 2012.

[78] O. H. Heckl, C. J. Saraceno, C. R. E. Baer, T. Südmeyer, Y. Y. Wang, Y. Cheng, F. Benabid, and U. Keller, "Temporal pulse compression in a

xenon-filled Kagome-type hollow-core photonic crystal fiber at high average power," *Optics Express*, vol. 19, no. 20, pp. 19 142–19 149, sep 2011.

[79] F. Emaury, C. J. Saraceno, B. Debord, D. Ghosh, A. Diebold, F. Gèrôme, T. Südmeyer, F. Benabid, and U. Keller, "Efficient spectral broadening in the 100-W average power regime using gas-filled kagome HC-PCF and pulse compression," *Optics Letters*, vol. 39, no. 24, pp. 6843–6846, 2014.

[80] M. Azhar, N. Y. Joly, J. C. Travers, and P. S. J. Russell, "Nonlinear optics in Xe-filled hollow-core PCF in high pressure and supercritical regimes," *Applied Physics B*, vol. 112, no. 4, pp. 457–460, 2013.

[81] W. J. Wadsworth, N. Joly, J. C. Knight, T. A. Birks, F. Biancalana, and P. S. J. Russell, "Supercontinuum and four-wave mixing with Q-switched pulses in endlessly single-mode photonic crystal fibres," *Optics Express*, vol. 12, no. 2, pp. 299–309, jan 2004.

[82] C. Harvey, F. Yu, J. C. Knight, W. Wadsworth, and P. Almeida, "Spectral Broadening and Pulse Compression Using Argon Filled Hollow-core Negative Curvature Fiber," *Cleo: 2016*, 2016.